Current-Voltage Characteristics of Carbon Nanotube Field Effect Transistor Considering Non-Ballistic Conduction

By

Nirjhor Tahmidur Rouf (10121002)

Ashfaqul Haq Deep (10121024)

Rusafa Binte Hassan (10221077)

A Thesis

Submitted as the partial Fulfillment for the Degree of

Bachelor of Science in Electrical and Electronic Engineering

Department of Electrical and Electronic Engineering

BRAC University

Dhaka-1212, Bangladesh

CERTIFICATE OF APPROVAL

The thesis entitled **"Current-Voltage Characteristics of Carbon Nanotube Field Effect Transistor Considering Non-Ballistic Conduction"** submitted by **Nirjhor Tahmidur Rouf, Ashfaqul Haq Deep** and **Rusafa Binte Hassan** has been accepted satisfactorily in partial fulfillment of the requirement for the degree of Bachelor of Science in Electrical and Electronic Engineering on September, 2013.

Supervisor

(Dr. Sharif Mohammad Mominuzzaman)

Department of Electrical and Electronic Engineering

Bangladesh University of Engineering and Technology (BUET)

CANDIDATE DECLARATION

It is hereby declared that this thesis or any part of it has not been submitted elsewhere for the award of any degree or diploma.

Author

Nirjhor Tahmidur Rouf

Author

Ashfaqul Haq Deep

Author

Rusafa Binte Hassan

ACKNOWLEDGEMENT

We are grateful to Almighty ALLAH for directing us on the right path in pursuing the requirement of the full thesis work.

There are many people we would like to thank who have helped us in completing our research. First of all we would like to express our gratitude towards our respected thesis supervisor, **Dr. Sharif Mohammad Mominuzzaman,** Professor of EEE department BUET, for his insight and direction. His faith in us and motivation has provided us with the confidence to achieve our goals.

We would also like to thank **Dr. A.K.M. Azad** who referred our group to Professor Mominuzzaman and always believed in our abilities.

We are indebted to **Sabbir Ahmed Khan** and **Mahmudul Hasan** for sharing their experience, ideas and at the same time stimulating our intellectual curiosity. Also, a special thanks to **Shakerul Islam Khan** for taking the time out of his busy schedule to help us out with our work. They have been extremely helpful and have guided us in times of difficulties.

Lastly, we thank our parents and well-wishers for supporting and encouraging us throughout our work.

ABSTRACT

The need for technological advancement in the field of electronics has been ever increasing. Till now silicon has been the prime material of choice for meeting the current demands. However, silicon has its own limitations; Silicon based integrated circuits and the scaling of silicon MOSFET design faces complications like tunneling effect, gate oxide thickness effect etc. which has given the scope for new materials to emerge.

The growing academic interest in carbon nanotubes (CNT) as a promising novel class of electronic material has led to significant progress in the understanding of CNT physics including ballistic and non-ballistic electron transport characteristics. In a nanotube, low bias transport can be nearly ballistic across distances of several hundred nanometers. Non-ballistic CNT transistors have been considered, and extended circuit-level models which can capture both ballistic and non-ballistic electron transport phenomenon, including elastic, phonon scattering, strain and tunneling effects, have been developed.

The purpose of this paper is to establish a comparative analysis of the transport characteristics of ballistic and non-ballistic carbon nanotubes. The simulation is carried out using MATLAB and the main focus is on the changes in the I-V characteristic curves of elastic scattering effect, bandgap strain effect, tunneling effect and the overall combined effect, varying the parameters such as gate oxide thickness, temperature, dielectric constant, and chirality. The obtained results were then compared to their respective ballistic results. We verified our work by further comparison of our findings with other established academic papers published under the same category.

Table of Contents

	Pages
Certificate of Approval	2
Candidate Declaration	3
Acknowledgement	4
Abstract	5
Table of Contents	6
List of Tables	10
List of Figures	11
Chapter One	
Introduction	14
1.1 Overview	14
1.2 Objectives of the Research	15
1.3 Scope of the Research	16
1.4 Outline of the Research Report	17
Chapter Two	
Silicon MOSFET, Carbon Nanotube and CNTFET	18
2.1 Review of the Silicon MOSFET	18
2.2.1 Scaling of the Silicon MOSFET	19
2.2.2 Limitations of Scaling	20
2.2.2.1 Short Channel Effect	20
2.2.2.2 Oxide Thickness	23
2.2.2.3 Tunneling Effect	23
2.2.2.4 Threshold Voltage	24
2.2.2.5 Contact Resistance	25
2.2.2.6 Power Consumption and Heat Dissipation	26

2.2.2.7 Theoretical Limitations 26
2.2.2.8 Design Limitations 26
2.2 Carbon Nanotube (CNT) 27
2.2.1 Physical Structure of CNT 28
2.3 Carbon Nanotube Field Effect Transistor 32
2.3.1 Back-gate CNTFET 33
2.3.2 Top-gate CNTFET 33
2.3.3 Electrodes dependent CNTFET 34
2.3.4 Schottky Barrier CNTFET 35
2.3.5 Partially gated CNTFET 36
2.3.6 Doped source or drain CNTFET 36
2.3.7 MOSFET-like CNTFET 37
2.3.8 Vertical CNTFET 38
2.4 Introduction to Carbon Nanotube Behavior 38
2.4.1 Metallic Carbon Nanotubes 39
2.4.2 Semiconducting Carbon Nanotubes 40
2.5 Ballistic Transport 42
2.5.1 Resonant Scattering Centers and Resonant Tunneling 44
2.5.2 Current Carrying Capacity, Current Saturation 44
2.6 Non-Ballistic Properties Analysis 46
2.6.1 Mobile Charge Density and Self-Consistent Voltage 47
2.6.2 Current Model and Spline-based Approximation of Charge density 50
2.7 Non-Ballistic Transport Effects 51
2.7.1 Elastic Scattering 52
2.7.2 Bandgap Tuning with Strain 54
2.7.3 Tunneling Effect 54
2.7.4 Phonon Scattering 56
2.8 Summary 58

Chapter 3
Results and Analysis of Non-Ballistic CNTFET Characteristics Using MATLAB 59

Simulation
3.1 The Model 59
3.2 Results and Analysis 62
3.2.1 Change of Electron Concentration at the Top of the Barrier 62
3.2.1.1 Effect of Temperature 62
3.2.1.2 Effect of Chirality 63
3.2.2 Effect of Gate Oxide Thickness 65
3.2.2.1 Elastic Scattering Effect 65
3.2.2.2 Bandgap Strain Effect 67
3.2.2.3 Tunneling Effect 68
3.2.2.4 Combined Non-Ballistic Effect 69
3.2.3 Effect of Temperature 70
3.2.3.1 Elastic Scattering Effect 71
3.2.3.2 Bandgap Strain Effect 72
3.2.3.3 Tunneling Effect 73
3.2.3.4 Combined Non-Ballistic Effect 74
3.2.4 Effect of Dielectric Constant 75
3.2.4.1 Elastic Scattering Effect 76
3.2.4.2 Bandgap Strain Effect 77
3.2.4.3 Tunneling Effect 78
3.2.4.4 Combined Non-Ballistic Effect 79
3.2.5 Effect of Chirality 80
3.2.5.1 Elastic Scattering Effect 81
3.2.5.2 Bandgap Strain Effect 84
3.2.5.3 Tunneling Effect 86
3.2.5.4 Combined Non-Ballistic Effect 88
3.2.6 Variation of I-V Characteristics with respect to Gate Voltage Vg 91
3.2.7 Change in Tunnel Control Parameter with Parameters 96
3.2.7.1 Change with Channel Length 96
3.2.7.2 Change with Temperature 97
3.2.7.3 Change with Chiral Index n 98

3.2.7.4 Change with Chiral Index m 98
3.2.8 Summary 99

Chapter Four
Conclusion and Future Research 100
4.1 Conclusion 100
4.2 Prospected Future Research 101

References 103
Appendix A (MATLAB Code) 113
Appendix B (Mathematical Derivation) 152

List of Tables

	Pages
1 Silicon MOSFET Roadmap	22
2 Physical Properties Comparison of Carbon Nanotube	31
3 Some properties of Carbon Nanotube	31
4 Comparison of Back-gate and Top-gate CNTFET	34
5 Table of Parameters	60

List of Figures

	Pages
1 Structure of MOSFET	19
2 Silicon ICs' sizes in different times	20
3 Short Channel Transistor Leakage Current Mechanisms	21
4 Potential Barrier between two Transistors	24
5 Single Wall Carbon Nanotube	28
6 Multiple Wall Carbon Nanotube	28
7 Graphene Sheet	29
8 3D model of SWCNT	30
9 CNTFET	34
10 Different types of CNTFET	35
11 MOSFET-like CNTFET	37
12 V-CNTFET	38
13 Bandstructure of Carbon Nanotube	39
14 Schematics of MOSFET and CNTFET	41
15 Ballistic Transport	42
16 Current Saturation in CNT	44
17 Structure layout of Top-gate CNT	47
18 Equivalent Circuit for CNTFET	50
19 Fermi Level Profile	53
20 Energy Band diagram	55
21 Flowchart of used simulation	61
22 Change rate of Electron Concentration at the top of barrier with Temperature	62
23 Change rate of Electron Concentration at the top of barrier with Chirality n	64
24 Change rate of Electron Concentration at the top of barrier with Chirality m	65
25 Effect of Gate Oxide Thickness considering Elastic Scattering effect	66
26 Effect of Gate Oxide Thickness considering Bandgap Strain effect	67
27 Effect of Gate Oxide Thickness considering Tunneling effect	68
28 Effect of Gate Oxide Thickness considering Combined Non-Ballistic effect	69
29 Effect of Gate Oxide Thickness considering Ballistic transport	70
30 Effect of Temperature considering Elastic Scattering effect	71

31 Effect of Temperature considering Bandgap Strain effect 72
32 Effect of Temperature considering Tunneling effect 73
33 Effect of Temperature considering Combined Non-Ballistic effect 74
34 Effect of Temperature considering Ballistic transport 75
35 Effect of Dielectric Constant considering Elastic Scattering effect 76
36 Effect of Dielectric Constant considering Bandgap Strain effect 77
37 Effect of Dielectric Constant considering Tunneling effect 78
38 Effect of Dielectric Constant considering Combined Non-Ballistic effect 79
39 Effect of Dielectric Constant considering Ballistic transport 80
40 Effect of Chiral index n considering Elastic Scattering effect 82
41 Effect of Chiral index m considering Elastic Scattering effect 83
42 Effect of Chiral index n considering Bandgap Strain effect 84

43 Effect of Chiral index m considering Bandgap Strain effect 85

44 Effect of Chiral index n considering Tunneling effect 86

45 Effect of Chiral index m considering Tunneling effect 87

46 Effect of Chiral index n considering Combined Non-Ballistic effect 88

47 Effect of Chiral index m considering Combined Non-Ballistic effect 89

48 Effect of Chiral index n considering Ballistic transport 90

49 Effect of Chiral index m considering Ballistic transport 91

50 Change in I-V characteristics with Vg considering Elastic Scattering effect 91

51 Change in I-V characteristics with Vg considering Bandgap Strain effect 92

52 Change in I-V characteristics with Vg considering Tunneling effect 92

53 Change in I-V characteristics with Vg considering Combined Non-Ballistic effect 93

54 Comparison of results with Rahman *et al.* 93

55 Non-Ballistic Effects observed by Kazmierski *et al.* 94

56 Non-Ballistic Effects observed in this work 95

57 Ballistic vs. Non-Ballistic Comparison 96

58 Change in Tunnel Control Parameter with Channel Length 97

59 Change in Tunnel Control Parameter with Temperature 97

60 Change in Tunnel Control Parameter with Chiral index n 98

61 Change in Tunnel Control Parameter with Chiral index m 98

Chapter 1

Introduction

The intention of this paper is to institute a comparative analysis of the transport characteristics of ballistic and non-ballistic carbon nanotubes by generating its corresponding I-V curves in MATLAB and observing the changes of these curves under the elastic scattering effect, bandgap strain effect, tunneling effect and overall combined effect when other varying parameters such as gate oxide thickness, temperature, dielectric constant, and chirality come into play. This chapter presents a background on the research, objectives, and our scope of study. It also provides a brief summary of our total thesis work.

1.1 Overview:

Silicon has been the building block for the progress in the field of electronics until today. However, the scaling limits of silicon are nearing the end since many problems arise as devices become smaller in size. Problems like tunneling effect, short-channel effect etc. come into the picture and these effects hinder the device performance. It is therefore vital that silicon be replaced by other materials which will take device advancement to a whole new level. Chemical synthesis, self-assembly, and template self-assembly promise the precise fabrication of device structures or even the entire functional entity. New materials with superior electronic, optical, and mechanical properties emerge as a result of the ability to manipulate matter on a nanoscale. Now it is achievable to consider new nanoelectronic systems based on new devices with completely new system architecture, for example: nanotubes, nanowires. Therefore, research on finding new molecular-scale devices with better electrical capabilities to allow device scaling to continue to the atomic level is a major issue in engineering today.

Significant progress has been achieved since the discovery of carbon nanotubes (CNTs) by Iijima in 1991, for both understanding the elementary properties and exploring potential engineering applications. The possible application for nanoelectronic devices has been broadly investigated since the demonstration of the first carbon nanotube transistors (CNTFETs). Due to its excellent electrical properties, carbon nanotubes are attractive for nanoelectronic applications.

Low bias transport can be nearly ballistic across a distance of about several hundred nanometers in nanotube. The conduction and valence bands are symmetric, which is beneficial for complementary applications. The band structure is direct, which enables optical emission, and finally, CNTs are highly resistant to electro migration. Noteworthy efforts have been dedicated to comprehend how a carbon nanotube transistor operates and to improve the transistor performance. Most of the up to date CNTFETs operate like non-conventional Schottky barrier transistors [1], [2], which results in quite different device and scaling behaviors from the MOSFET-like transistors [3], [4]. In the near future it is hoped that transistor exceeding the performance of the traditional Silicon MOSFETs can be achieved.

In this work, simulations are developed to explain how differently ballistic and non-ballistic CNTFETs behave. In order to exploit the infinite possibilities there is with carbon nanotubes, understanding their basic physics is extremely essential. This research therefore deals with the
I-V characteristics of ballistic and non ballistic carbon nanotubes and this has increased our depth of knowledge regarding the fundamental physics that governs their behavior in other devices.

1.2 Objectives of the Research:

Due to the limitations imposed by the silicon-based transistors, researchers have been motivated to explore and discover other alternative technology like carbon nanotubes for better functioning of the current devices. Carbon nanotubes are a potential material for future nanoelectronics, both as interconnects and as critical elements for field-effect transistors because of their low dimensionality and outstanding electronic properties. At the present time, ballistic carbon nanotube field-effect transistor (CNTFET) is treated as one of the nanoelectronic devices that have immense prospective to be treated as a switching device for future. We plan to explore the possibilities that lie within non-ballistic CNTFETs. The core objectives of the research work to summarize are:

- Understand the operation and limitation of Silicon MOSFETs.
- Identify with the fundamental physics of carbon nanotubes and their electrical properties.
- Scrutinize the carbon nanotube device model.

- Understand the physical and theoretical differences between silicon field effect transistor (MOSFET) and carbon nanotube field effect transistor (CNTFET).
- Get familiar with the device characteristics, fundamental equations, and mathematical models of CNTFET.
- Understand the differences between ballistic and non-ballistic theories, characteristics, and equations.
- Using MATLAB model simulation investigate the I-V characteristics of both ballistic and non-ballistics CNTFETs by varying different parameters and comparing our results with those of other established thesis groups working under the same topic category.

By examining the objective stated above, we can deduce an overall CNTFET characterization of ballistic and non-ballistic electron transport which is important for other device simulations.

1.3 Scope of the Research:

This research paper is confined to the following scope of work as there was a lack of expertise and resources on this field:

- Using CNTFETTOY in MATLAB to generate the I-V curves non-ballistic carbon nanotubes.
- Simulating the transfer characteristic of non-ballistic CNTFETs taking into account some of the major non-ideal effects like elastic scattering, band gap tuning with strain and tunneling effects altering different parameters (like gate oxide thickness, chirality (leads to diameter), temperature and dielectric constant) and calculating the respective data.
- Comparing the obtained results from the simulation with those of other research groups' data and observe the deviation in the data.
- Comparison between ballistic and non-ballistic CNTFETs.

1.4 Outline of the research report:

This thesis is divided into four chapters:

Chapter 1 deals with the background, scopes of the research and objectives of our work.

Chapter 2 consists of an elaborate discussion of the Silicon MOSFETs and its limitations due to scaling. Then we provided a detailed background explanation on carbon nanotubes and the working principles of carbon nanotubes field effect transistors. Next we gave a comprehensive discussion of ballistic and non-ballistic CNTFETs where all the aspects of these two types have been noted down explicitly.

Chapter 3 contains the results and analysis of our main work where we generated the I-V curves for both ballistic and non-ballistic CNTFETs. Non-ballistic curves have been obtained by incorporating the non-ideal effects such as elastic scattering, band gap tuning with strain and tunneling effect and at the same time varying parameters such as temperature, gate oxide thickness, dielectric constant and chirality. We also generated the tunneling parameter 'F' in MATLAB and further investigated the changes in F by altering the parameters mentioned above.

Chapter 4 concludes our whole research and discusses about our future prospects and feasible research in carbon nanotubes and CNTFETs.

Chapter 2

Silicon MOSFET, Carbon nanotube and CNTFET

2.1 Review of the Silicon MOSFET:

In 1930, Lilienfeld [8] patented the basic concept of the field effect transistor (FET). After thirty years in 1959, the concept was finally materialized in Si-SiO_2 by Kahng and Atalla [5], [6]. The first MOSFET was invented in 1959 and since then it has completely changed the world of digital electronics. MOSFETs have dominated all fronts of digital applications especially modern computers; because it offers many advantages to the user. MOSFETs are relatively small in size and this contributes to the fact that they can be packed in large numbers on a single integrated circuit. It is also very reliable and offers low consumption of power. The progress up to now is well described by "Moore's law." Gordon Moore predicted in 1965 that for each new generation of memory chip and microprocessor unit on the market, the device size would reduce by 33 percent, the chip size would increase by 50 percent, and the number of components on a chip would quadruple every three years. So far this trend has shown no signs of stopping [11].

Several properties of silicon have made these developments in microelectronics possible. Silicon can be grown in single crystals that are more than 1 m long and 30 cm across. The purity of the crystal and the number of electrically active defects can be controlled. The number of atomic crystal defects in sub-micrometresized MOSFETs is now limited to individual centers that act as traps for electrons. Such traps may be identified, individually characterized, and counted, so that single-electron transistors are possible. The reason behind Silicon being the semiconductor of choice for MOSFET, is its native oxide. Silicon dioxide (SiO_2) is an almost perfect insulating material with a resistivity in excess of 1016 Vcm. The insulating films of SiO_2 grown on silicon are smooth and coherent with no holes, in a thickness ranges down to single atomic layers [11].

The metal–oxide–semiconductor field-effect transistor (MOSFET) is a transistor used for amplifying or switching electronic signals. Although the MOSFET is a four-terminal device with source (S), gate (G), drain (D), and body (B) terminals; [66] the body (or substrate) of the

MOSFET often is connected to the source terminal, making it a three-terminal device like other field-effect transistors. The gate terminal is a metal electrode that controls the current flow from source to drain [69]. The gate voltage needs to be higher than the threshold voltage in order for the current to flow in MOSFET. The source terminal is usually grounded and the drain voltage applied is relatively very small. As the gate voltage rises above the threshold voltage; an inversion layer or channel is created. This causes electrons to flow from source to drain terminal and as a result of which the current flows from drain to source terminal. There is no current flow to gate terminal since there is an oxide barrier which acts as an insulator. Figure 2.1 shows the structure of MOSFET.

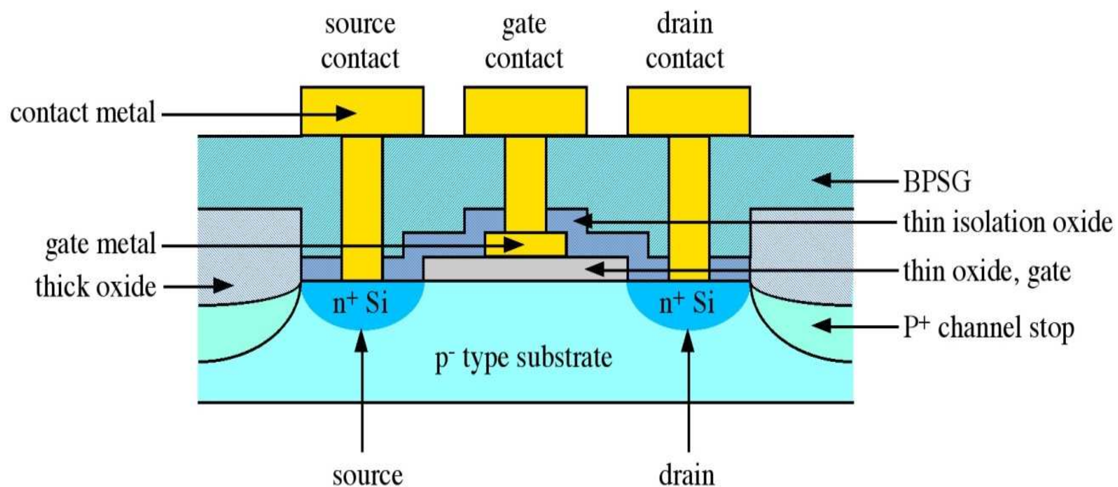

Figure 2.1: Structure of MOSFET [Source-internet image]

2.1.1 Scaling of the Silicon MOSFET:

Scaling is a process which involves reducing the size of MOSFET and at the same time improving its performance. The first method was introduced in 1974 in which by reducing the MOSFET dimension, the device density, switching speed and energy was also improved. Each new generation has approximately doubled logic circuit density and increased performance by about 40% while the memory capacity has increased by four times. In ideal scaling, as the dimension and the operating voltage is reduced by a factor of 0.7, the area density doubles, switching delay decreases by a factor of 0.7 and the switching energy is halved. The switching speed can be estimated when the gate capacitance, operating voltage, and drive current are

known. Switching energy is reduced as a result of the lower total combination parasitic capacitance due to smaller device size and lower operating voltage. Reduction of switching energy is very important since the overall circuit power is very crucial especially if the system is used for a long period continuously [69].

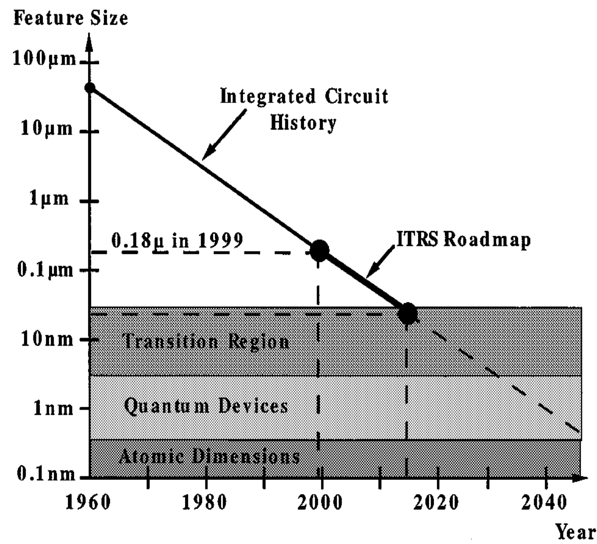

Figure 2.2: Feature size versus time in silicon ICs [67]

2.1.2 Limitations of Scaling:

There have been many articles and papers on the current situation and future prospects for Si-MOSFETs; many different scaling limits for MOSFETs have also been discussed and proposed [6]. There are a number of factors which needs to be taken under consideration with continued MOSFET scaling that present challenges for the future and, ultimately, fundamental limits. There are quite a few problems which arise as the MOSFET size reaches nanometer scale and ultimately limits the performance of the MOSFET itself. These problems are crucial and must be taken under consideration if the MOSFET is to survive in the near future.

2.1.2.1 Short Channel Effect:

The first factor to be considered is the short channel effect. The short channel effect introduces several leakage currents in MOSFET which are discussed below and shown in the figure- 2.3[7].

- Reverse bias p-n junction current occurs due to the minority carriers, diffusion near the depletion region and also due to the generation of electron-hole pairs.
- Weak reverse current occurs when gate voltage is lower than threshold voltage.
- DIBL current is present when source's potential barrier is reduced as a result of the drain's depletion region interacting with the source. The existence of DIBL lowers the threshold voltage.
- Gate-Induced Drain Lowering (GIDL) current occurs in high electric field between gate and drain, and it also occurs along the channel width between gate and drain.
- Another leakage current mechanism, punchthrough, occurs when the drain and source depletion regions touch deep in the channel.
- Narrow-width current arises when the channel length is reduced to less than 0.5μm.
- Gate-oxide tunneling current occurs when the oxide layer is made very thin and also causes gate leakage current tunneling through oxide bands.
- Hot-carrier injection occurs when hot carriers is injected into the oxide.

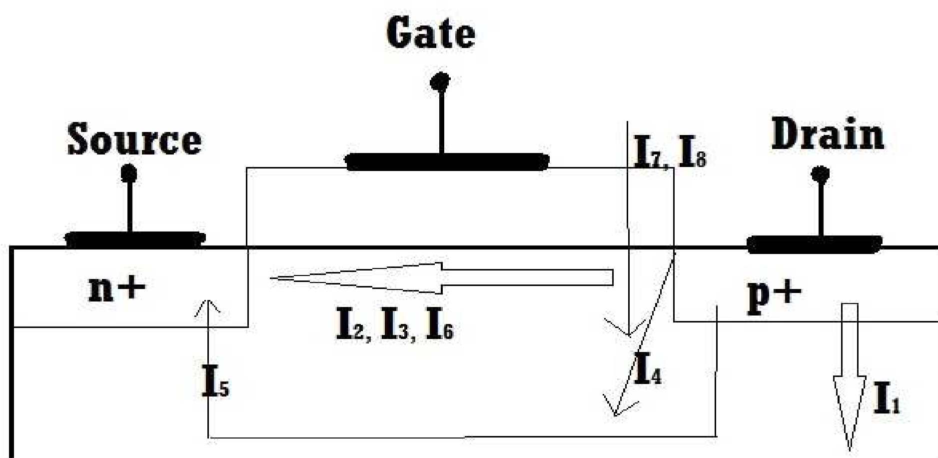

Figure 2.3: Short-channel-transistor leakage current mechanisms: reverse-bias p-n junction leakage (I_1), weak inversion (I_2), drain-induced barrier lowering (I_3), gate-induced drain leakage (I_4), punch-through (I_5), narrow-width effect (I_6), gate oxide tunneling (I_7), and hot-carrier injection (I_8).

Table 2.1: schematically illustrates the MOSFET used in today's silicon chips. The basic fabrication process steps to manufacture such a device have been broadly described. The basic structure will continue to evolve to allow continued performance improvements, but fundamental changes are unlikely until 2015 [67].

Year of 1st DRAM Shipment	1997	1999	2002	2005	2008	2011	2014
Minimum Feature Size	250 nm	180 nm	130 nm	100 nm	70 nm	50 nm	35 nm
Isolated Gate Length	-	100 nm	70 nm	50 nm	35 nm	25 nm	18 nm
DRAM Bits/Chip	256M	1G	(3G)	8G	(24G)	64G	(192G)
DRAM Chip Size (mm^2)	280	400	460	530	630	710	860
Equivalent Physical Gate Oxide Thickness (nm)	3-5	1.9-2.5	1.5-1.9	**1.0-1.5**	**0.8-1.2**	**0.6-0.8**	**0.5-0.6**
Dielectric Constant of DRAM Capacitor		22	50	250	700	**1500**	**1500**
Max Gate Electrode Resistivity (μΩ cm)		60	43	33	**23**	**16**	**11**
Max Silicide/Si Contact Resistivity ρ_C (Ω cm^2)		$30x10^{-8}$	$17x10^{-8}$	**$10x10^{-8}$**	**$5x10^{-8}$**	**$2.5x10^{-8}$**	**$1.5x10^{-8}$**
S/D Extension Sheet Resistance (Ω/sq)		350-800	250-700	**200-625**	**150-525**	**120-450**	**100-400**
S/D Extension x_J (nm)	50-100	42-70	25-43	**20-33**	**16-26**	**11-19**	**8-13**
S/D Extension Lateral Abruptness (nm/decade)		14	8.5	6.5	**4.5**	**3.2**	**2.2**
Minimum Supply Voltage (volts)	1.8-2.5	1.5-1.8	1.2-1.5	0.9-1.2	0.6-0.9	0.5-0.6	0.5

2.1.2.2 Oxide Thickness:

The gate insulator in a MOSFET needs to be thin compared to the device channel length in order for the gate to exert dominant control over the channel potential. This avoids "short channel effects," which are largely the result of the drain electric field penetrating throughout the channel and influencing the channel potential at the source of the device [67].

Gate-oxide thickness causes two kinds of limitations. Firstly, the thin layer of oxide eventually increases leakage current. This effect is also related to quantum effect tunneling that dominates in MOSFET as the oxide thickness is reduced. The tunneling current due to thick oxide layer may look negligible in comparison with "on state" current. However, it has a major effect when the chip is in standby mode. Secondly, due to the oxide thickness there is a loss of inversion charge and also the transconductance as a result of inversion-layer quantization and polysilicon gate depletion effect [9].

The gate electrode itself also presents some significant challenges. Polysilicon has been used for more than 25 years as the gate electrode material. However, decreasing its resistivity, as shown in table-2.1, implies increasing the doping levels in the polysilicon, which minimizes the resistivity of the gate electrode. This aids in avoiding polysilicon depletion effects. However, this approach is limited by dopant solubility limits and by dopant out diffusion from the polythrough to the thin gate dielectric and into the silicon. This later problem is particularly acute with p-gates because boron diffuses rapidly through SiO_2. The likely solution is again new materials. But there are no known materials solutions that are known to work in manufacturing [67].

2.1.2.3 Tunneling Effect:

Under normal conditions, in an operating or computational system integrated transistors are separated sufficiently enough so that operation of one transistor does not in any way affect the operation of another transistor. This separation is made by inserting a material that acts as a barrier between two transistors. However, the barriers are also scaling down along with the MOSFETs. So there is a possibility of carriers from one MOSFET crossing over to another and distorting the performance. This effect increases exponentially as the barrier distance decreases.

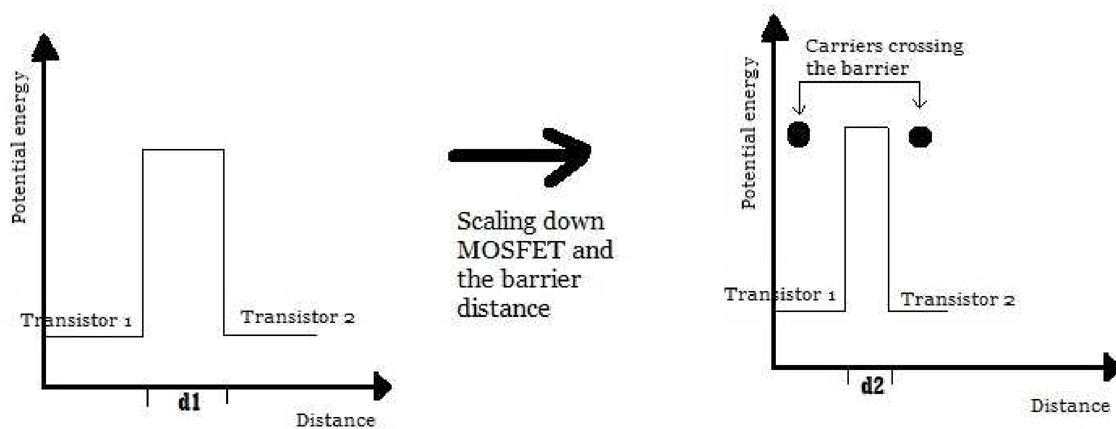

Figure 2.4: Potential barrier between two transistors.

2.1.2.4 Threshold Voltage Effect:

A notable limitation to MOSFET is that the threshold voltage is not proportionally decreasing with respect to transistor scaling. The threshold voltage is maintained at a constant level when the channel length is between 0.1µm-1µm and it deviates further when the channel length is below 0.1µm [69], [8]. If the transistor is scaled below 0.1µm, the threshold voltage current does not drop to zero immediately but it decreases exponentially, and is inversely proportional to the thermal energy [69]. There are some thermally distributed electrons at source terminal that have enough energy to overcome the barrier potential regulated by gate terminal. This behavior is independent of channel length and power supply. So, higher threshold voltage causes higher leakage current. Denoting leakage current as I_{off} gives:

$$I_{off} = I_o\ (-qV_t / mKT) \tag{1}$$

I_o = Extrapolated current per width at threshold voltage.

m= Dimensionless ideality factor

V_t= Threshold voltage.

Lower leakage current is essential for a transistor in order to reduce the power loss. However lower threshold voltage can reduce the leakage current. So, designing a transistor should be in

such a way that its threshold voltage remains very low. According to Sanudin, the leakage current is reduced ten times for every 0.1V reduction of threshold voltage [69].

2.1.2.5 Contact Resistance:

Contacts are normally made by self-aligned silicides which are in contact with heavily doped silicon. This process provides an ohmic contact; which completely covers the area of the source/drain diffusions and this leads to the minimization or reduction of the contact resistance. Current flows in a distributed manner from the source/drain extension to the contact. The exact flow lines depend on the doping profile in the silicon and on the physical geometry. The contact resistance depends on the effective area of the contact. Current crowding on the leading edge of the contact can have a significant effect. In this structure, the contact resistance is given by:

$$R_{contact}=\sqrt{(\rho_c R_{SD})}/(W \times \coth(L_c/L_t)) \approx \rho_c/(WL_c) \quad (2)$$

Where,

ρ_c= specific contact resistivity of the silicide/semiconductor contact (Ω cm^{-2});

R_{sd}= sheet resistance of the source/drain diffusion (Ω/square);

W= contact width;

L_c= contact length.

L_t= $\sqrt{(\rho_c/R_{sd})}$ is called the transfer length and is the average distance that carriers travel in the diffusion before entering the contact.

For typical values of ρ_c, R_{sd} and L_t, is greater than the physical contact length L_c, which results in the approximation shown above. In this case, the current flows into the entire length of the contact and current crowding effects are minimal. Thus, the contact resistance varies inversely with the contact area if ρ_c is constant.

The silicide formation process itself often consumes silicon since the metal component (Ti, for example) is usually deposited and then reacted to form the silicide. This has several important consequences. Firstly, some of the volume of the heavily doped source/drain regions is lost or

consumed by the silicide formation. The portion of the source/drain region which is “lost” is the top portion, which is normally the most heavily doped and, therefore, the most conductive. This increases the sheet resistance of the remaining diffusion in which current can flow to the contact and, therefore, increases the effective contact resistance [67].

2.1.2.6 Power Consumption and Heat Dissipation:

Power consumption and heat dissipation are two obstacles for further advancement in Si-based transistors. For the past three years power density has grown with the rate of 0.7 for every generation [10]. Large amount of power consumption boosts up the heat generation, increasing the possibility of transistors interfering with each other. As MOSFETs are scaling down these small transistors consume small amount of power but IC chips are becoming denser because of large number of transistors on each of them. So it uses large amount of power to drive all transistors and therefore generates more heat. Heat dissipation and power consumption are two major limitations. Therefore, there is the need of searching for alternative media, which can overcome the limitations of conventional Si based MOSFET. And this is where the idea of using carbon nanotubes instead of Silicon is conceived.

2.1.2.7 Theoretical Limitations:

Thermal limit and quanta limit are a major problem. Amount of energy needed to write a bit must be greater than the thermal function in order to avoid the bit error to occur. This is called the thermal limit. Currently CMOS needs 10-13 J to write a bit and the trend is to reduce it, in order for the power dissipation to reduce [69].

Quantum limit is associated with E/f where, E is the thermal energy and f is the frequency. Currently CMOS is operating higher than the quantum limit and if the scale reaches to 100nm then it is expected the limit is approached as E is decreased and f is increased.

2.1.2.8 Design Limitations:

Due to the scaling down of MOSFETs lead to the discovery of its design limitations. MOSFET does not work effectively when it is scaled to only around 30nm. The limit is because of the fact of Zener breakdown at source/substrate junction [69]. Leakage at gate also starts to surface and it becomes very difficult to have control over the channel.

2.2 Carbon Nanotube (CNT):

Carbon nanotubes were first discovered in 1991 by S. Iijima, also known as the father of carbon nanotubes. Carbon nanotubes are formed when graphene layers are folded into a seamless cylindrical form. Carbon nanotubes are quasi-one-dimensional and look like long thin cylinders of carbon with diameters of about 1nm. There are two types of carbon nanotubes depending on their composure. When the nanotube is composed of several shells of carbon, it is known as multi wall nanotube (MWNT). On the other hand, when only one shell composes the nanotube it is known as single wall nanotube (SWNT). Carbon nanotubes display a versatile range of properties which has attracted researchers all around the globe. They are good conductors of heat, electricity and also display semiconducting characteristics. Carbon nanotubes can be metallic, semiconducting or insulating depending on their rolling helicity most importantly and then on its length and diameter. What is fascinating is the fact that carbon nanotubes require no doping. The bandgap can also be varied just by changing the diameter of the nanotube. Bandgap decreases with increasing diameter. Carbon nanotubes have a very high current density; individual tubes are able to carry currents at a higher density than most metals and other semiconductors. Carbon nanotubes are also inert and this makes them very compatible with other materials. Currently, SWNTs are synthesized by one of three different techniques: pulsed laser vaporization, arc discharge growth, or chemical vapor deposition (CVD) on supported or gas phase catalysts. Transition metals in their nanoscales are used as catalysts in the processes. Pure carbon nanotubes are highly polarizable, smooth-sided structures, they tend to aggregate into parallel bundles that are held together by non-covalent interactions of approximately 0.5 eV per nanometer. These substantial Van der Waals cohesive forces are sufficient to bundle the nanotubes in raw samples. This makes it really difficult to separate and collect individual tubes for further research or device construction. One of the greatest needs in nanotube research and commercialization is the development of effective methods for obtaining samples of SWNTs with uniform electronic character. Ultrasonic agitation in surfactant solution followed by ultracentrifugation can often give stable suspensions that are rich in individual nanotubes. However, physical separation of the semiconducting and metallic species is much more difficult particularly for larger batch sizes. Obtaining SWNT samples of specific (n, m) types is the most difficult goal and it is one of the major factors disrupting the commercialization of carbon nanotubes [3].

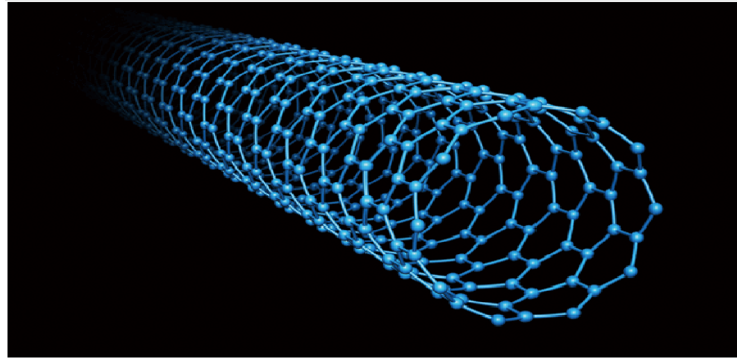

Figure 2.5: Single Wall Nanotube (SWNT) [Internet image]

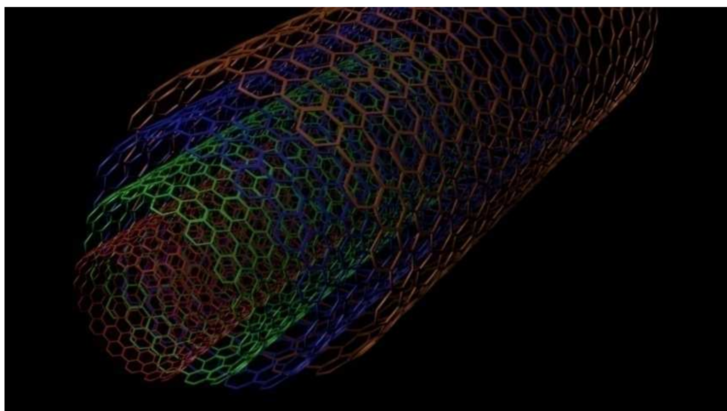

Figure 2.6: Multi Wall Nanotube (MWNT) [Internet Image]

2.2.1 Physical Structure and Properties of CNT:

SWNTs are more pliable than their multi-walled counterparts and can be twisted, flattened and bent into small circles or around sharp bends without breaking [13]. They can be conducting, like metal or semiconducting, which means that the flow of current through them can be controlled by varying an electrical field. Whereas, multi-walled carbon nanotubes are basically like Russian dolls made out of SWNTs concentric cylindrical graphitic tubes. In these more complex structures, the different SWNTs that form the MWNT may have quite different structures (length and chirality). MWNTs are typically 100 times longer than they are wide and have outer diameters mostly in the tens of nanometers. Although it is easier to produce significant quantities of MWNTs than SWNTs, their structures are less well understood than single-wall nanotubes because of their greater complexity and variety. Multitudes of exotic shapes and arrangements,

often with imaginative names such as bamboo-trunks, sea urchins, necklaces, or coils, have also been observed under different processing conditions. The variety of forms may be interesting but also has a negative side—MWNTs always (so far) have more defects than SWNTs and these diminish their desirable properties [13].

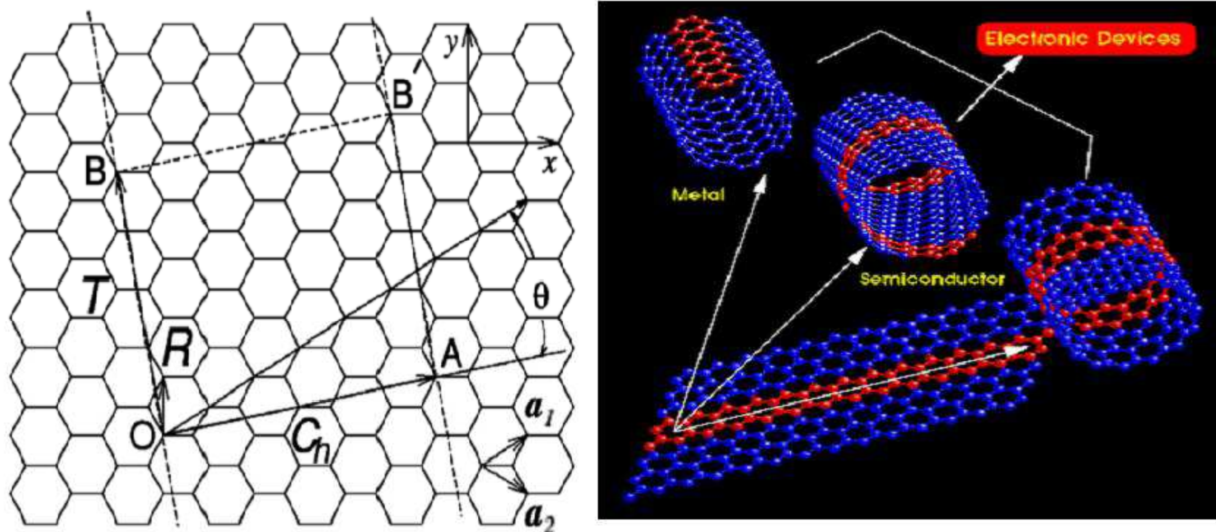

Figure 2.7: Graphene sheet [14] and rolling graphene sheet to create carbon nanotube [18].

A SWNT is described as a graphene sheet rolled up into a cylindrical shape with axial symmetry, exhibiting a spiral conformation called chirality [13]. Graphene has a hexagonal structure, and rolling up the graphene sheet in different directions and diameter would yield the nanotubes with different symmetries, which induces different electronic structures. Since electronic properties of SWNTs depend on their structures, it is very important to find a way to specify the geometric structure of a SWNT. As shown in Fig. 2.7, we can roll up the graphene sheet alone vector OA, which is perpendicular to the nanotube axis in the direction of OB. Here, we can see that O, A, B and B' are four crystallographically equivalent sites. By rolling up the paper plane and making OB overlap with AB', we get a seamless single-walled tubular structure. Then it would be straightforward to define the vectors $C_h = OA$ as chiral vector and $T = OB$ as translational vector. If we use a1 and a2 as the base vectors of graphene 2-D crystal lattice, we can have the chiral vector as [14]:

$$C_h = na_1 + ma_2 = (n, m) \qquad (3)$$

$$0 \leq m \leq n.$$

The way the graphene sheet wraps can be represented by a pair of indices (n, m) called the chiral vector. The relationship between n and m defines three categories of CNTs. Arm chair (n = m) and chiral angle equal to 30°); zigzag (n = 0 or m = 0 and chiral angle equal to 0°); and chiral (other values of *n* and *m* and chiral angles lie between 0 and 30°) [12]–[17]. These are shown in figure 2.8

$$C_h = a/\sqrt{n^2 + m^2 + n} \qquad (4)$$

Where, a = 2.49 Å.

$$d_t(\text{diameter}) = C_h / \pi \qquad (5)$$

$$\theta(\text{chiral angle}) = \text{arc cos } (2n+m/2\sqrt{n^2 + m^2 + nm}) \qquad (6)$$

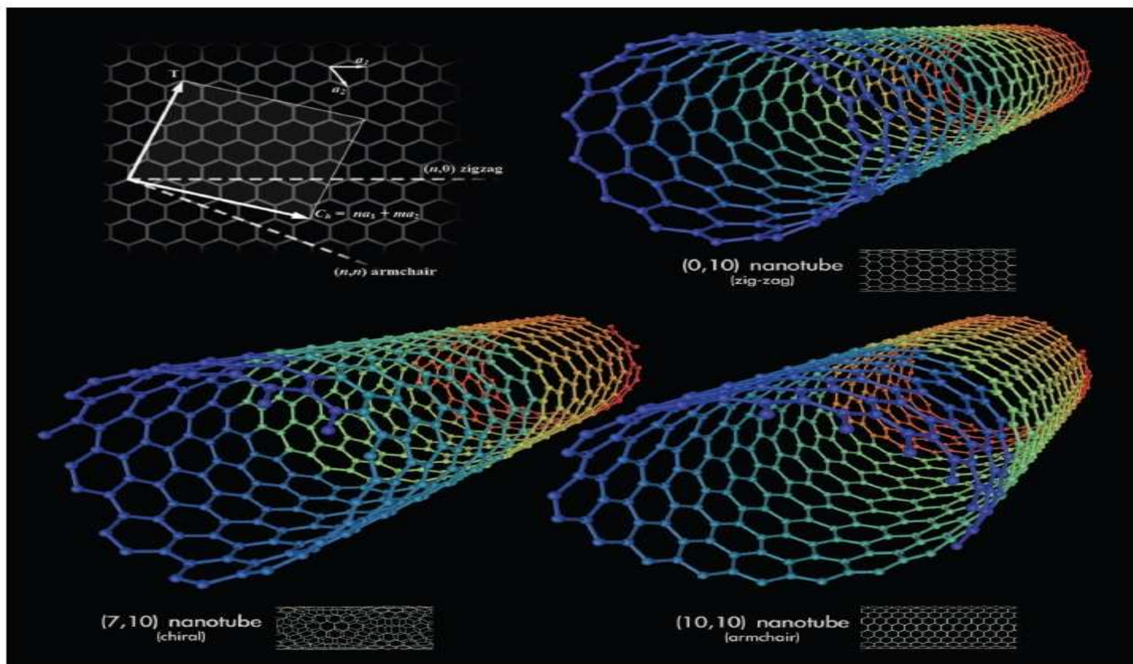

Figure 2.8: 3D model of the three types of single walled carbon nanotubes [12].

Material	Young's Modulus(Gpa)	Tensile Strength (Gpa)	Density (g/cm3)
Single wall nanotube	1054	150	
Multi wall nanotube	1200	150	2.6
Steel	208	0.4	7.8
Epoxy	3.5	0.005	1.25
Wood	16	0.008	0.6

Table 2.2: Young's modulus, Tensile strength, and density of carbon nanotubes compared with other materials [12]

Average diameter of SWNTs	1.2-1.4 nm
Distance from opposite carbon atoms (Line 1)	2.830 Å
Analogous carbon atom separation (Line 2)	2.456 Å
Parallel carbon bond separation (Line 3)	2.450 Å
Carbon bond length (Line 4)	1.420 Å
C-C tight bonding overlap energy	~ 2.50 eV
Group symmetry (10, 10)	C5V
Interlayer spacing:	
(n, n) Armchair	3.380 Å
(n, 0) Zigzag	3.410 Å
(2n, n) Chiral	3.390 Å
Optical properties	
Fundamental gap:	
For (n, m); n-m is divisible by 3 [Metallic]	0 eV
For (n, m); n-m is divisible by 3 [Semiconducting]	~0.5 eV
Maximum current density	1013 A/m2
Thermal transport	
Thermal conductivity (room temperature)	~ 2000 W/m K
Phonon mean free path	~ 100 nm
Relaxation time	~ 10-11 s
Elastic behavior	
Young's modulus (SWNT)	~ 1 TPa

Table 2.3: Some parameters for carbon nanotubes [12]

2.3 Carbon Nanotube Field Effect Transistor (CNTFET):

CNTFETs were first brought to life in the year of 1998 by Dekker et al. Basic principle of operation of CNFET is the same as MOSFET. Electrons are supplied by source and drain collects the electrons. In other words, current flows from drain to source terminal. Gate terminal controls current intensity in the transistor channel and the transistor is in off state if no gate voltage is applied. The main reason that is attracting research on CNTFET is their high channel mobility. A carbon nanotube field-effect transistor (CNTFET) refers to a field-effect transistor that utilizes a single carbon nanotube or an array of carbon nanotubes as the channel material instead of bulk silicon in the traditional MOSFET structure [20]. The most important reason behind choosing carbon nanotube FETs is their 1 dimensional characteristic; because of which the carriers are confined on the cylinder of the tube and this gives rise to a strong quantization of electron and hole states and charge transport in 1-D sub band becomes feasible even at room temperature. The reduced phase space for scattering events reduces the probability of back scattering and manifests itself in a high conductivity of carbon nanotubes [21]. Secondly, all chemical bonds of the C atoms are satisfied and there is no need for chemical passivation of dangling bonds as in silicon. This implies that CNT electronics would not be bound to use silicon oxide as an insulator. High dielectric constant and crystalline insulators can be used, allowing, among other things, the fabrication of three dimensional structures. The strong covalent bonding gives the CNTs high mechanical and thermal stability and resistance to electromigration. Their key dimension, their diameter, is controlled by chemistry, not conventional fabrication. In principle, both active devices (transistors) and interconnects can be made out of semiconducting and metallic nanotubes, respectively [22]. By using a single-wall CNT as the channel between two electrodes, like the source and drain contacts of a FET, a coaxial CNTFET can be fabricated. Coaxial devices, due to their geometry allows for better electrostatics since the gate contact wraps all around the channel (CNT) and has a very good control on the transportation of carriers. The type of Metal-CNT contacts plays crucial role in the output characteristics of the transistor. Heavily doped semiconductors because of the ability to form Ohmic contacts can be used as ideal electrodes but they suffer from high parasitic resistance [19]. Carbon nanotube FETs can be classified into two categories:

- Back gate CNTFET

- Top gate CNTFET

2.3.1 Back Gate CNTFET:

CNTFET was first demonstrated in 1998 by Tans et al. [24] to show a technologically exploitable switching behavior and this work marked the inception of CNFET research progress. In this structure a single SWNT was the bridge between two noble metal electrodes on an oxidized silicon wafer. The silicon oxide substrate can be used as the gate oxide and adding a metal contact on the back makes the semiconducting CNT gateable. Here the SWCNT plays the role of channel and the metal electrodes act as source and drain. The heavily doped silicon wafer itself behaves as the back gate. These CNTFETs behaved as p-type FETs with an I (on) / I (off) ratio~10^5 [23]. This suffers from some of the limitations like high parasitic contact resistance (≥1Mohm), low drive currents (a few nanoamperes), and low transconductance, gm ≈ 1nS. To reduce these limitations the next generation CNTFET developed which is known as top gate CNTFET.

2.3.2 Top Gate CNTFET:

To get better performance Wind et al. proposed the first top gate CNTFET in 2003 [23]. In the first step, single-walled carbon nanotubes are solution deposited onto a silicon oxide substrate. Then by using either atomic force microscope or scanning electron microscope the individual nanotubes are located. After which, source and drain contacts are defined and then patterned using high resolution electron beam lithography. High temperature annealing reduces the contact resistance and also increases union between the contacts and CNT. A thin top-gate dielectric is then deposited on top of the nanotube, either via evaporation or atomic layer deposition. Finally, the top gate contact is deposited on the gate dielectric. Arrays of top-gated CNTFETs can be fabricated on the same Silicon wafer, since the gate contacts are electrically isolated from each other, unlike in the back-gated case. Also, due to the thinness of the gate dielectric, a larger electric field can be generated with respect to the nanotube using a lower gate voltage. These advantages mean top-gated devices are generally favored over back-gated CNTFETs, regardless of their more complex fabrication process [25].

The advantages of top gated CNTFET over back gated CNTFET is summarized in table- 2.4 [23].

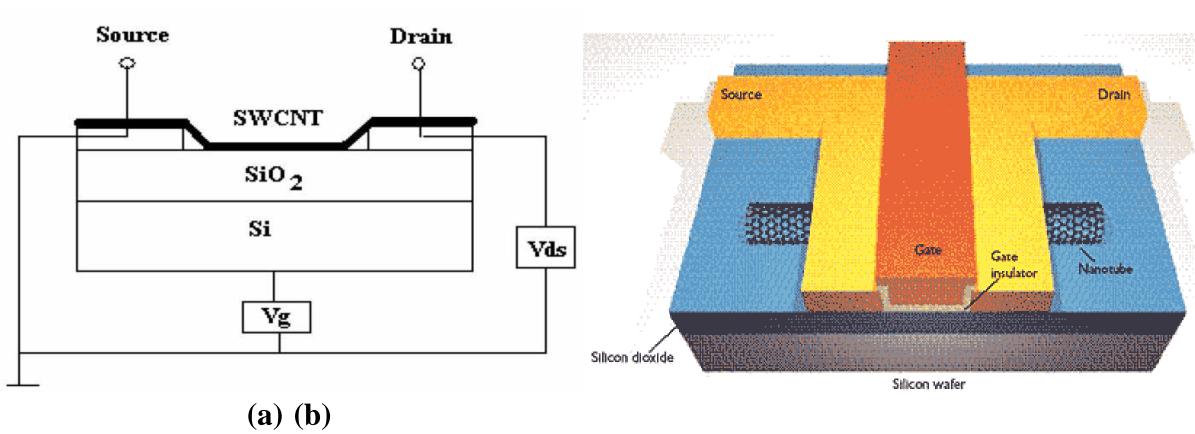

(a) (b)

Figure 2.9: (a) Back gate CNTFET [23], **(b)** Top gate CNTFET [Source- Internet image]

Table 2.4: Comparison between Back gate CNTFET and Top gate CNTFET [23]

Parameters	Back gate CNTFET	Top gate CNTFET
Threshold voltage	-12V	-0.5V
Drain current	Of the order of nanoampere	Of the order of microampere
Transconductance	1nS	3.3μS
I(on)/I(off)	10^5	10^6

2.3.3 Electrodes dependent CNTFET:

Based on the type of electrodes used CNTFET is classified into three categories.

(a) Schottky-barrier (SB) CNTFET

(b) Partially gated (PG) CNTFET and

(c) Doped-S/D CNTFET. [26], [27]

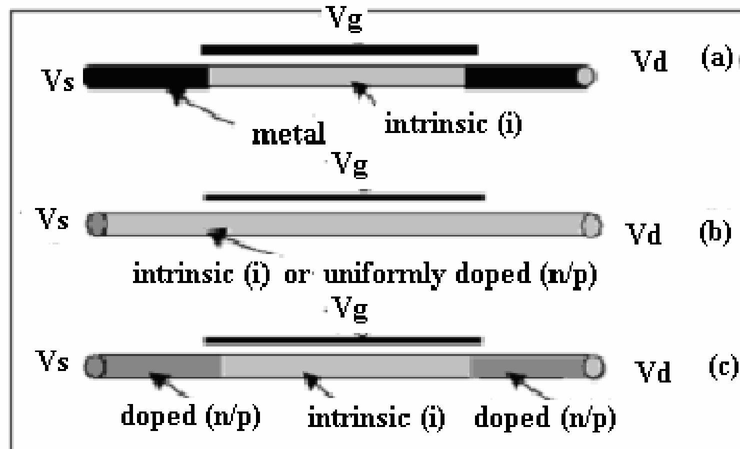

Figure 2.10: Different types of CNTFET: **(a)**Schottky-barrier (SB) CNTFET, **(b)** partially gated (PG) CNTFET **(c)** doped-S/D CNTFET [23].

2.3.4 Schottky-barrier (SB) CNTFET:

As shown in figure 2.10, an intrinsic CNT is used in the channel region. This is connected to metal Source/Drain and forms Schottky barriers at the junctions. Carbon nanotube transistors operate as alternative Schottky barrier transistors in which transistor action occurs above all by varying the contact resistance rather than the channel conductance. The barrier height is determined by the filling of metal-induced gap states. These states become available in the energy gap of semiconductor due to boundary formed with the metal. The SB is controlled by the difference of the local work functions of the metal and the carbon nanotube [70]. SB-CNFET works on the principle of direct tunneling through the Schottky barrier at the source-channel junction. The barrier width is controlled by the gate voltage and hence the transconductance of the device depends on the gate voltage. At low gate bias, large barrier limits the current in the channel. As gate bias is increased, it reduces the barrier width, which increases quantum mechanical tunneling through the barrier, and therefore increases current flow in transistor channel. In SB-CNFET, the transistor action occurs by modulating the transmission coefficient of the device [70], [72]. These types of FET require careful alignment of the Schottky barrier and gate electrode which leads to manufacturing challenge. Another concern regarding is that this

type of transistor suffers from metal-induced-gap states which limit minimum channel length and thus increases source to drain tunneling [28], [29], [30].

2.3.5 Partially gated (PG) CNTFET:

PG-CNTFET, shown in Figure-2.10 is a depletion mode CNTFET in which the nanotube is uniformly doped or uniformly intrinsic with ohmic contacts at their ends. PGCNTFETs can be of n-type or p-type. In these devices the gate locally depletes the carriers in the nanotube and turns off the p-type (n-type) device with an efficiently positive (negative) threshold voltage that approaches the theoretical limit for room-temperature operation [25], [26].

2.3.6 Doped- source or drain (S/D) CNTFET:

Doped-S/D CNTFETs presented in Figure-2.10 are composed of three regions. The region below the gate is intrinsic in nature and the two ungated regions are doped with either p-type or n-type. The ON-current is limited by the amount of charges that can be induced in the channel by the gate and not by the doping in the source. They operate in a pure p-type or n-type enhancement-mode or in a depletion-mode, based on the principle of barrier height modulation when applying a gate potential. Out of these three, doped S/D CNTFETs are promising because they show unipolar characteristics unlike SB-CNTFETs. The absence of SB reduces the OFF leakage current. In ON-state, the source-to-channel junction has a significantly higher ON current. Depending on the doping profile doped source or drain CNTFETs can again be classified into two groups.

- Conventional CNTFET (C-CNTFET): This comprises of CNTFETs with p/i/p or n/i/n doping method where the source or drain are doped with either p-type or n-type material.

- Tunneling CNTFET (T-CNTFET): CNTFETs with n/i/p doping scheme (source and drain are oppositely doped) comes under this group [23]. All the CNTFETs discussed till are of planer structure

2.3.7 MOSFET-like CNTFET:

The structure of this device is slightly dissimilar to SB-CNTFET since it uses heavily doped terminals instead of metal. This was formed in order to overcome problems in SB-CNTFET and operates like MOSFET. Unlike SB-CNTFET, source and drain terminals are heavily doped like MOSFET and hence it is called as MOSFET-like CNTFET. This device, as shown in Figure 2.11, operates on the principle of modulation the barrier height by gate voltage application. The drain current is controlled by number of charge that is induced in the channel by gate terminal.

This type of transistor has several advantages over SB-CNTFET. This device is able to suppress ambipolar conduction in SB-CNTFET. It also provides longer channel length limit because the density of metal-induced-gap-states is significantly reduced. Parasitic capacitance between gate and source terminal is greatly reduced and thus allows faster operation of the transistor. Faster operation can be achieved since length between gate and source/drain terminals can be separated by the length of source to drain, which reduces parasitic capacitance and transistor delay metric. It operates like SB-CNTFET with negative Schottky barrier height during on-state condition and thus it delivers higher on-current than SB-CNTFET. Previous work has shown that this type of device gives higher on-current compared to SB-CNTFET and therefore it can justify the upper limit of CNTFET performance. Based on the device performance, it is obvious that this device can be used to investigate the ballistic transport in CNTFET [88], [90].

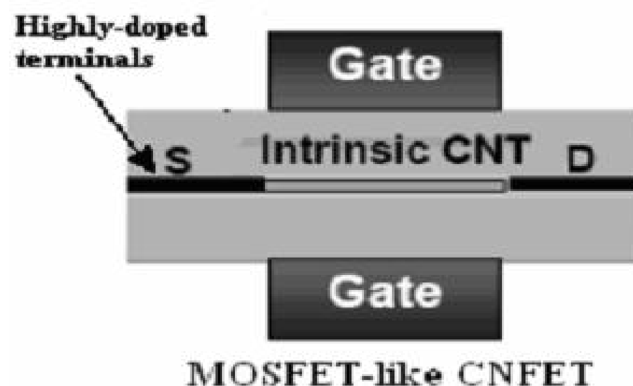

Figure 2.11: MOSFET-like CNTFET [89]

2.3.8 Vertical CNTFET (V-CNTFET):

The most recent development is the V-CNTFET conceptualized in 2004, by Choi *et al*. They are made of a SWCNT with a coaxial gate. The improvement of V-CNTFET is that vertical growth in CNT is easier and aligned than horizontal growth. The SWCNT is either grown from a bottom source contact in a hole defined through separating dielectric layers and a ring gate, or the dielectric and gate are built on the nanotube after growth. A top drain contact completes the device. The advantages of these devices include the self-adjusted alignment of the nanotube and gate, optimum gate control, and the minimal footprint required. The vertical CNFET allows higher packing densities that can be achieved since source and drain areas can be arranged on top of each other [71]. On the other hand, real 3-D structures can be made possible because the active devices are no longer bound to the surface of mono-crystalline silicon wafer. Figure 2.12 shows the concept of the device.

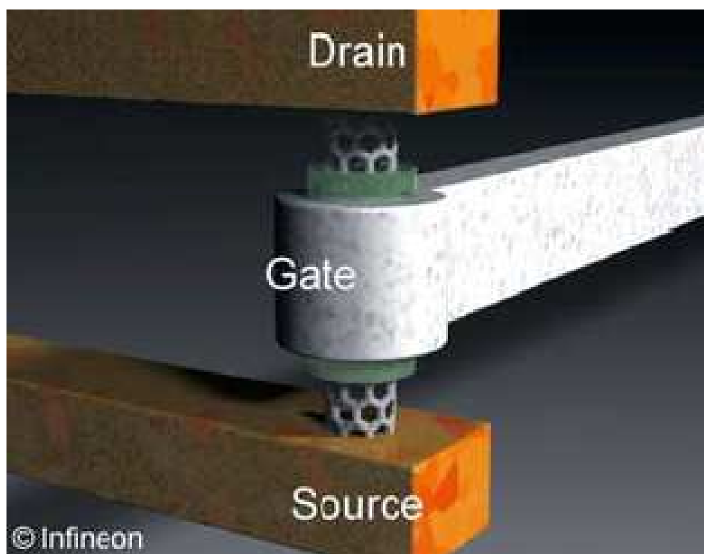

Figure 2.12: Vertical carbon nanotube field-effect transistor (V-CNTFET) concept [Source-Internet image]

2.4 Introduction to Carbon Nanotube behavior:

Carbon Nanotubes can either be metallic or semiconducting. It depends precisely to the way they are wrapped which is shown in figure 2.13(a) and 2.13(b). In metallic carbon nanotubes, low-bias transport is ballistic over a length range that can reach micrometers. This phenomenon is

possible because acoustic phonon scattering is extraordinarily weak in this one-dimensional conductor, and only few defects that act as resonant scattering centers are present. Nevertheless, at high bias the electrons strongly excite optical phonons, which lead to energy dissipation in the tube and current saturation.

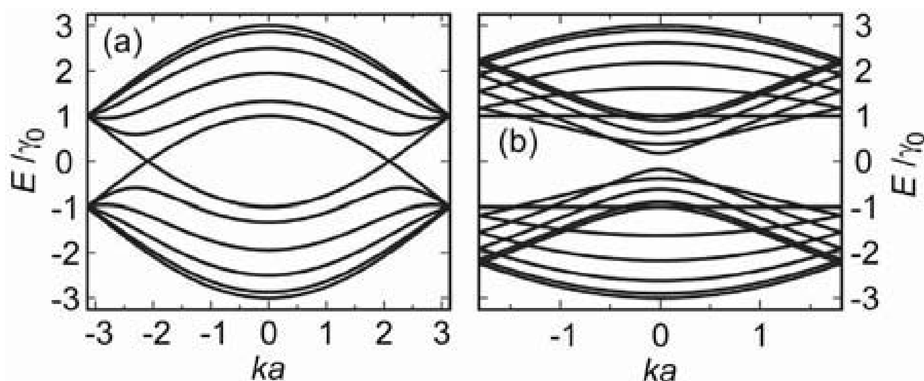

Figure 2.13: Band structure of **(a)** a metallic (5, 5) CNT and **(b)** a semiconducting (10, 0) nanotube

The wave vector k is plotted in units of 1/a, where a = 0.249 nm is the graphene lattice constant. The low-energy band structure of metallic CNTs consists of two pairs of crossing bands right at the Fermi level. In semiconducting nanotubes a band gap on the order of 1 eV opens up at k = 0.

2.4.1 Metallic carbon nanotubes:

The fact that metallic behavior is observed in CNT tubes of 1 nm is significant. Most one-dimensional materials show Peierls instability that leads to the opening of an energy gap and thus the material undergoes a metal-to-insulator transition [73]. The Peierls instability occurs because the total energy of a one-dimensional chain can often be reduced by doubling the unit cell. For say, two neighboring atoms move closer together, while the next pair goes farther apart. A good thing about carbon nanotubes is that it does not show Peierls instability even at the lowest measured temperatures. This is due to the massive strength of the carbon–carbon bond in graphitic materials and the cylindrical rather than chain-like array of carbon atoms.

It can be demonstrated via tight-binding calculations that all chiral (m = n) carbon nanotubes are truly metallic, shown in Figure 2.14(a). Their band structure consists of two sets of linear bands

that cross right at the Fermi level. Among the chiral tubes, about 2/3 are semiconducting [(m – n) mod3 = 1 or 2], while the remainder [(m – n) mod3 = 0] exhibit a small band gap on the order of a few meV. Small-gap semiconductors are included in this section on metallic carbon nanotubes because at room temperature (k_BT= 26 meV) the effects related to the small band gaps are not very prominent.

The low-energy band structure of a metallic carbon nanotube comprises of four linear bands that intersects at two distinct K-points (Figure 2.13a). [76] In each K-point, one band carries the forward-moving electrons, while the other carries the backward moving electrons. Moreover each band is spin degenerate so that in a metallic carbon nanotube, there are a total of four forward-moving conduction channels. The theoretical limit for the conductance through an individual single-wall carbon nanotube is as a result $G = 4 \times e^2/h$, which is equivalent to a resistance of 6.5 kΩ. Experimentally, the low bias resistance of carbon nanotube was found to be in a range between 10kΩ to a several 100KΩ [78], which suggest the transmission coefficients to be in the range between 75 and 1%. Palladium contacts on chemical vapor deposition (CVD)-grown tubes were found to make the best contacts with almost unity transmission [79], [80].

2.4.2 Semiconducting carbon nanotubes:

Semiconducting carbon nanotubes have band gap that has an inverse relationship with tube diameter and its band gap is E_g = 0.84eV/d nm. Conduction through semiconducting tubes is dependent on the exact position of the Fermi level with respect to the band edges, and chemical or electrostatic doping can be used to change the conductivity significantly. Highly doped CNT which has for example, the Fermi level is deep into the valence band, they conduct almost as good as metallic tubes, as they also have four available channels: two quasi-degenerate valence bands, each of which can carry spin up or down. The low-bias conduction is ballistic over 100-nm-length scales, and the maximal achievable currents with optimized contacts are about 20 µA, similar to what is observed in metallic tubes. The strong dependence of the conductivity on the electrochemical potential in the carbon nanotube can be utilized to make a device that acts like a switch. It conducts current acting as a metal when the potential on a capacitively coupled gate moves the Fermi level into the valence — or conduction — band and acts as an insulator when the Fermi level is in the band gap. This kind of device is well known in the semiconductor

industry and called a field effect transistor (FET). The silicon metal-oxide semiconductor field effect transistor (MOSFET)[88], [89] is of massive technological importance. Fundamentally all modern computer chips are based on MOS logic. Fortunately, this device is the most straightforward to replicate with a semiconducting carbon nanotube in the channel as the inversion layer instead of silicon (Figure 2.14) [90], [91].

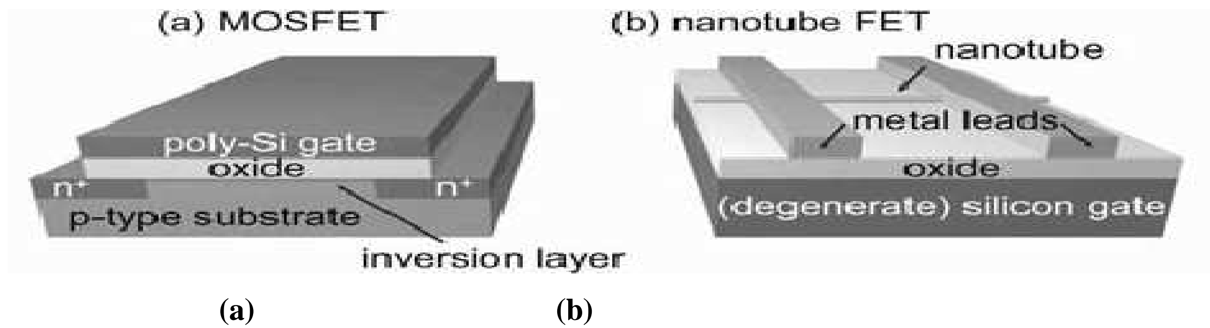

(a) **(b)**

Figure 2.14: Schematic of **(a)** a silicon MOSFET and **(b)** a carbon nanotube FET. The channel in the case of the MOSFET is an *n*-type inversion layer in the *p*-type substrate close to the interface with the silicon oxide. In the nanotube FET, the inversion layer is replaced by the carbon nanotube

Similar to metallic carbon nanotubes but unlike silicon, semiconducting carbon nanotubes are ballistic at low bias and length scales below hundreds of nanometers [95]. Reducing the channel length below this value will not result in any change in resistance. Due to time-of-flight considerations, however, the device will still switch faster. On the other hand, CNTFETs with very long channel lengths, above 10 μm behave more like bulk-switching MOSFETs .This means that they show current saturation, because the channel resistance gets larger than the resistance of the contact barriers. In these nanotubes transport is dominated by drift of carriers in a charge gradient that builds up inside the nanotube channel. It then makes sense to use a geometric capacitance to model conduction [92] and extract material quantities such as mobility. Low-bias mobility ofμ~ 100,000 cm^2/Vs, that exceeds any other known semiconductor mobility was found by Fuhrer et al [93], [94].The eventual breakdown of saturation in and the crossings in the various *I-V* curves are due to the opening of an electron channel for conduction in addition to the predominant hole conduction. Due to the cylindrical geometry of carbon nanotubes, the gate capacitance in long-channel devices scales with the inverse logarithm of the oxide thickness *Cox* ~ 1/ln(*tox*), rather than inversely, as in the planar MOSFET geometry.

2.5 Ballistic transport:

The resistance of short one-dimensional conductors depends neither on their composition nor on the length of the conductor. It depends only a function on the number of available conduction channels for example, one-dimensional subbands, and the transmission at the contacts [74]. For a single conduction channel with 100% transparent contacts, the quantum resistance is a universal constant, which is given by,

$$R_Q = h/e^2 \sim 26K\Omega \qquad (7)$$

This activity is known as the ballistic conduction, since electrons travel with zero scattering effect between two terminals (Figure 2.15a).Although there is no scattering in the conduction channel or any back scattering of the electrons leaving the conductor, the resistance of a ballistic conductor is not zero.

The quantum resistance, also known as contact resistance, develops from the difference between the large number of modes in the macroscopic contacts that the current is distributed over and few electronic modes (1Dsubbands) available in the one-dimensional conductor [75].

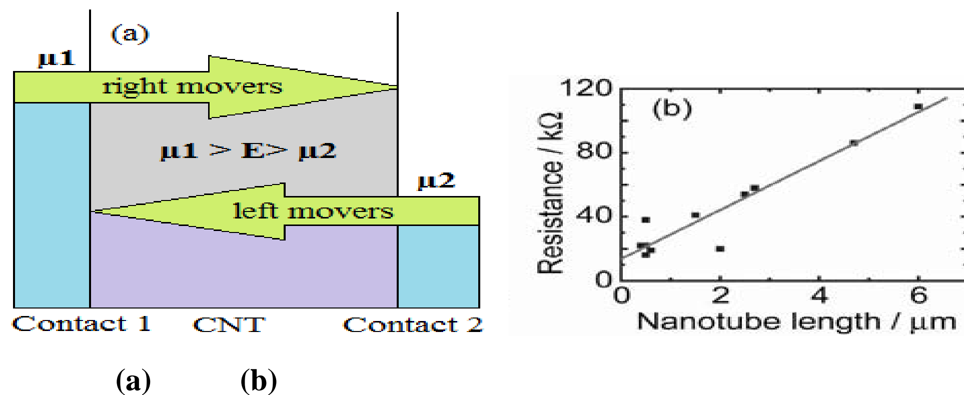

(a) **(b)**

Figure 2.15: **(a)** Design of ballistic transport in a short metallic carbon nanotube where energy is plotted as a function of position. Carriers with energy up to μ_1 are injected into the CNT from contact 1 and those from energies up to μ_2 are injected from contact 2. There is no scattering in the CNT, and carries injected with certain energy E traverse the tube without any energy loss. **(b)** Low-bias resistance vs. nanotube length for 11 metallic chemical vapor deposition (CVD) tubes after 10. The solid line is a linear fit to the data with slope 15 kΩ/μm and y-axis intercept of 14 kΩ. The y-axis intercept suggests transmission coefficients of t_i= 0.5 and the slope an electron mean free path of 0.4 μm.

Equation 7 can be generalized to include M conduction channels and contacts with non unity transmission coefficient t_i:

$$G = e^2/h.\sum_{i=1}^{M} t_i(E_f) \quad (8)$$

Where,

- $G = 1/R_Q$ is the quantum conductance,
- E_F is the Fermi energy.

Equation 8 is called the Landauer formula for a ballistic conductor. For 100% transparent contacts the conductance is simply $M \times e^2/h$. The quantum resistance (or contact resistance) goes to zero when there is a large number of conduction channels, such as a macroscopic system.

The Landauer formula can be further generalized to include scattering in the conduction channel by introducing an electron mean-free path (momentum scattering length l_m):

$$R = R_Q \cdot L/l_m \quad (9)$$

Here,

- L is the length of the conductor,
- $R_Q = 1/G$ is the quantum resistance.

In this form, the classical length dependence of the resistance is recovered

The mean free path can be extracted from Equation 9 by using the length dependence of the low-bias resistance. In carbon nanotubes, this has been done by contacting a tube with one lithographic contact as well as one movable scanned probe [81] and also by comparing the resistances of many similarly fabricated two-terminal devices with varying nanotube lengths (Figure 2.15b) [82] Both methods give a mean-free path on the order of lm ~ 500 nm at room temperature. This is much larger than the typical values of about 10 nm in most other materials. Due to the perfect lattice with no localized surface states and the large momentum transfer required for backscattering, the scattering is decreased or suppressed in carbon nanotubes. (Cumulative small-angle scattering that adds up to 180° is impossible in a one-dimensional system.).The two most significant sources of scattering in metallic carbon nanotubes in the low-bias regime are called ‘acoustic phonon scattering’ [83], [84] and ‘elastic scattering from defects’ [85]. Acoustic phonon scattering typically dominates at room temperature, whilst on the

contrary, elastic scattering from defects rules at low temperatures, where the mean-free path can be several micrometers long.

2.5.1 Resonant scattering centers and resonant tunneling:

Metallic carbon nanotubes are not expected to respond to varying gate voltages due to their constant density of states. The gate voltage is applied at the silicon substrate which is separated from the CNT by a SiO_2 layer. In some devices a moderate amount of gate voltage dependency of current (up to a factor of 2) is found. A process called ‘Scanning gate microscopy’ (SGM) is used to show that these changes happens because of the localized scatterers in the CNT [85].

2.5.2 Current-carrying capacity, current saturation:

A single carbon nanotube can carry up to 25µA of current, which corresponds to an astonishingly high current density of 10^9 A/cm^2. A typical I-V characteristic for a metallic carbon nanotube is shown in Figure 2.16 [77] .At low bias (the ballistic region) the current is seen to be increasing linearly. But at high bias, it rolls over and saturates.

In the small figure inserted to the larger one, the data are plotted in a different way, explicitly, resistance R =V/I as a function of bias voltage.

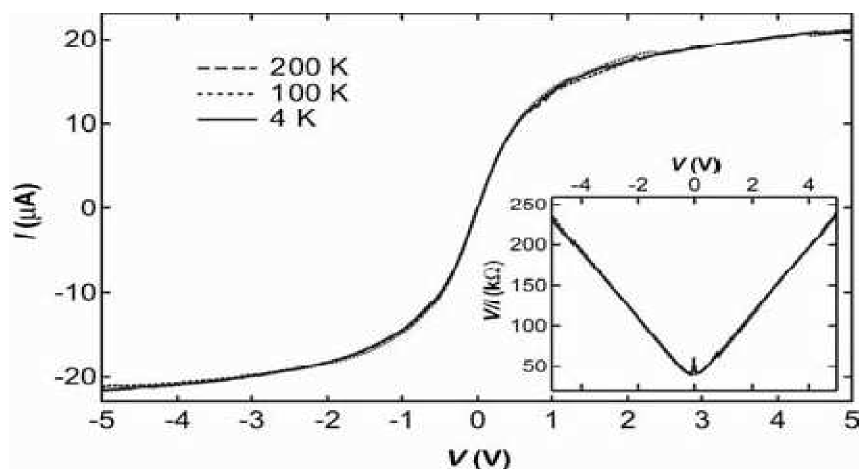

Figure 2.16: Current saturation in metallic carbon nanotube.
Main image: current voltage characteristics showing current saturation at high bias. Inset: resistance R = V/I vs. bias voltage [77]

Above a few 100 mV the resistance increases linearly with voltage. A simple model [77] where phonon excitation is included can explain the linear increase in resistance and also correctly predict the value for the saturation current to be about 25 μA.

Two important assumptions made in the model are:

I. There is an energy threshold $eV= \hbar\Omega$ below which the excitation of phonons is impossible and the transmission is ballistic. (V is the bias voltage and$\hbar\Omega$ is the energy of the phonon.)

II. The electron excites the optical phonon immediately as it gains enough excess energy to do so. Unless the electron reaches the opposite contact, the process of acceleration in the applied electric field and optical phonon excitation is repeated.

The Landauer formula (Equation 9) and Matthiessen's rule is used to combine the scattering mechanisms,

$$R= \frac{h}{4e^2}\left(\frac{L}{l_m} + \frac{L}{l_\Omega}\right) \quad (10)$$

Where,

- L is the length of the carbon nanotube,
- l_m is the low-bias mean-free path that may include elastic defect scattering and acoustic phonon scattering,
- $l_\Omega = \hbar\Omega\ L/eV$, is the length it takes an electron in the applied electric field to gain the optical/zone boundary phonon energy $\hbar\Omega$.

The functional form of resistance, $R= R_0+ V/I_0$ of the experimental data yields the low-bias resistance $R_0 = \frac{h}{4e^2}\left(\frac{L}{l_m}\right)$and saturation current $I_0 = \frac{4e}{h}\hbar\Omega$. With L = 0.5μm and R_0 = 40KΩ the low-bias mean-free path for the device in Figure 2.15becomes lm ~ 100 nm. This value is a lower limit because of likely nonunity transmission at the contacts. More importantly, the saturation current of I_0 ~ 25 μA proposes a phonon energy of $\hbar\Omega$ ~ 0.16 eV, which is right in the approximate range for zone boundary or optical phonons in carbon nanotubes.

As long as the electron–phonon scattering length for optical/zone boundary phonons, lop, is much shorter than l_{Ω}, the second assumption made before is acceptable. On the other hand, experimentally observed divergence from the current saturation at 25 µA can be used to infer lop. This is very noteworthy because devices that are smaller than the electron–phonon scattering length will remain ballistic even at high bias. It is confirmed by two experiments
that the current does not saturate in short devices of ≤100 nm [81], [87] and instead it reaches values as high as 60 µA with no sign of saturation before breakdown. Javey et al used electron beam lithography to fabricate carbon nanotube devices with lengths down to 10 nm and derived optical/zone boundary phonon scattering lengths between 11 and 15 nm [87]. Park et al. used a mobile scanned probe as an electronic contact and obtained lop = 10 nm [81].

2.6 Non-Ballistic Properties Analysis:

Recent investigations of carbon nanotube transistors has shown its potential to play a very important role in future electronic systems as a descendant of the CMOS technology because they have excellent electrical properties including high electron mobility [31]. Studies were more focused on two terminal devices such as PN junctions and Schottky diodes before, but in case of applications transistors are the most feasible ones. Till now CNFETS have used channels lengths of hundreds of thousand nanometers and shows a large contact resistance between metal and nanotube. One possible way of them operating, which is still ambiguous, is that the gate field modulated the width of a barrier at the source contact, analogous to the Schottky barrier metal–oxide–semiconductor field-effect transistor commonly known as MOSFET [32]. Furthermore, other experiments with CNTFETs have demonstrated that these devices have large transconductances, indicating a great prospective for nanoelectronic circuits, but not so comprehensive about large scale nanoelectronics. The practicability of CNTFET electronics depends on the responses of the logic gates that are made up of multiple CNTFETs and used in larger circuits [33], [34].
CNTFETs exhibit the potential of becoming an attractive solution in addition to their silicon twins, chiefly due to their electrostatic properties such as ballistic or near ballistic transport of electrons and very low conduction threshold voltages which makes carbon nanotubes suitable for significantly very high speed and ultra low power circuit design [35], [36], [37]. The want for numerically efficient CNT transistor models suitable for implementation in circuit-level

simulators has been elevating since, especially in the light of the recently reported successful implementations of logic circuits built with CNTs. Breakthrough improvements to accurate spice compatible CNT transistor modeling have been proposed where not only ballistic but also a number of non-ballistic effects have been included [38], [39].

2.6.1 Mobile Charge Density and Self-Consistent Voltage:

Accurate calculations of the mobile charge require numerical integration of the densities of states over the number of allowed energy levels using the Fermi probability distribution. Moreover, the total drain current is affected not only by the non-equilibrium mobile charge in the nanotube but also by the charges present at terminal capacitances. That is why, an iterative approach using Newton-Raphson method is needed for the solution of an implicit non-linear algebraic equation [35], [40].

A non-equilibrium mobile charge is induced in the nanotube when an electric field is applied between the drain and the source of a CNT transistor demonstrated in Figure 2.17 [35], [41].

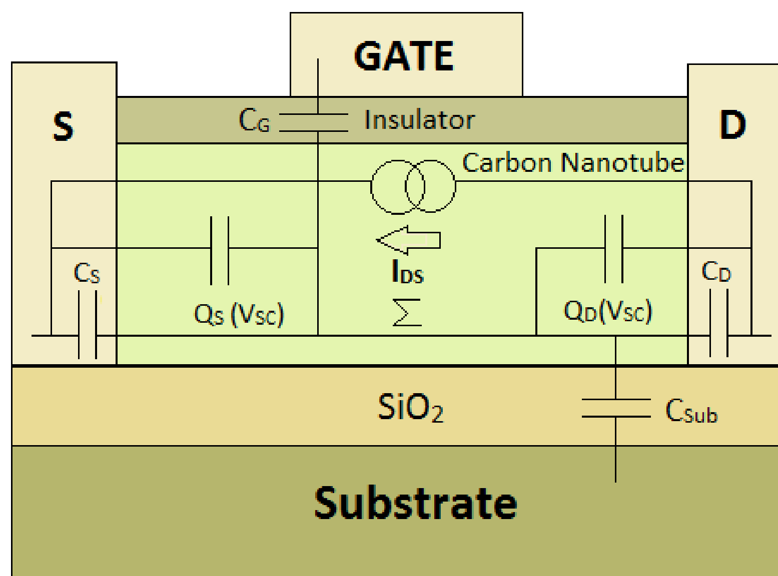

Figure 2.17: Structure layout of a top-gate CNT transistor showing components of the proposed equivalent circuit model with the virtual node Σ for V_{SC}.

$$\Delta Q = q\ (N_S + N_D - N_0) \quad (11)$$

Where,

- N_S is the density of positive velocity states filled by the source
- N_D is the density of negative velocity states filled by the drain
- N_0 is the equilibrium electron density.

Fermi-Dirac probability distribution is used to determine these densities by the following method:

$$N_S = \frac{1}{2}\int_{-\infty}^{+\infty} D(E) f(E - U_{SF}) dE \quad (12)$$

$$N_D = \frac{1}{2}\int_{-\infty}^{+\infty} D(E) f(E - U_{DF}) dE \quad (13)$$

$$N_0 = \frac{1}{2}\int_{-\infty}^{+\infty} D(E) f(E - U_F) dE \quad (14)$$

D (E), U_{SF} and U_{DF} are defined as,

$$D(E) = D_0 \frac{E}{\sqrt{E^2 - \left(E_g/2\right)^2}} \Theta\left(E - E_g/2\right) \quad (15)$$

$$U_{SF} = E_F - qV_{SC} \quad (16)$$

$$U_{DF} = E_F - qV_{SC} - qV_{DS} \quad (17)$$

Where,

- $D(E)$ is the density of states at the channel,
- $D_0 = 8/(3\pi V_{cc} a_{cc})$ is the constant density of states of a metallic nanotube,
- E_g is the band gap which can be calculated using $E_g = 2accVcc/d$ [12],
- a_{cc} is the carbon $\pi - \pi$ nearest-neighbor bond length ,
- V_{cc} is the energy of the tight bonding model.
- $\Theta(E - E_g/2) = 1$ when $E > Eg/2$ and $\Theta(E - E_g/2) = 0$ when $E \leq E_g/2$
- E_F is the Fermi level,
- f is the Fermi probability distribution,
- q is the electronic charge,
- E represents the energy levels per nanotube unit length,

- V_{SC} *is* the self-consistent voltage, a recently discovered concept [35] which exemplifies that the CNT energy band is affected by external terminal voltages.

The self-consistent voltage V_{SC} is without a doubt related to the device terminal voltages and charge sat terminal capacitances by the following non-linear algebraic equation [35], [43]:

$$V_{SC} = \frac{-Q_t + qN_S(V_{SC}) + qN_D(V_{SC}) - qN_0}{C_\Sigma} \tag{18}$$

The standard approach to the solution of Equation 18 of V_{sc} is to use the Newton-Raphson iterative method and in each iteration to evaluate the integrals in Equation 13 of N_D and Equation 14 of N_0 to obtain the state densities Equation 13 N_D and Equation 12 N_S.

$$Q_t = V_G C_G + V_D C_D + V_S C_S + V_{Sub} C_{Sub} \tag{19}$$

Where,

- Q_t represents the charge stored in terminal capacitances,
- C_G, C_D, C_S and C_{Sub} are the gate, drain, source and substrate capacitances respectively. C_{Sub} also implies that the body effects may be taken into account in further work.
- C_Σ is the total terminal capacitance given by,

$$C_\Sigma = C_G + C_D + C_S + C_{Sub} \tag{20}$$

$$C_{ox} = \frac{2\pi k_1 \varepsilon_0}{\ln\left((2t_{ox} + d)/d\right)} \tag{21}$$

$$C_{Sub} = \frac{2\pi k_2 \varepsilon_0}{\ln(4H_{Sub}/d)} \tag{22}$$

Where,

- d is the diameter of the carbon nanotube,
- H_{Sub} is the thickness of the SiO_2 layer on the substrate,
- t_{ox} is the thickness of the gate insulator and,
- k_1, k_2 are the relative permittivities of the gate and the substrate respectively [44].

The capacitances between terminals can be calculated as follows: [42].

$$C_G = C_{ox} \tag{23}$$

$$C_S = 0.097C_{ox} \tag{24}$$

$$C_D = 0.040C_{ox} \tag{25}$$

2.6.2 Circuit Model and Spline-Based Approximation of Charge Densities:

Equal parts of the equilibrium mobile charge density N_0 to the drain and source was apportioned in the earlier works [45]. This facilitates circuit implementation of the model because now the corresponding non-equilibrium mobile charge densities Q_S and Q_D can be modeled as non-linear circuit capacitances, dependent on the self-consistent voltage V_{SC}, and connected between a conceptual inner node, which represents the self-consistent potential, and CNT terminal nodes:

$$Q_S(V_{SC}) = q\left(N_S(V_{SC}) - \frac{1}{2}N_0\right) \tag{26}$$

$$Q_D(V_{SC}) = q\left(N_D(V_{SC}) - \frac{1}{2}N_0\right) \tag{27}$$

The resulting equivalent circuit is shown in Figure 2.18.

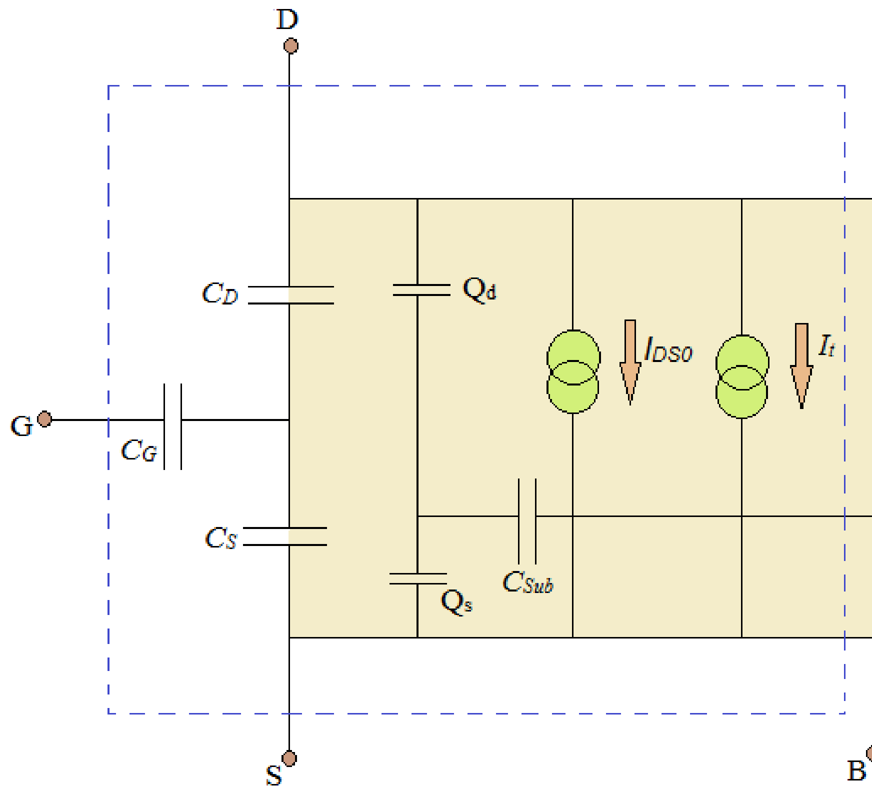

Figure 2.18: Equivalent circuit for the proposed CNT transistor model.

Where,

- Σ is the hypothetical inner node described above, which comprises all the CNT charges,

- I_t represents the tunneling current which is one of the non-ballistic effects,
- I_{DS} is the transport current determined by the self-consistent voltage V_{SC} if only the ballistic transport is considered. I_{DS} is equivalent to current I_{DSB} given by equation of I_{DS0}.Later we consider models of non-ballistic effects which allow a more accurate representation of the transport current I_{DS}.

According to the ballistic CNT ballistic transport theory [35], [42], the drain current caused by the transport of the non-equilibrium charge across the nanotube can be calculated using the Fermi-Dirac statistics as follows:

$$I_{DS_0} = \frac{2qkT}{\pi\hbar}\left[\mathcal{F}_0\left(\frac{U_{SF}}{kT}\right) - \mathcal{F}_0\left(\frac{U_{DF}}{kT}\right)\right] \tag{28}$$

Where,

- F_0represents the Fermi-Dirac integral of order 0,
- K is Boltzmann's constant,
- T is the temperature and,
- $\hbar$ is the reduced Planck's constant.

2.7 Non-Ballistic Transport Effects:

Further research of CNTFETs has produced some new theories in the energy domain which reveals that the insufficient system within a non-ideal nanotube indicates the existence of a general non-ballistic regime [46]. The transport type in carbon nanotubes if it I ballistic or non-ballistic basically depends on the energy region. Ballistic transport will take over if the length of the CNTFET is smaller than the carrier mean free path but larger than the Coulomb blockade length. To travel through a single defect Coulomb potential, the transmission coefficient can be calculated by [47],

$$T_{defect}\,(E) = G_{filled}\,(E)/G_{empty}\,(E) \tag{29}$$

Where, E is the energy of the hole in a nanotube. Therefore, the charging and discharging decides the maximum differential conductance through single transport channels, and E is directly determined by the terminal voltage V_{DS}.

For non-ballistic CNTFETs this transmission coefficient fluctuation could be caused by mobility fluctuation. Yet, under the effects of scattering, E is much smaller than qV_{DS}in this case. Studies

have also shown that a short mean free path may arise due to the mismatch of helicity between the adjacent shells [48]. Furthermore, non-ballistic transport can be caused by various other defects such as contamination, vacancies, contact to the substrate and absorbed molecules [48]. Four major non-ballistic affects are:

- Elastic Scattering
- Band gap tuning with strain
- Tunneling effect
- Phonon Scattering effect

.

2.7.1 Elastic scattering:

There are three typical scattering mechanisms in the channel region:

1) Acoustic phonon scattering (near elastic process [35])

2) Optical phonon scattering (inelastic process [34])

3) Elastic scattering.

The elastic-scattering rate and thus the mean free path (MFP) are assumed to be independent of the carrier energy. Although the elastic-scattering MFP of the intrinsic CNT can be longer than 1 μm [33], the fabricated CNTs often contain non-ideal scattering centers for example defects, which may decrease the MFP significantly and can cause additional potential drop along the channel region.

The elastic scattering mechanism in the CNT channel region affects the channel resistance and therefore makes a potential drop of the channel voltage. Assuming that,

$$l_{eff} \infty d \quad (30)$$

$$l_{eff} = d/(d_0)\lambda_{eff} \quad (31)$$

Where,

- l_{eff} is the mean free path which is proportional to the diameter of the nanotube [49], [50],
- d is the CNT diameter
- d_0 is the reference diameter with a value of 1.5nm,
- λ_{eff} is the elastic-scattering MFP[9], $\lambda_{eff} \approx 200nm$ [51]

- $T_{eff}= l_{eff}/ (L+l_{eff})$ is the transmission probability in the elastic-scattering channel region,
- L is the channel length,

Therefore the potential drop at the channel can hence be derived as [53],

$$V_{DSeff} = \frac{L}{L+(d/d_0)\lambda_{eff}} V_{DS} \tag{32}$$

$$V_{DS}= V_{ch,DS}+ V_{ch,el}, \tag{33}$$

$$V_{ch,DS}= I_{DS}.R_{ch,c}, \tag{34}$$

$$V_{ch,el}= I_{DS}.R_{ch,el} \tag{35}$$

$$R_{ch,el}= (1 - T_{eff}) / T_{eff} \cdot R_{ch,c} \tag{36}$$

The total potential drop (V_{DS}) across the channel region is a summation of the potential drop ($V_{ch,DS}$) due to the channel quantum resistance $R_{ch,c}$, and the potential drop ($V_{ch, el}$) over the channel resistance $R_{ch,el}$ due to the elastic scattering (Fig. 2.19).

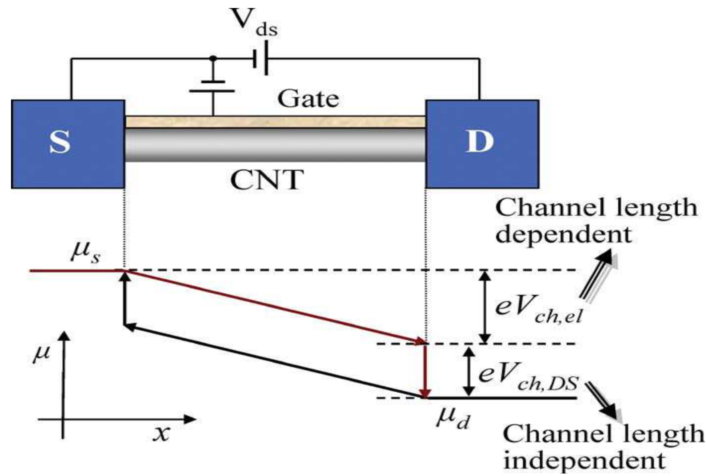

Figure 2.19: Fermi-level profile for 1-D device with series resistance (finite MFP along CNT). The Fermi-level profile is approximated as a linear function of the position along the channel. The contribution to the device current characteristics can be computed directly from the variable voltage V_{DSeff} due to the elastic scattering instead of the channel resistance, which simplifies the calculation efficiently [58].

2.7.2 Band gap tuning with strain:

It has been proved that the transport property of CNT can vary under strain [41]. Experiments have shown that the strain applied onto a nanotube can change the band gap and thus affect the transport characteristics. A shape distortion is formed by the strain which can be treated as a key factor when calculating the extra band gap caused by the effect.

$$E_{g\text{eff}} = E_g + \frac{dE_{g\text{strain}}}{d\chi}\chi \tag{37}$$

Where,

- E_{geff} is the effective band gap under strain,
- $dE_{gstrain}$ is the gap shift due to the strain,
- χ is definedas the distortion factor under strain. $\chi = 0.1$,

Studies have also shown that in presence of the strain, the rate of change of band gap $\frac{dE_{g\text{strain}}}{d\chi}$ is dependent on the chirality of the CNT. The rate of change of band gap is calculated using the following formula:

$$\frac{dE_{g\text{strain}}}{d\chi} = 3\sigma(1 + r_0)\text{sign}(2p + 1)\cos(3\phi) \tag{38}$$

In this equation,

- σ is the overlap integral of the tight-binding C-C model, with a value of circa $2.7eV$,
- $r_0 \approx 0.2$ is the Poisson's ratio,
- φ is the chiral angle of the nanotube, $\varphi=20^\circ$
- p comes from the CNT chirality and p=1. For a CNT with the chirality (m,n),$m-n=3l+p$, where l and p are both integrals.

It should be noted that the band gap change of a CNT can be influenced both by chirality and strain. The total band gap E_{geff} could be either more than or less than the ideal diameter-based calculation E_g, which might cause the transport to decrease or increase correspondingly.

2.7.3 Tunneling effect:

There are basically three current sources in the CNTFET model:

1) The thermionic current contributed by the semiconducting subbands (I_{semi}) with the classical band theory;

2) The current contributed by the metallic subbands (I_{metal});

3) The leakage current (I_{btbt}) caused by the band-to-band tunneling (BTBT) mechanism through the semiconducting subbands. [54]

$I_{\mathbf{btbt}}$: The BTBT current from drain to source becomes significant in the sub-threshold region; mainly with negative gate bias (nFET).There are two possible tunneling regions:

I. The "n"-shape called the region 1

II. The "L"-shape known as the region 2

This phenomenon is depicted in figure 2.20 given below. With $V_{\mathrm{ch,DS}} > E_{1,0}$, the tunneling through the drain junction in region 1 causes the holes (electrons) to pile up in the nFET (pFET) channel region because the source junction forbids the holes (electrons) from escaping away. The piling up of holes (electrons) results in the lowering of the surface-potential and thereby leads to a higher current and worse sub-threshold behavior [55].But for well-tempered devices this effect is very minor and so for simplification of the modeling, this effect in region 1 is ignored [55], [56].Since tunneling through the source junction in region1 is prohibited, only band-to-band-tunneling (BTBT) current through the drain junction in region 2 is considered. Assuming a ballistic transport for the tunneling process, the BTBT current (I_{btbt},) is estimated by the BTBT tunneling probability (T_{btbt}) times the maximum possible tunneling current integrating from the conduction band at the drain side up to the valance band at the source side[55].

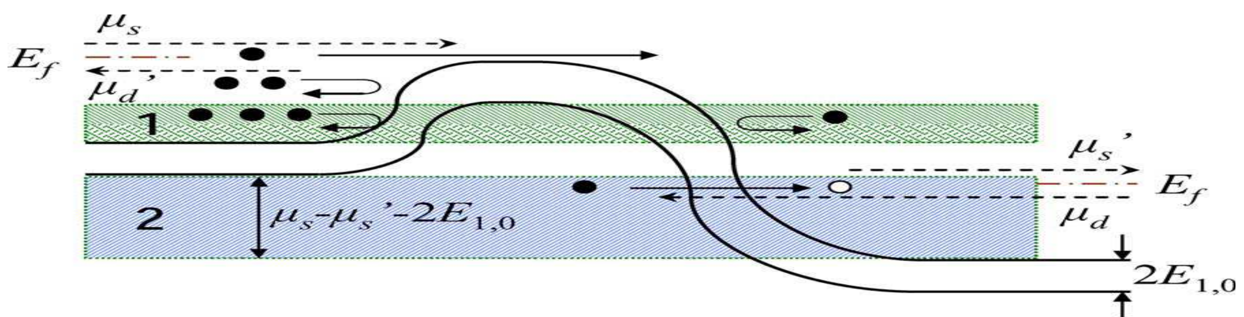

Figure 2.20: Energy-band diagram (only the first subband is shown) and the associated Fermi levels at the source/drain side for CNFET with moderate gate/drain bias. There are two possible tunneling regions: regions 1 and 2, which are shaded on the plot. Only the tunneling through region 2 is considered in this paper [54]

The tunneling current then can be obtained by T_t timing the maximum possible tunneling current using:

$$I_t = \frac{4qkT}{h} T_t \sum_{m=1}^{M} \left[\ln\left(1 + e^{(qV_{\text{DSeff}} - E_{g\text{eff}}/2 - E_F)/K_B T}\right) - \ln\left(1 + e^{qV_{\text{DSeff}} - E_F/K_B T}\right) \right] \frac{\max(qV_{\text{DSeff}} - E_{g\text{eff}}, 0)}{qV_{\text{DSeff}} - E_{g\text{eff}}} \quad (39)$$

Where, E_f *is* the Fermi level of the doped source/drain nanotube in electron-volt unit.

The tunneling current increases the total drain current throughout the V_{DS} *r*ange, but the effect only becomes obvious when the bias voltage is getting large and exceeds a certain turning point depending on the coefficients. [57]

The tunneling effect is also inevitable in the sub-threshold region, which may cause the lowering of the self-consistence potential and thereby worsen the threshold characteristics of the transistor. One simplified method to describe the tunneling effect is to introduce a parameter *Tt*, called the tunneling probability [44],

Following the work of Kane [58], [59], theWentzel–Kramers–Brillouin like transmission coefficient is given by:

$$T_t \approx \frac{\pi^2}{9} e^{-\left(\pi \sqrt{m^* E_g^3} / \sqrt{8q\hbar F}\right)} \quad (40)$$

Where *F* is a parameter which triggers the tunneling under high electrical field [44]

$$\text{F} = (V_{\text{ch,DS}} + (Ef - \Delta\Phi B)/e)/l_{\text{relax}} \quad (41)$$

F is known as the electrical field triggering the tunneling process near the drain-side junction. The potential drop across the drain-channel junction is assumed to relax over the distance l_{relax}, which affects both the BTBT current slope and its magnitude. $m*$ is the effective electron mass, which is defined as $\hbar^2/(\partial^2 E_{m,l}/\partial k_l^2)^2$ [54].

2.7.4 Phonon scattering:

CNT transistors operating close to the ballistic limit have been experimentally reported to be at low temperature [60], [61]. However, at room temperature carrier transport in short tubes is still influenced by phonon scattering [62]. At low bias, the associated interface is known to be nearly

elastic and dominated by acoustic phonon (AP) scattering and the mean free path (MFP) detected to be very long in CNTs (~0.6–1.5 μm) in comparison to the channel length of a CNT .Whereas on the other hand at high bias, optical phonon (OP) emission dominates and the electron MFP is short (∼15 nm) compared to the channel length of a CNT [63].

For semiconducting carbon nanotubes, the scattering effects are related to the band energy. The effective phonon scattering mean free path in a semiconducting nanotube can be calculated by:

$$\frac{1}{l_{sc}(V_x)} = \frac{1}{l_{\text{ap}}}\left[1 - \frac{1}{1 + e^{(E_F - qV_{SC} + qV_x)/K_B T}}\right] + \frac{1}{l_{\text{op}}}\left[1 - \frac{1}{1 + e^{\left(E_F - qV_{SC} - \hbar\omega_{\text{op}} + qV_x\right)/K_B T}}\right] \tag{42}$$

Where,

l_{ap}= 500nm is a typical acoustic phonon scattering MFP value,

l_{op}= 15nm is a typical optical phonon scattering MFP,

ħωop≈0.16eV is atypical optical phonon (OP) energy[64], [65].

At low carrier energy (e.g. <0.15eV), the acoustic scattering dominates; while the optical scattering takes place at high kinetic energy.

$$T_S = \frac{l_{SC}(0)}{l_{SC}(0)+L} \tag{43}$$

$$T_D = \frac{l_{SC}(V_{\text{DS}eff})}{l_{SC}(V_{\text{DS}eff})+L} \tag{44}$$

$$I_{DS_p} = \frac{2qkT}{\pi\hbar}\left[T_S \ln\left(1 + e^{E_F - qV_{SC}/kT}\right) - T_D \ln\left(1 + e^{E_F - q\left(V_{SC}+V_{\text{DS}eff}\right)/kT}\right)\right] \tag{45}$$

The phonon scattering effects may limit the transport capability of carriers in the channel and hence restrain the drain current.

2.8 Summary:

From the non-ideal effects discussed earlier and others like contact junction effects, it is noticed that the transport characteristics of CNT becomes non-ballistic when these parameters exist. Some other factors present include scattering mechanisms, parasitic capacitances and energy barriers as well and the transport phenomenon discussed above is just a part of them. Practically, the non-ballistic effects are caused by a number of factors, including fabrication technologies, materials etc and thus it is difficult to determine which effect is of more importance as certain effects are dominant when the related coefficients posses more value in the provided device. For a CNT model with non-ballistic effects, the transport equation can be treated as the summary of the transport current and the tunneling current.

Chapter 3

Results and Analysis of Non-Ballistic CNTFET characteristics Using MATLAB Simulation

This chapter discusses the methodology of this research. Simulation model used to study the characteristics is explained here. Also, obtained results are scrutinized and compared with the reported results of other research groups.

This work uses the model developed by Rahman *et al* [35]. The detailed calculation and modeling is provided in Appendix B. The input parameters and different constant values are shown in table 3.1. Also, to generate 3D plots, a model developed by Khan *et al.* [96] has been followed.

3.1 The Model:

The equations have been collected from the work of Kazmierski *et al.* [45]. Step by step process of the calculation of tunnel control parameter is described below:

1) Firstly, effective drain to source voltage was calculated using the following equation.

$$V_{DSeff} = \frac{L}{L+(d/d_0)\lambda_{eff}} V_{DS} \tag{46}$$

Due to non-ballistic conduction, applied drain voltage will suffer some loss and will be reduced to effective drain voltage.

2) Then, bandgap will also be affected because of non-ballistic conduction. The effective bandgap is calculated using the follow formulae.

$$\frac{dE_{g\text{strain}}}{d\chi} = 3\sigma(1+r_0)\text{sign}(2p+1)\cos(3\phi) \tag{47}$$

$$E_{g\text{eff}} = E_g + \frac{dE_{g\text{strain}}}{d\chi}\chi \tag{48}$$

3) Tunneling current is calculated by reproducing the results of Tom J. Kazmierski, Dafeng Zhou, Bashir M. Al-Hashimi and Peter Ashburn [45].

4) Value of tunneling current is put into the following equation to evaluate T_t.

$$I_t = \frac{4qkT}{h} T_t \left[\ln\left(1 + e^{(qV_{\text{DSeff}} - E_{geff}/2 - E_F)/K_B T}\right) - \ln\left(1 + e^{qV_{\text{DSeff}} - E_F/K_B T}\right) \right] \quad (49)$$

5) The following equation was used to find out the value of tunnel control parameter.

$$F = \sqrt{8} \times q \times \hbar \times \frac{-\ln(I_{t \times} \pi^2/9)}{\pi \sqrt{m^* E_g^3}} \quad (50)$$

Detailed modeling has been discussed in Appendix A.

Table 3.1: Parameters used in the simulation

Input parameters:	**List of values (Physical parameters):**
Gate insulator thickness t (m);	(Permittivity of free space)€o:8.85*10^-12 (Relative permittivity of dielectric cons.) €:3.9
Gate insulator Dielectric constant (€);	C-C bond length (ac-c): 1.42*10^-10
Tube diameter (d);	Oxide thickness(Default) t= 1.5*10^-9
Temperature (T);	No. of bias point NV(Default)= 11
Number of bias point (NV);	Range (VI-Vf) :(0-1) v
Initial voltage (Vi);	(Fermi level for source) (Default)Ef=-0.3
Final „ (Vf);	αg (Default)= .88 αd(Default)= .035
Source Fermi level (Ef)eV;	C-C bond energy: (Default) 3ev
Gate control parameter alphag (αg);	Tunnel control parameter, f=9.798e36 Reduced Planck's constant,hbar=1.05e-34; (m^2-kg-/s)
Drain control parameter alphad (αd);	**Non-ballistic effect parameters:** Channel length, L=300e-9; Elastic scattering MFP, lambda_eff= 200e-9 (m); Reference diameter, d0=1.5e-9 (m),
Chiral axis(n,m);	Overlap integral of tight bonding c-c model ,sigma=2.7 (eV); Poisson's ratio, r0=.2; Distortion factor under strain, chi=.1; Fermi energy, EF=-.32 (eV) p=mod(n-m,3); Chiral angle, phi=atan((sqrt(3)*m)/(m+(2*n))); effective mass of electron, m_eff=.19*m0;

The flowchart used in generating the results is given below:

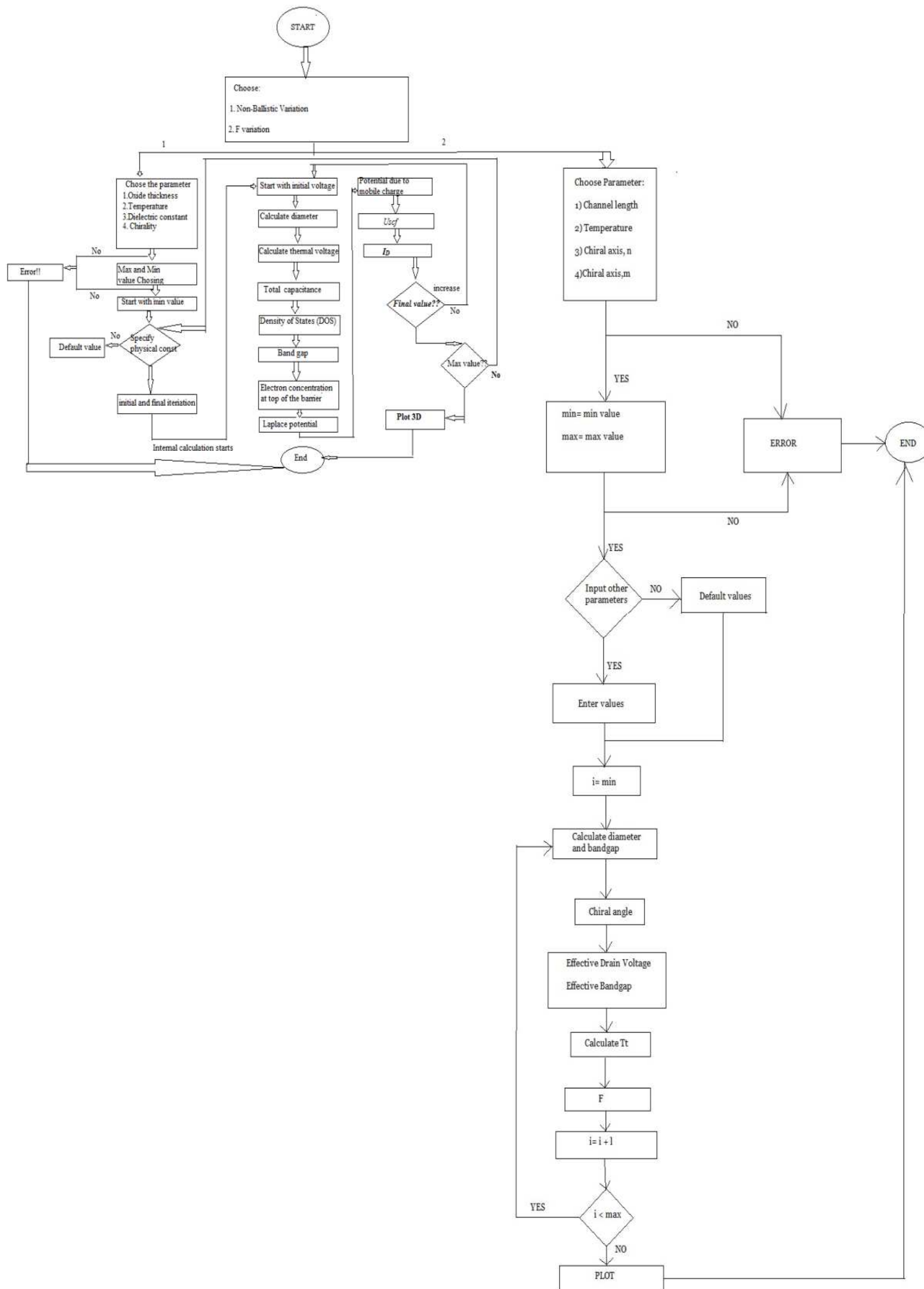

Figure 3.1: Flowchart of MATLAB simulation used in this research

3.2 Results and Analysis:

This work starts by observing the change in electron concentration at the top of the barrier of a neutral device with respect to different parameters. The change rate is plotted to have a better understanding of its tendencies. In the simulation, the change in I-V characteristics of non-ballistic Carbon Nanotube Field Effect Transistor is observed with the change of different parameters. The output characteristics are shown in three different 3D views for better understanding. Firstly, a linear 3D plot is shown, which is followed by another 3D plot without mesh and finally, a logarithmic view of the result is displayed. In this research, the considered CNTFET structure is similar to that of a MOSFET. In addition to these, this work evaluates the total non-ballistic effect and compares the result to that of ballistic CNTFET. The deviation in performance is thoroughly studied. Also, change rate of tunnel control parameter with the change of parameters is calculated.

3.2.1 Change of Electron Concentration at the Top of Barrier:

Electron concentration was calculated by varying temperature and chirality and change rate was studied by plotting the results.

3.2.1.1 Effect of Temperature:

Firstly, the effect of temperature is varied to study its effect on electron concentration. Temperature was varied from 300 K to 500 K. Electron concentration shows significant change with this variation. The other parameters involved were gate oxide thickness which was fixed at 1.5 nm, dielectric constant was taken to be 3.9, gate and drain control parameters which were .88 and .035 respectively. Also, chiral axis n was set to 13 while m was 0. Fermi level was -.32 eV. Figure 3.2 shows the effect of temperature on electron concentration.

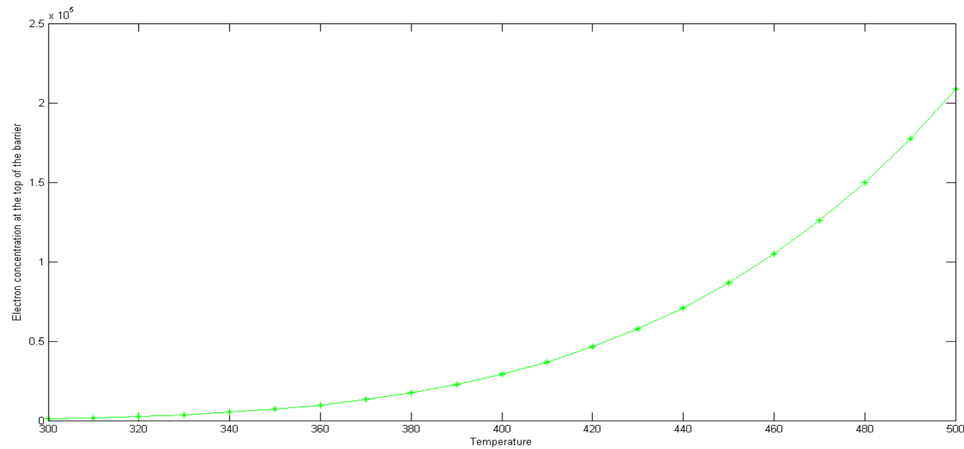

Figure 3.2: Change rate of electron concentration with Temperature

It can be seen from the plot that electron concentration increases as the temperature goes up.

3.2.1.2 Effect of Chirality:

After this, the change rate was studied due to chiral effects. Since electron concentration depends on diameter and diameter in turns is dependent on chirality, electron concentration was studied by varying the chiral indices.

This was done in two separate steps.

Firstly, chiral axis m was varied from 11 to 23 while m was constant at 0. Temperature was taken at 300 K. Temperature was set to 300 K, gate oxide thickness was 1.5 nm, and dielectric constant was fixed at 3.9. Gate control parameter was .88 and drain control parameter was taken to be .035. Fermi level was set to -.32 eV. Figure 3.3 shows the obtained result.

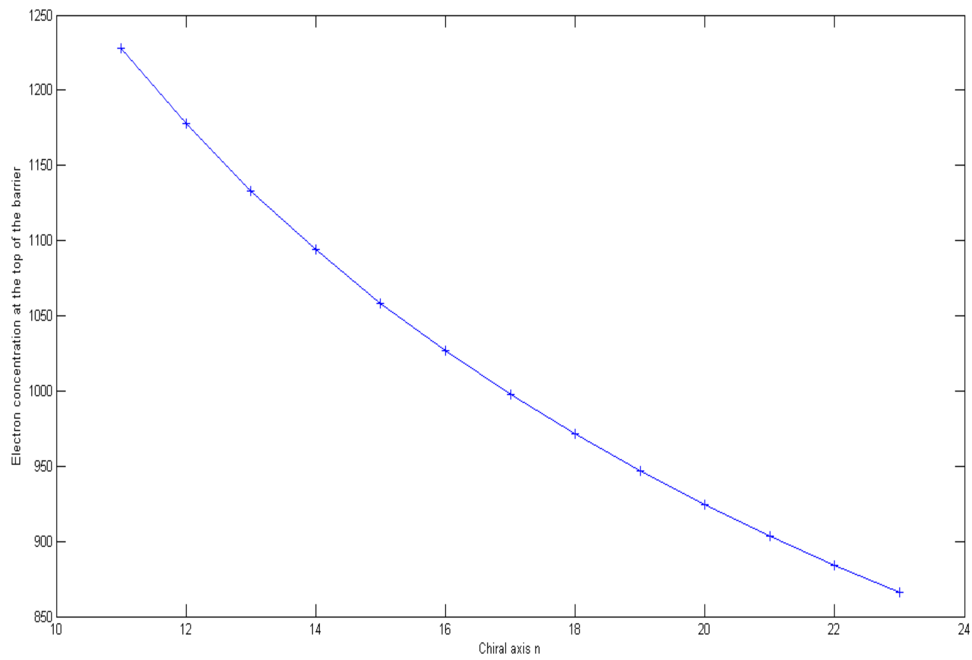

Figure 3.3: Change of electron concentration with Chiral Axis n

Lastly, chiral axis m was varied from 0 to 12, this time chiral axis n was fixed at 13. Temperature was again set to 300 K, gate oxide thickness was 1.5 nm, and dielectric constant was fixed at 3.9. Gate control parameter was .88 and drain control parameter was taken to be .035. Fermi level was -.32 eV for this experiment. The obtained result can be seen in figure 3.4.

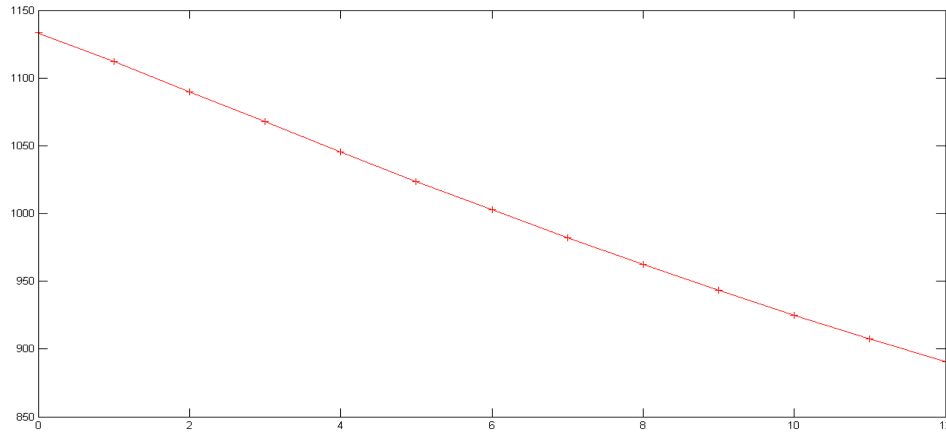

Figure 3.4: Change of electron concentration with Chiral Axis m

Therefore, electron concentration at top of the barrier maintains an inverse relation with chirality.

3.2.2 Effect of Gate Oxide Thickness:

Gate oxide thickness wields strong influence on the performance of CNTFET. In this section, the changes in I-V characteristics of non-ballistic carbon nanotube transistor with the increase of gate oxide thickness are observed and then, the obtained results are compared with a previously reported ballistic result to understand the effects of non-ballistic considerations on the performance of the transistor.

Gate oxide thickness was varied from 1 nm to 4 nm. Chirality was fixed at n=13 and m=0 and so, diameter of the nanotube was also constant at 1.0184 nm. Other parameters were also kept constant. Temperature was 300 K, source Fermi level was -.32 eV, gate and drain control coefficients were .88 and .035 respectively. The dielectric constant was set at 3.9.

Gate Oxide thickness values were taken at an interval of .25 nm. For all cases, the largest currents were found at 1 nm, the initial value. The currents gradually decrease with the increase of oxide thickness. At 4 nm the drain currents decrease to the lowest value.

3.2.2.1 Elastic Scattering Effect:

From the following figure 3.5, we can see the effect of elastic scattering. For elastic scattering effect, the highest current at 1 nm oxide thickness was found to be 1.021×10^{-5} A and at 4 nm the current was valued at 5.29×10^{-6} A.

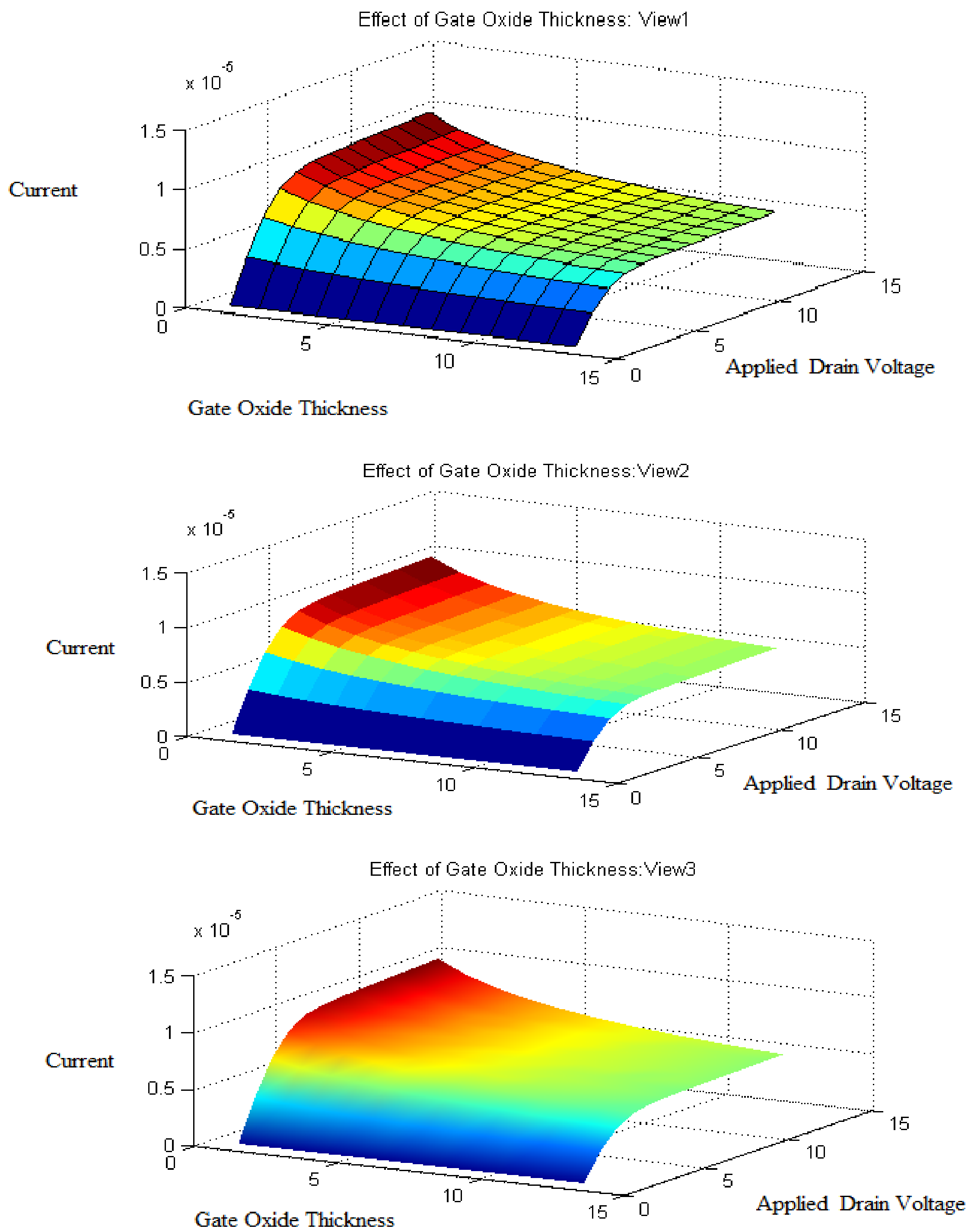

Figure 3.5: Effect of Gate Oxide Thickness variation on I-V characteristics of Carbon Nanotube Field Effect Transistor with Elastic Scattering Factor

3.2.2.2 Bandgap Strain Effect:

Next, we will discuss and show the effects of bandgap strain. From the following figure 3.6, we can easily see the effect of bandgap strain. For 1 nm gate oxide thickness the current was found to be 7.552×10^{-6} A and for 4 nm it decreased to the value of 3.809×10^{-6} A.

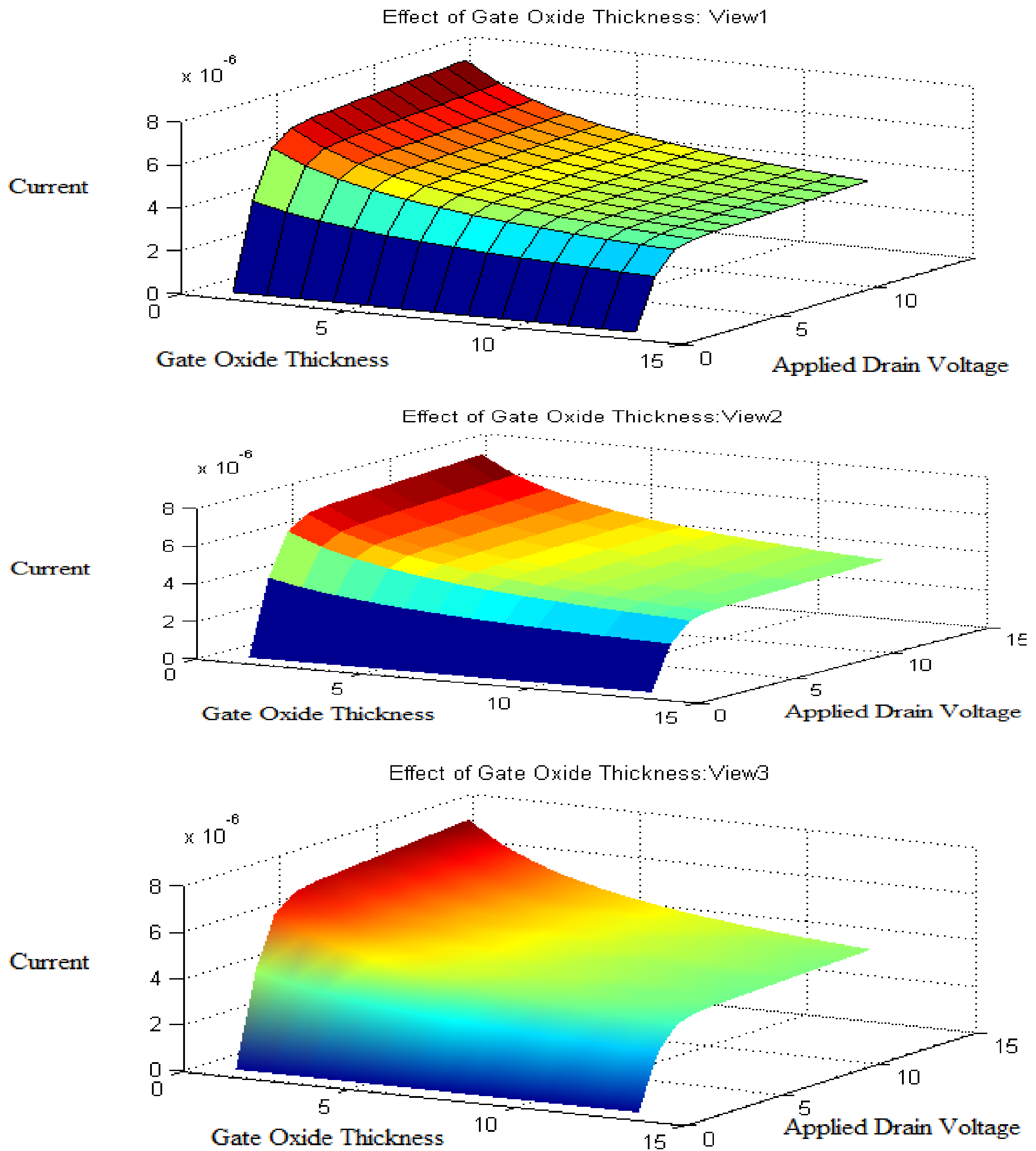

Figure 3.6: Effect of Gate Oxide Thickness variation on I-V characteristics of Carbon Nanotube Field Effect Transistor with Bandgap Strain Factor

3.2.2.3 Tunneling Effect:

The following figure 3.7 clearly shows the effect of tunneling on CNTFET. For 1 nm gate thickness the largest amount of current was observed. The value of this current was 1.072×10^{-5} A and for 4 nm the smallest amount of current was found with a value of 5.604×10^{-6} A.

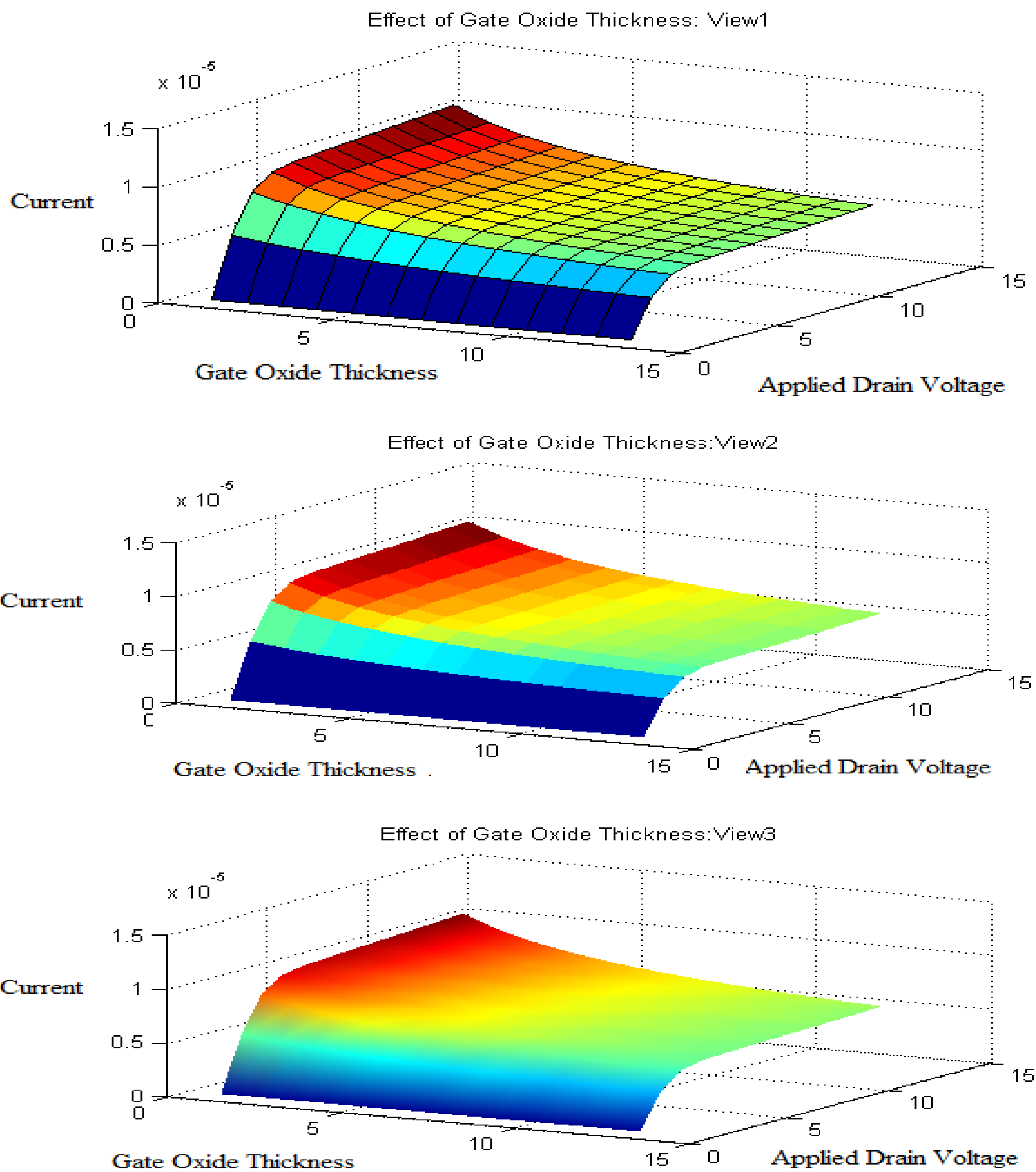

Figure 3.7: Effect of Gate Oxide Thickness variation on I-V characteristics of Carbon Nanotube Field Effect Transistor with Tunneling Factor

3.2.2.4 Combined Non-Ballistic Effect:

From the following figure 3.8, we can clearly observe the combined non-ballistic effect on CNTFET. For 1 nm gate thickness the largest amount of current was observed. The value of this current was 7.431×10^{-6} A and for 4 nm the smallest amount of current was found with a value of 3.833×10^{-6} A.

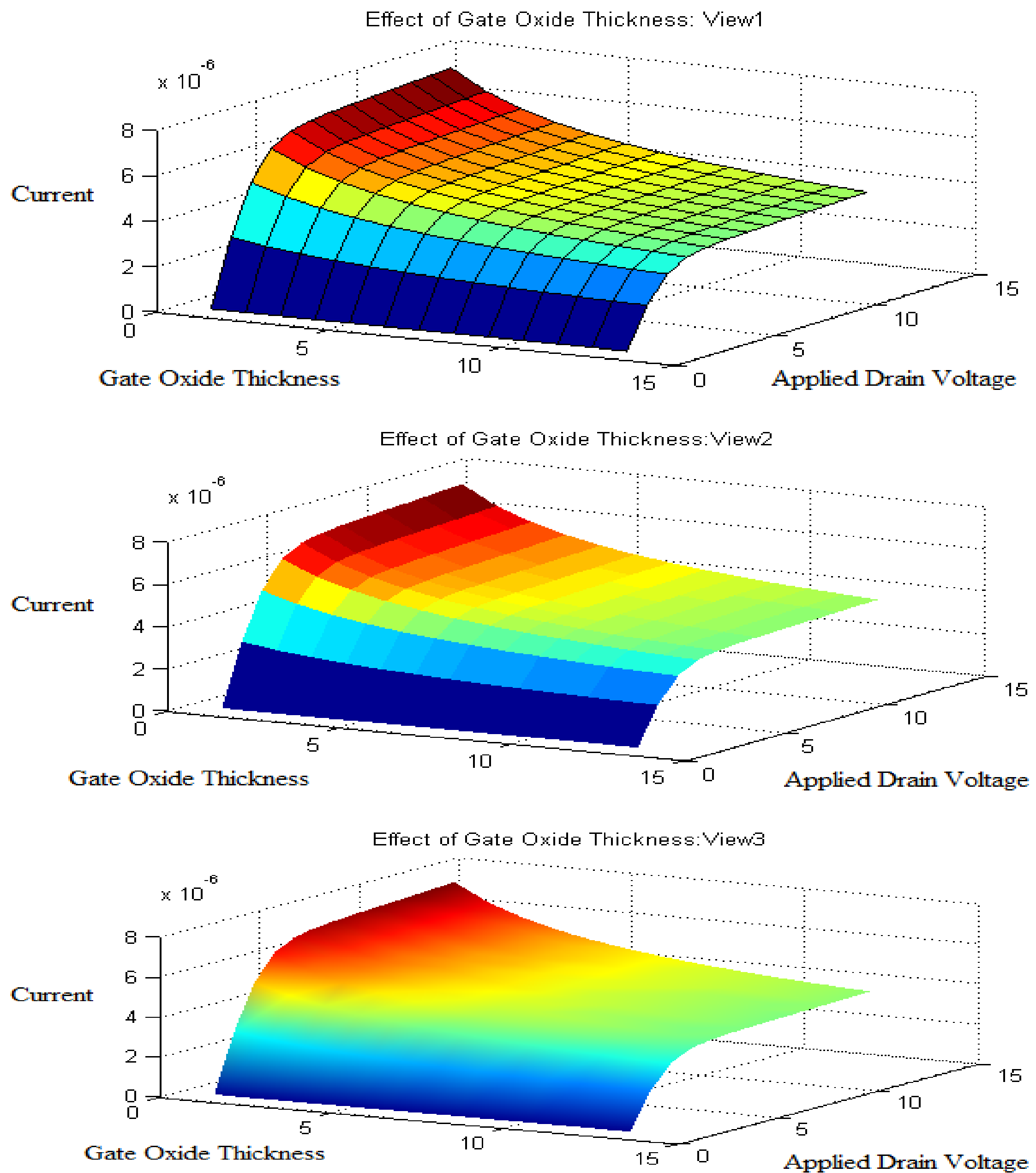

Figure 3.8: Effect of Gate Oxide Thickness variation on I-V characteristics of Carbon Nanotube Field Effect Transistor with Combined Non-Ballistic Effect

Therefore, from our finding, we can assume that theoretically thinner Oxide layer at the gate will yield better drain current.

The deviation from ideal behavior due to non-ballistic effects can be easily observed once the results have been compared with ballistic results found Khan *et al*. [96]. The ballistic simulation was run with the same values of the parameters and it was found that for 1 nm gate oxide thickness, the drain current was 1.049×10^{-5} A and for 4 nm thickness, it was 5.468×10^{-6} A. This is clearly superior to the obtained non-ballistic results. The figure 3.9 shows the ballistic characteristics in 3D.

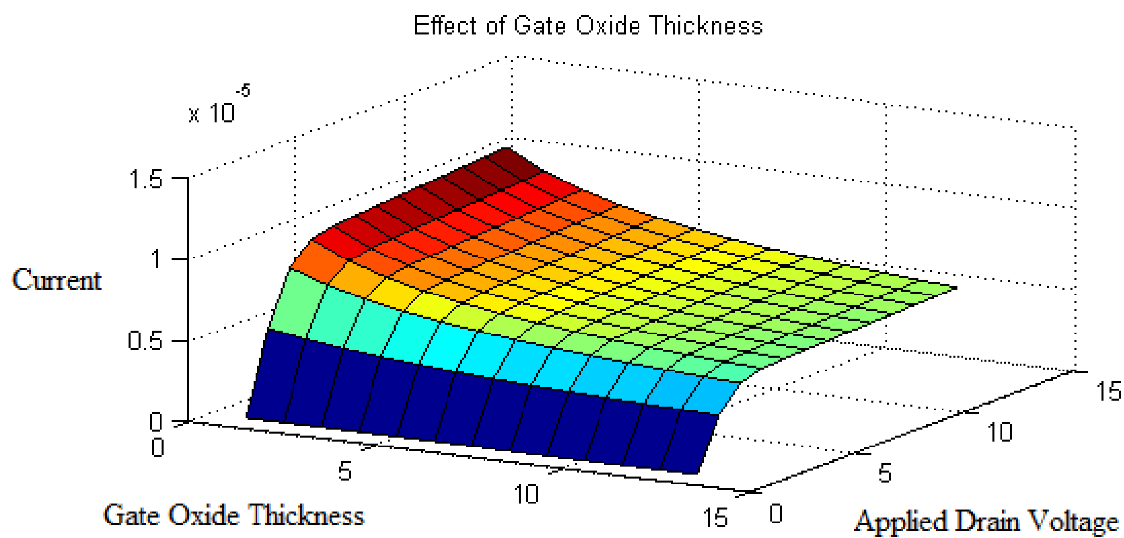

Figure 3.9: Effect of Gate Oxide Thickness variation on I-V characteristics of Carbon Nanotube Field Effect Transistor with Ballistic Effect [96]

3.2.3 Effect of Temperature:

Effect of temperature on the performance of non-ballistic CNTFET is also considered in this work. Temperature was changed from 273 K to 323 K. All other parameters were kept constant. For this case, gate oxide thickness was considered to be 1.5 nm. The temperature values were taken at an interval of 1 K. From the following figures, it can be seen that the effect of temperature is very negligible on the performance of CNTFET. Here, the drain currents at higher temperature are slightly higher than the drain currents at lower temperature. In all cases, the minimum currents were found for 273 K. The currents slowly rise to the peak values at 323 K.

3.2.3.1 Elastic Scattering effect:

The figure 3.10 deals with the effect of elastic scattering. For elastic scattering effect, the lowest current at 273 K temperature was found to be 8.086×10^{-6} A and at 323 K the current was valued at 8.399×10^{-6} A.

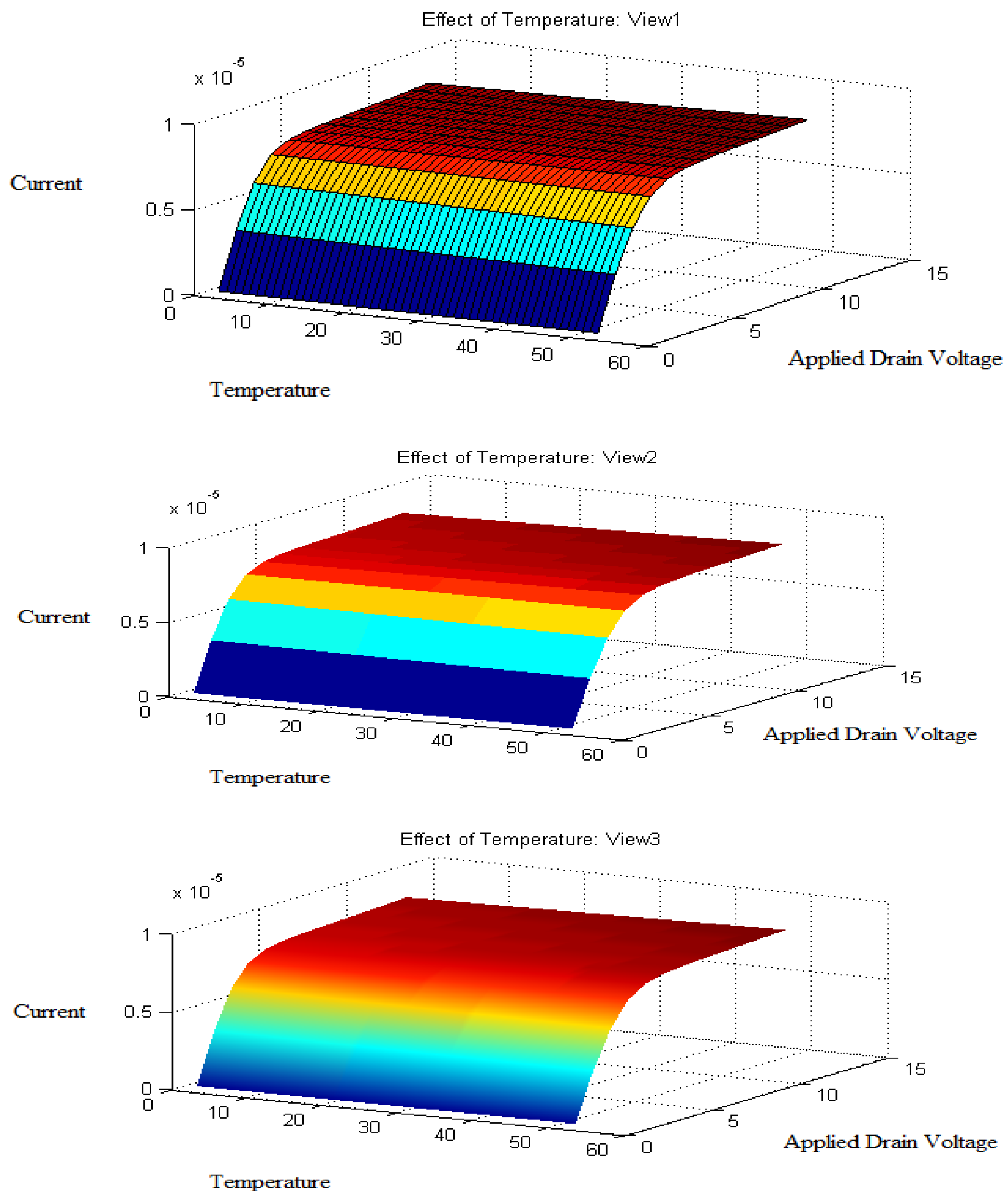

Figure 3.10: Effect of Temperature variation on I-V characteristics of Carbon Nanotube Field Effect Transistor with Elastic Scattering Factor

3.2.3.2 Bandgap Strain Effect:

The next figure, figure 3.11 clearly shows the effect of bandgap strain on CNTFET. For 273 K, the smallest amount of current was observed. The value of this current was 5.83×10^{-6} A. This current kept slowly increasing until it reached its peak value at 323 K. The peak value was observed to be 6.162×10^{-6} A.

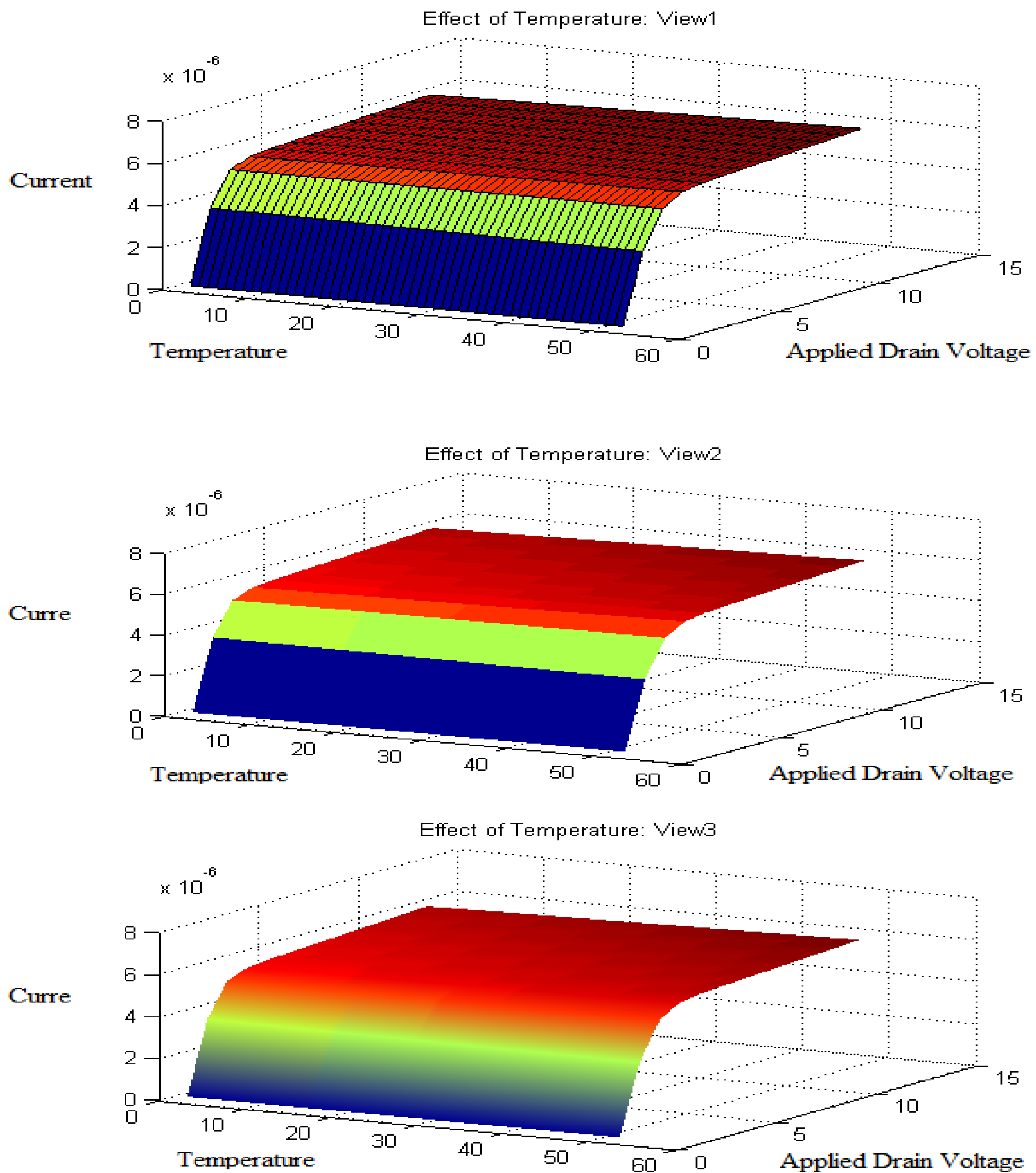

Figure 3.11: Effect of Temperature variation on I-V characteristics of Carbon Nanotube Field Effect Transistor with Bandgap Strain Factor

3.2.3.3 Tunneling Effect:

The figure 3.12 clearly shows the effect of tunneling on CNTFET. For 273 K gate thickness the smallest amount of current was observed. The value of this current was 8.517×10^{-6} A and for 323 K the largest amount of current was found with a value of 8.827×10^{-6} A.

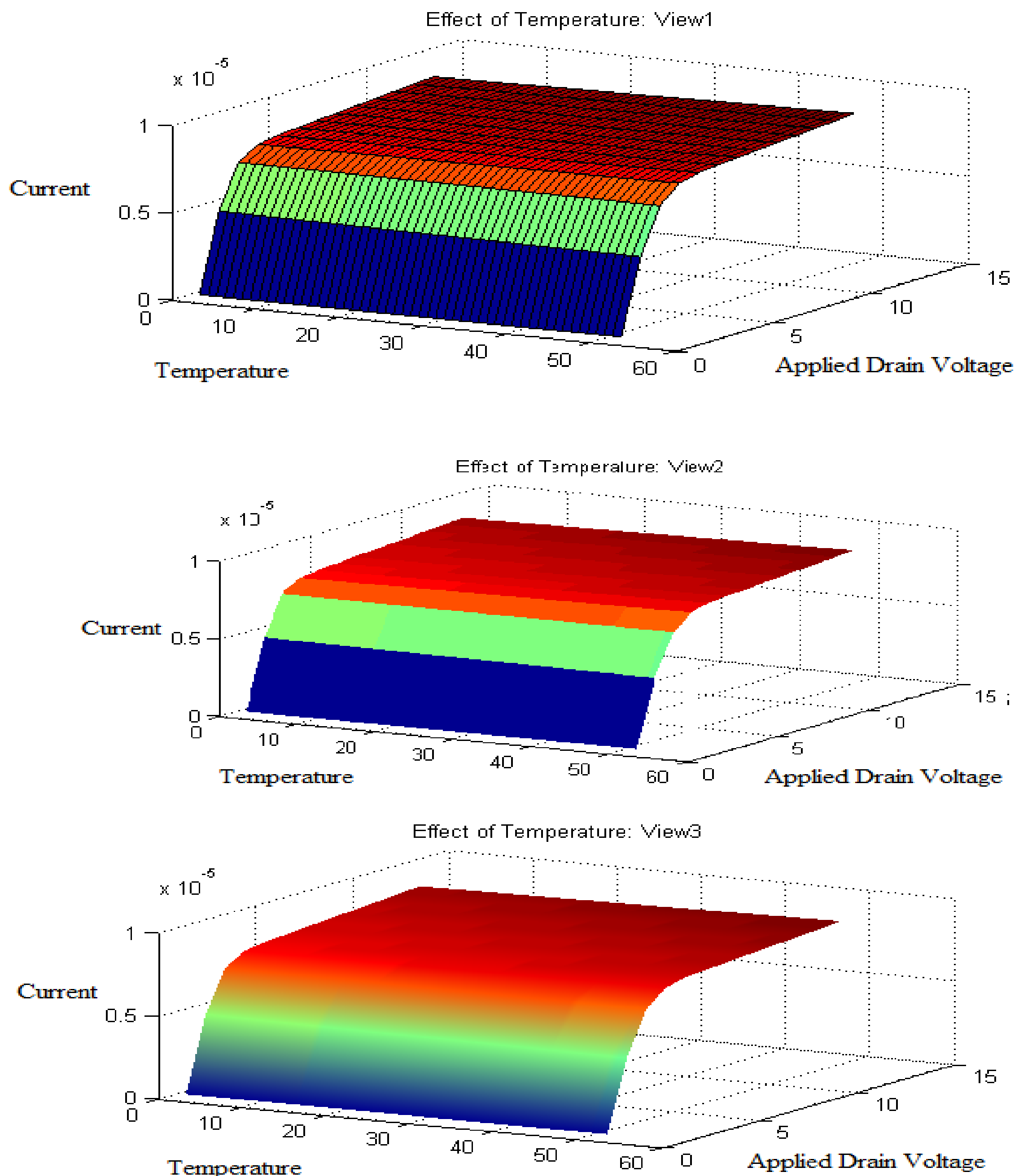

Figure 3.12: Effect of Temperature variation on I-V characteristics of Carbon Nanotube Field Effect Transistor with Tunneling Factor

3.2.3.4 Combined Non-Ballistic Effect:

From the following figure 3.13, we can clearly observe the combined non-ballistic effect on CNTFET. For 273 K, the lowest amount of current was observed. The value of this current was 5.771×10^{-6} A and for 323 K the highest amount of current was found with a value of 6.101×10^{-6} A.

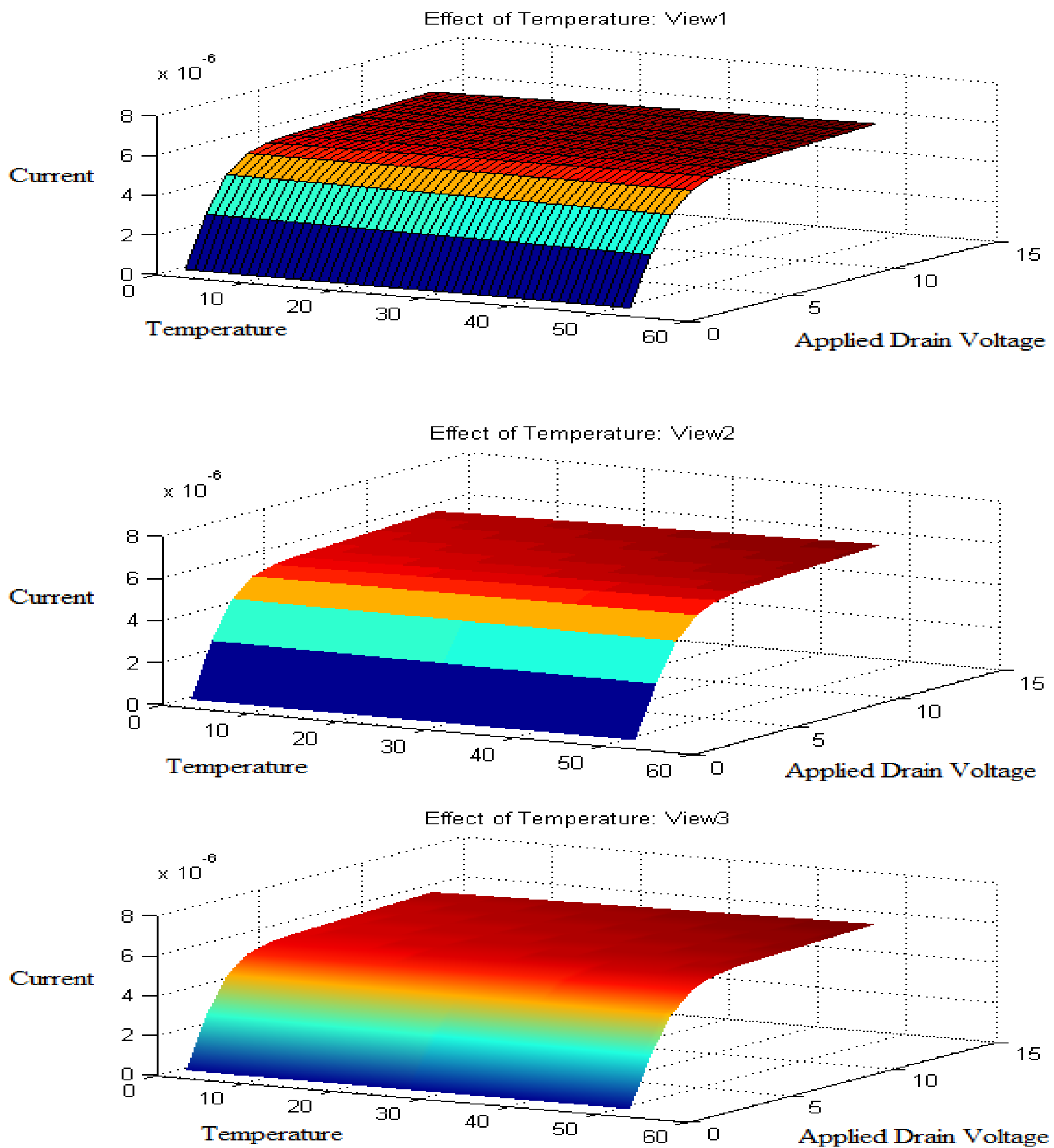

Figure 3.13: Effect of Temperature variation on I-V characteristics of Carbon Nanotube Field Effect Transistor with Combined Non-Ballistic Effect

Based on our result, we can deduce that drain current will increase very slowly with temperature and temperature has a minimum impact on the characteristics of CNTFET.

The deviation from ideal behavior due to non-ballistic effects can be easily observed once the results have been compared with ballistic results found Khan *et al*. [96]. The ballistic simulation was run with the same values of the parameters and it was found that for 273 K temperature, the drain current was 8.382×10^{-6} A and for 323 K, it was 8.692×10^{-6} A. This is clearly superior to the obtained non-ballistic results. The figure 3.14 shows the ballistic characteristics in 3D.

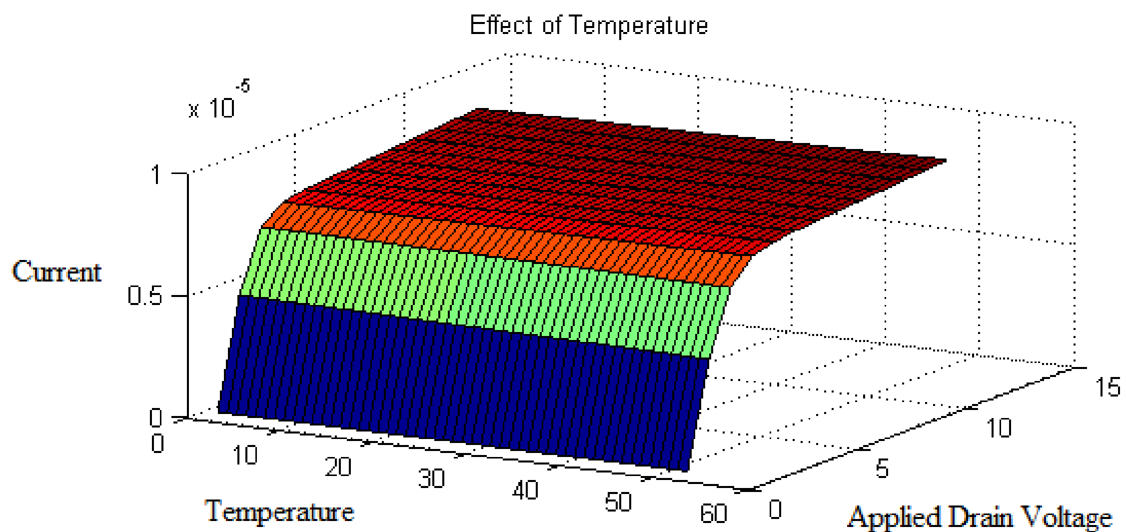

Figure 3.14: Effect of Temperature variation on I-V characteristics of Carbon Nanotube Field Effect Transistor with Ballistic Effect [96]

3.2.4 Effect of Dielectric Constant:

To observe how the dielectric constant of used gate material affects the I-V characteristics of CNT transistors, 3D I-V plots were generated with respect to different of dielectric constants.

In this case, the dielectric constant was changed from 3 to 15. The values were taken at an interval of .5. The other parameters were kept constant as usual. Also, this is to be mentioned that the value was temperature was taken to be 300 K. It is evident from the figures that dielectric constant has a profound impact on the drain current I_D. It has been observed that in all the cases, the currents are increasing as the value of dielectric constant is going higher. The lowest currents were found for dielectric constant 3. The highest currents were for dielectric constant 15.

3.2.4.1 Elastic Scattering Effect:

The following set of graphs in figure 3.15 show the effect of dielectric constant when elastic scattering is considered. The smallest current for dielectric constant 3 was found to be 6.432×10^{-6} A and the largest current at 15 was 2.153×10^{-5} A.

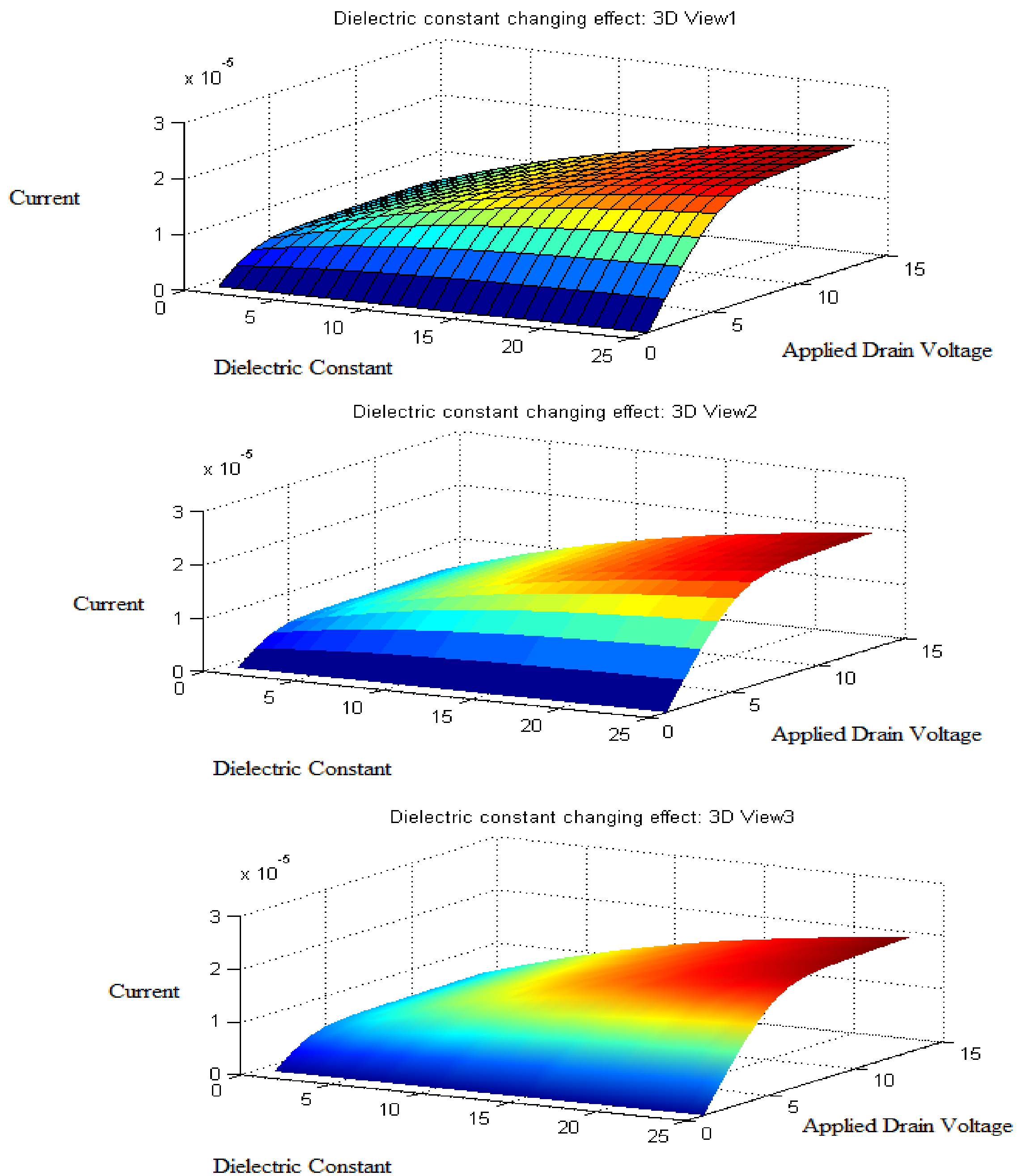

Figure 3.15: Effect of Dielectric Constant variation on I-V characteristics of Carbon Nanotube Field Effect Transistor with Elastic Scattering Factor

3.2.4.2 Bandgap Strain Effect:

The following figure 3.16 deals with the effect of bandgap strain on CNTFET. For dielectric constant 3, the smallest amount of current was observed. The value of this current was 2.459×10^{-5} A. This current kept increasing until it reached its peak value at dielectric constant 15. The peak value was observed to be 3.146×10^{-5} A.

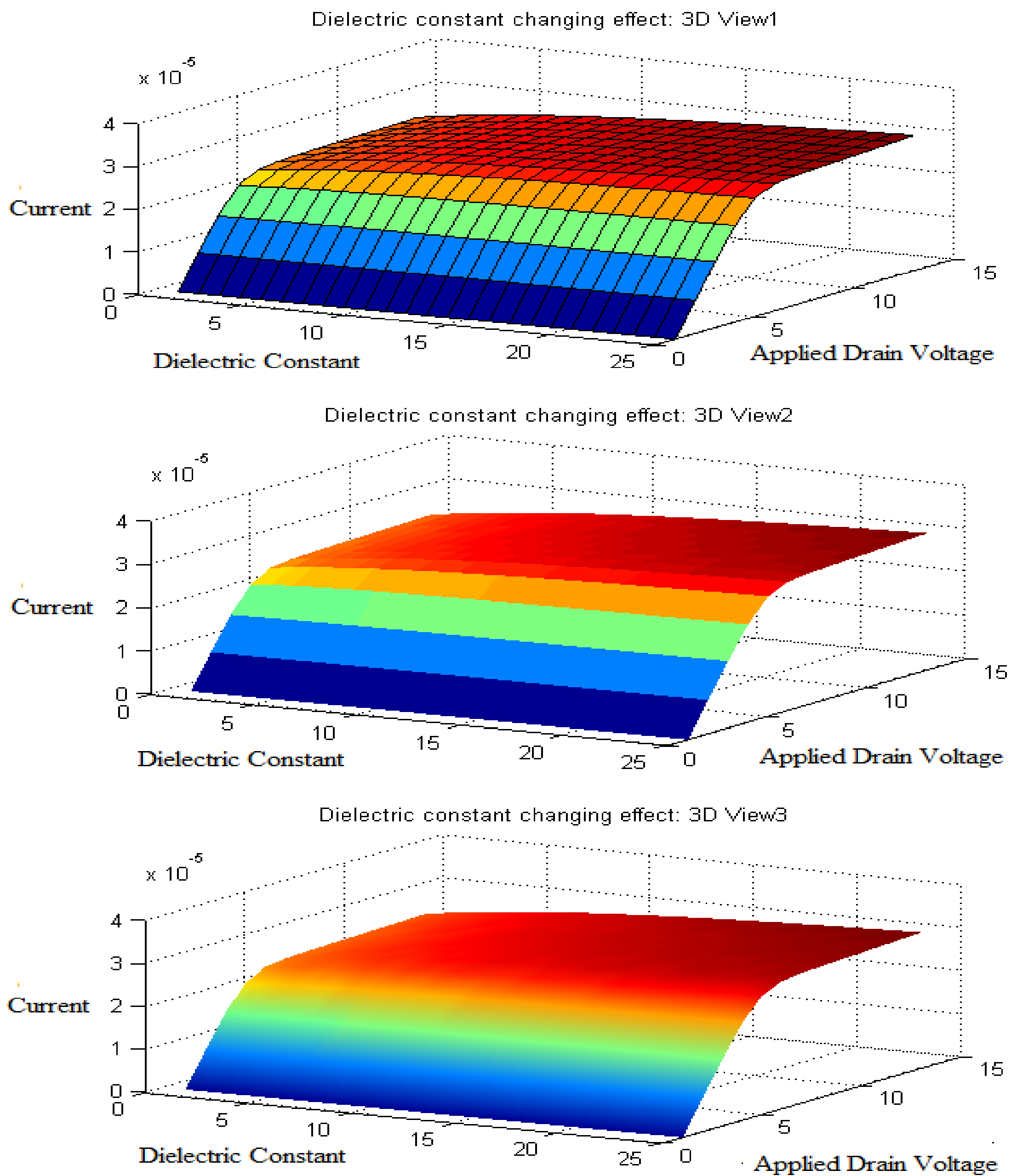

Figure 3.16: Effect of Dielectric Constant variation on I-V characteristics of Carbon Nanotube Field Effect Transistor with Bandgap Strain Factor

3.2.4.3 Tunneling Effect:

Figure 3.17 clearly shows the effect of tunneling on CNTFET. For dielectric constant 3 the smallest amount of current was observed. The value of this current was 1.817×10^{-5} A and for dielectric constant 15 the largest amount of current was found with a value of 3.38×10^{-5} A.

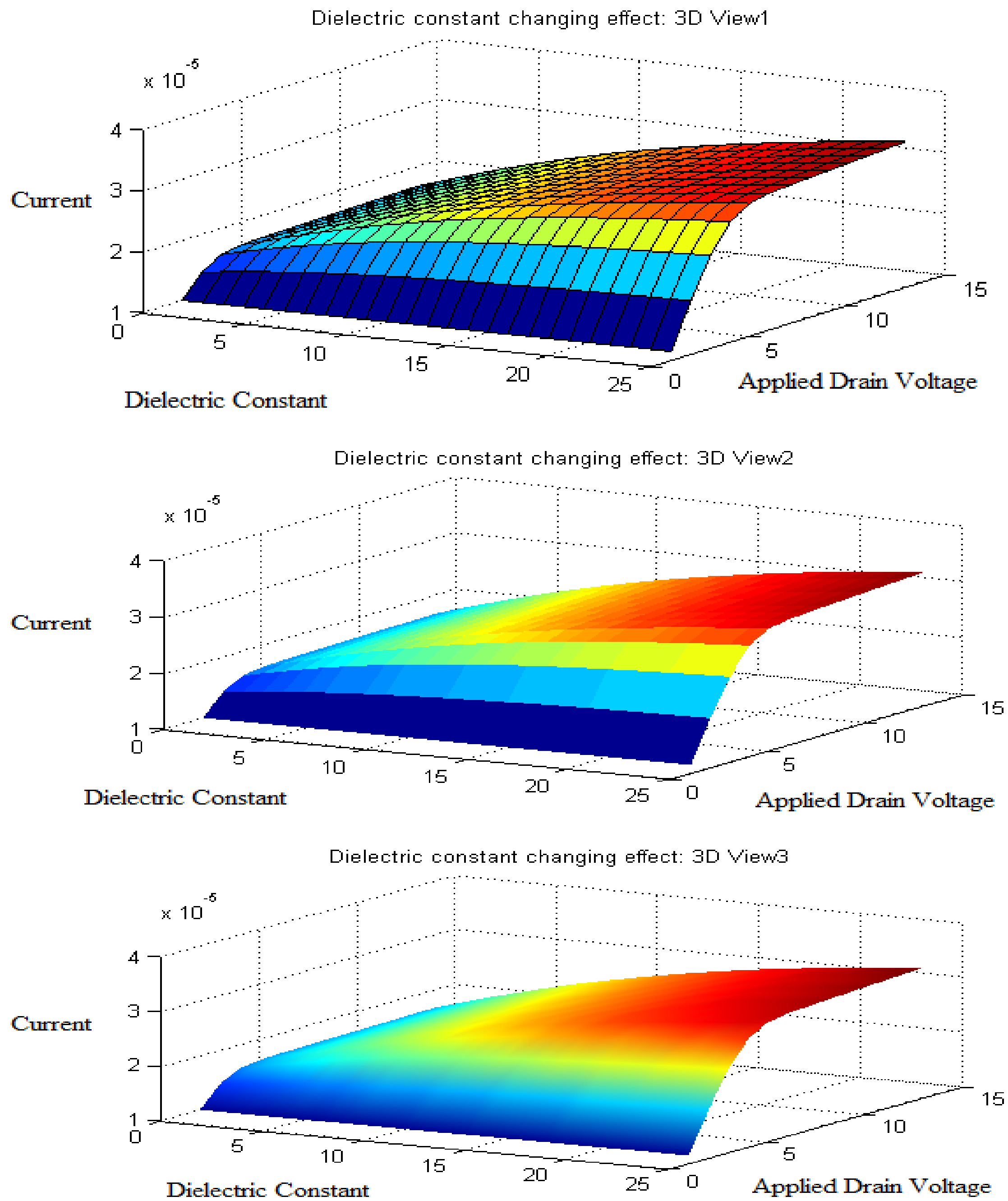

Figure 3.17: Effect of Dielectric Constant variation on I-V characteristics of Carbon Nanotube Field Effect Transistor with Tunneling Factor

3.2.4.4 Combined Non-Ballistic Effect:

From the following figure 3.18, we can clearly observe the combined non-ballistic effect on CNTFET. For dielectric constant 3, the lowest amount of current was observed. The value of this current was 3.568×10^{-5} A and for when dielectric constant was 15, the highest amount of current was found with a value of 4.218×10^{-5} A.

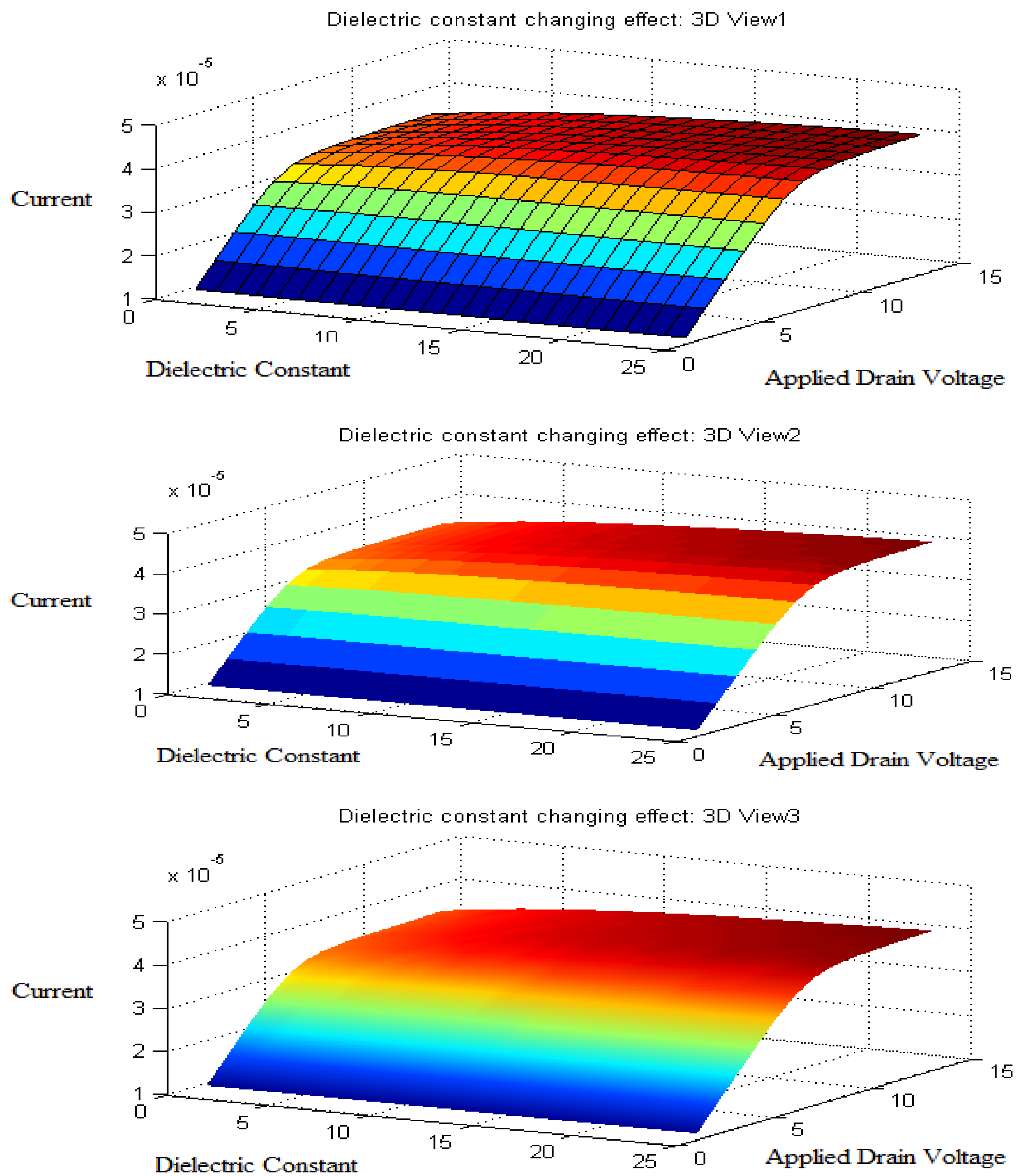

Figure 3.18: Effect of Dielectric Constant variation on I-V characteristics of Carbon Nanotube Field Effect Transistor with Combined Non-Ballistic Effect

From our results, we can say that higher dielectric constant will produce higher drain current. Therefore, drain current is directly proportional to dielectric constant.

The deviation from ideal behavior due to non-ballistic effects can be understood once the results have been compared with ballistic results found Khan *et al.* [96]. The ballistic simulation was run with the same values of the parameters and it was found that for dielectric constant 3, the drain current was 6.651×10^{-6} A and when dielectric constant was 15, current was 2.228×10^{-5} A. This is clearly superior to the obtained non-ballistic results. The figure 3.19 shows the ballistic characteristics in 3D.

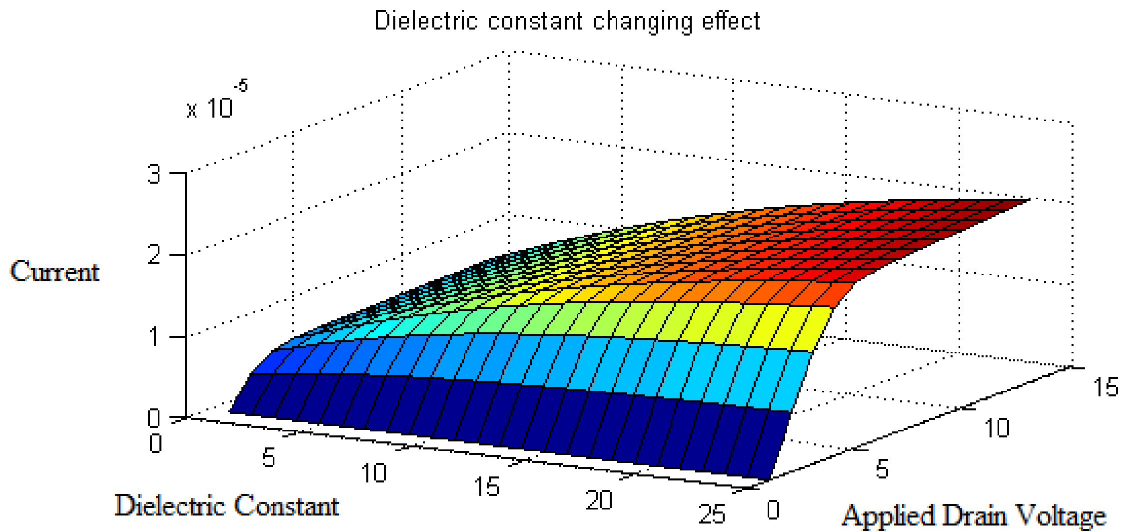

Figure 3.19: Effect of Dielectric Constant variation on I-V characteristics of Carbon Nanotube Field Effect Transistor with Ballistic Effect [96]

3.2.5 Effect of Chirality:

One of the most important aspects of a carbon nanotube is Chirality. Diameter of a carbon nanotube depends entirely on the chirality and diameter changing effect has a profound effect on the performance of CNTFET. Diameter of a CNT is calculated by the formula:

$$d_t = a/\pi\left(\sqrt{n^2 + nm + m^2}\right) \tag{50}$$

Where, n and m are the chiral index for (n,m) carbon nanotube and a is a constant valued at .246 nm. This is to be mentioned that n should always be greater than m.

At the same time, energy bandgap is inversely proportional to the diameter.

$$E_g = 2 \times (C - C\ bond\ length) \times (C - C\ bond\ energy)/d_t \tag{51}$$

Where, C-C bond length is considered constant at 1.42×10^{-10} m and C-C bond energy is constant at 3 eV. It is evident from the previous equation that since diameter of the nanotube plays a major part in controlling the bandgap, the drain current is also dependent on the diameter as energy bandgap is dependent on the diameter. So, ultimately the drain current depends on the chirality of the nanotube.

In this experiment, we observed the change in the I-V characteristics of non-ballistic carbon nanotube field effect transistor by changing both of the chiral indices n and m. First, we changed chiral index n and kept m constant. 3D plots were generated with respect to these conditions and change effect was observed. Then chiral index m was varied for a fixed value of n and again another set of 3D curves were produced to observe the changes in the current vs. voltage characteristics. For both sets of experiments, other parameters remained constant at their default values as usual. This should be mentioned that for this case, the value of dielectric constant was taken to be 3.9 which was the operating subject of the previous experiment.

From the figure, we can see that the value of drain current increases quite rapidly with the increasing chiral index n. Chiral index n was varied from 11 to 21 for all cases, whereas, m was considered to be 0. The values were taken at an interval of 1. In all the simulations, the minimum currents were found for n=11 A and the maximum currents were measured at n=21.

Then, chiral axis m was varied from 1 to 12 with n being constant at 13. The other parameters maintained their default values. From the figures, it is evident that chiral index m has a strong influence on drain current. The current increased with the increasing chiral index m. For all the simulations, the minimum currents were measured for m=1 and m=12 gave out the maximum currents. However, this should be noted that chiral index n influences the drain current more than chiral index m. The current changes more rapidly for chiral index n than chiral index m.

3.2.5.1 Elastic Scattering Effect:

Figure 3.20 shows the effect of change of chiral index ‘n’ when elastic scattering factor is taken into consideration. The minimum current for n=11 was 7.079×10^{-6} A and the maximum measured at n=21 was 1.25×10^{-5} A.

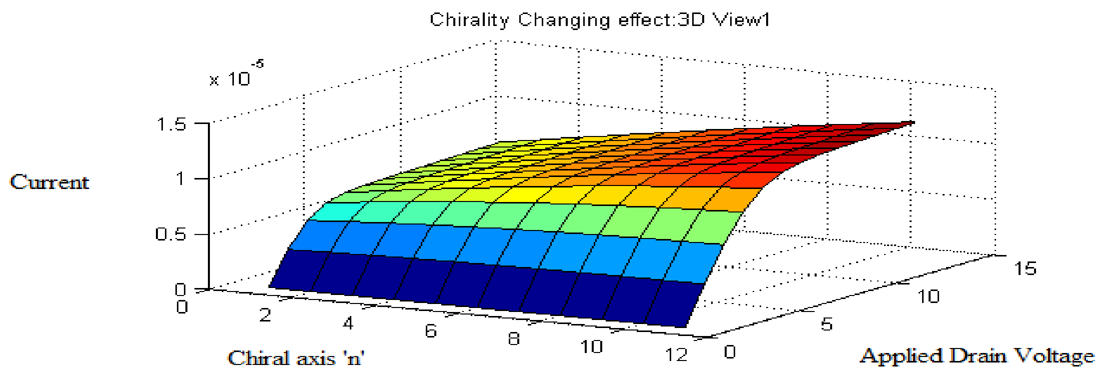

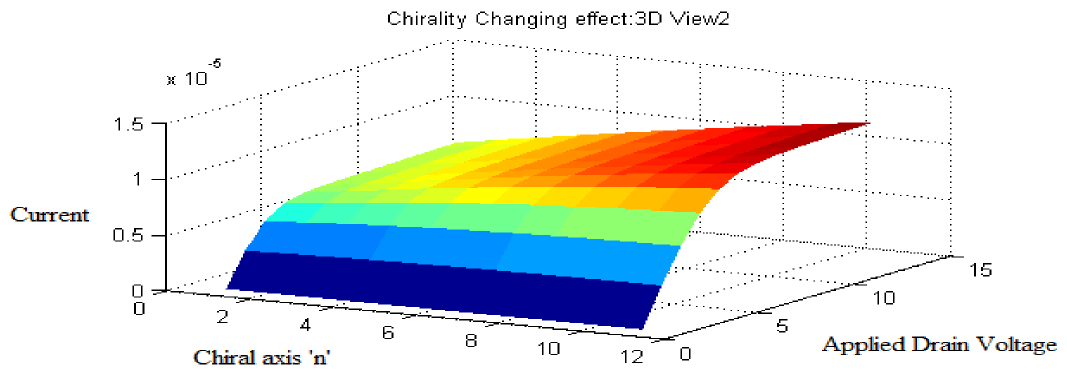

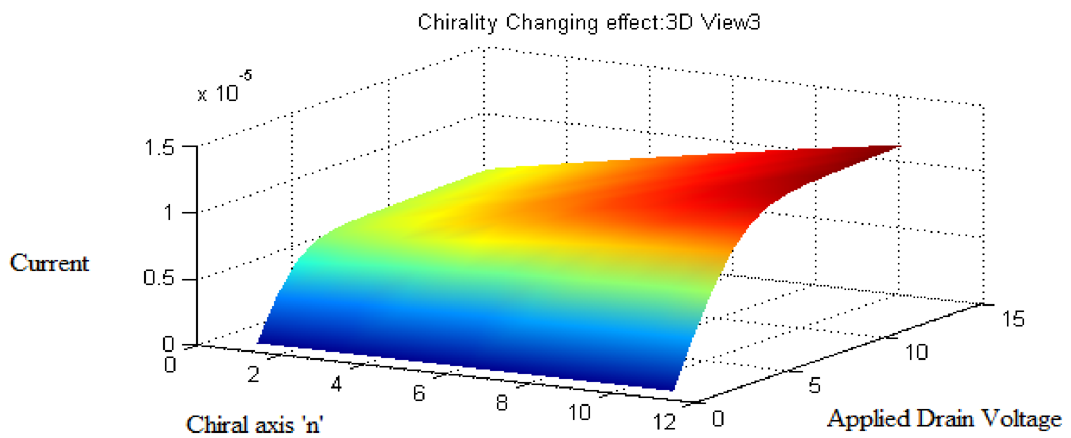

Figure 3.20: Effect of Chiral Axis 'n' variation on I-V characteristics of Carbon Nanotube Field Effect Transistor with Elastic Scattering Factor

The following figure 3.21 displays the change effect of chiral index ‘m’ when elastic scattering factor is accounted for. The minimum current was measured for m=1 which held the value of 8.559×10^{-6} A and m=12 gave out the maximum current of 1.281×10^{-5} A.

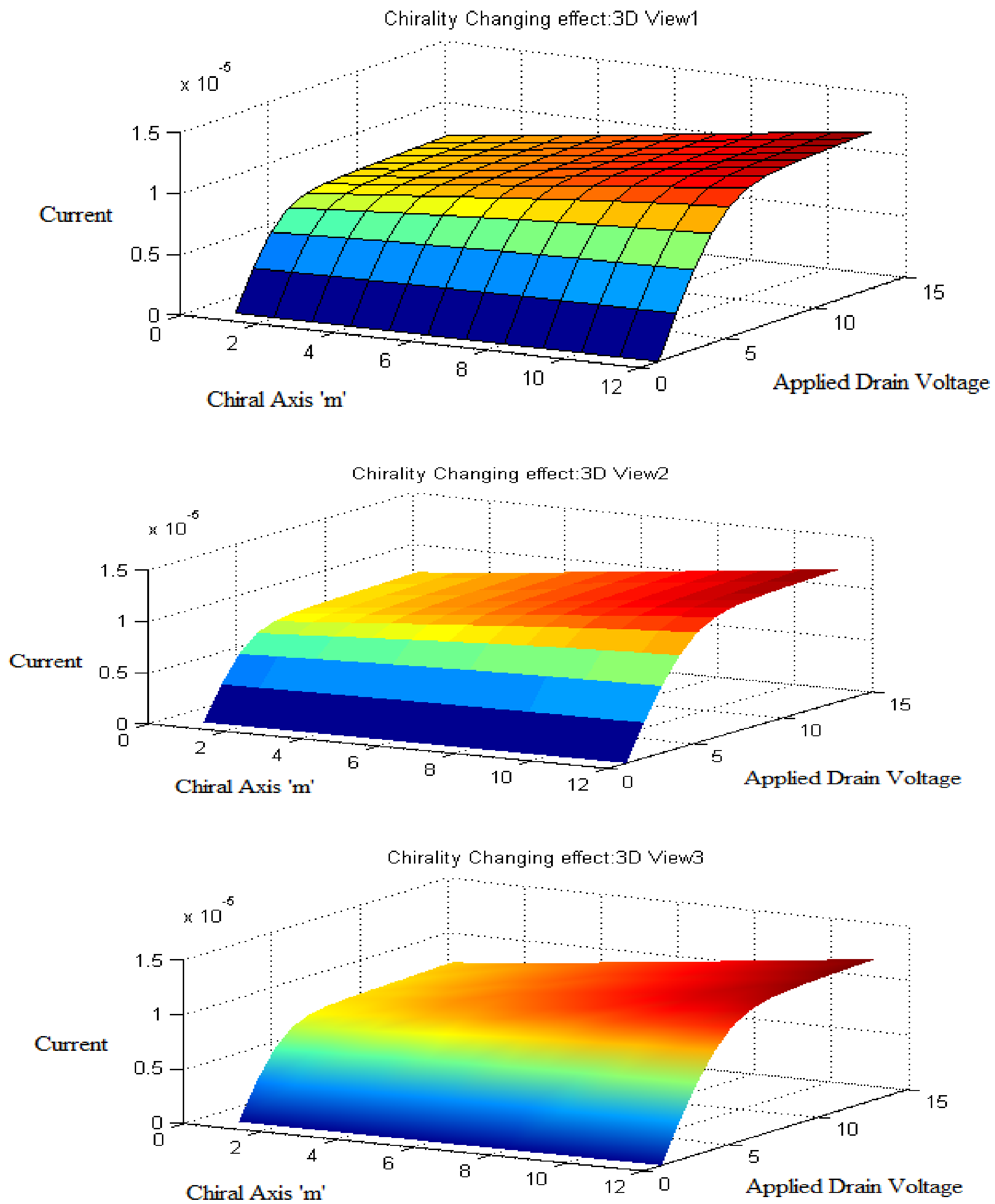

Figure 3.21: Effect of Chiral Axis ‘m’ variation on I-V characteristics of Carbon Nanotube Field Effect Transistor with Elastic Scattering Factor

3.2.5.2 Bandgap Strain Effect:

We can see the effect of bandgap strain on CNTFET from the figure 3.22. While the chiral index n held a value of 11, the smallest amount of current was observed. The value of this current was 5.299×10^{-6} A. This current kept increasing until it reached its peak value when value of n is 21. The peak value was observed to be 8.623×10^{-6} A.

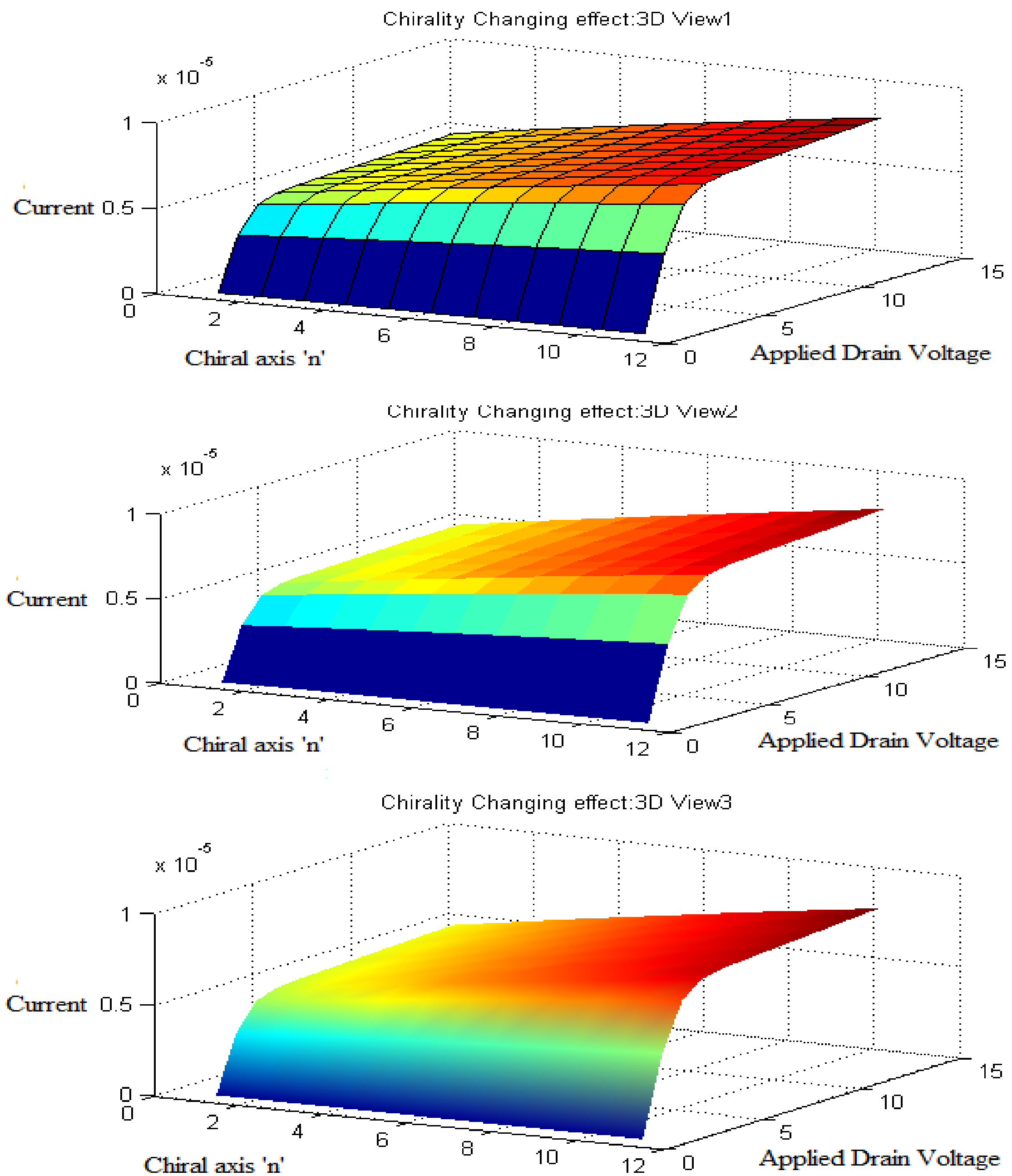

Figure 3.22: Effect of Chiral Axis 'n' variation on I-V characteristics of Carbon Nanotube Field Effect Transistor with Bandgap Strain Factor

Again, from figure 3.23, when value of chiral index m was 1, the smallest amount of current was observed. The value of this current was 6.223×10^{-6} A. The current kept increasing until it reached its peak value of 1.291×10^{-5} A when the value of m was 12.

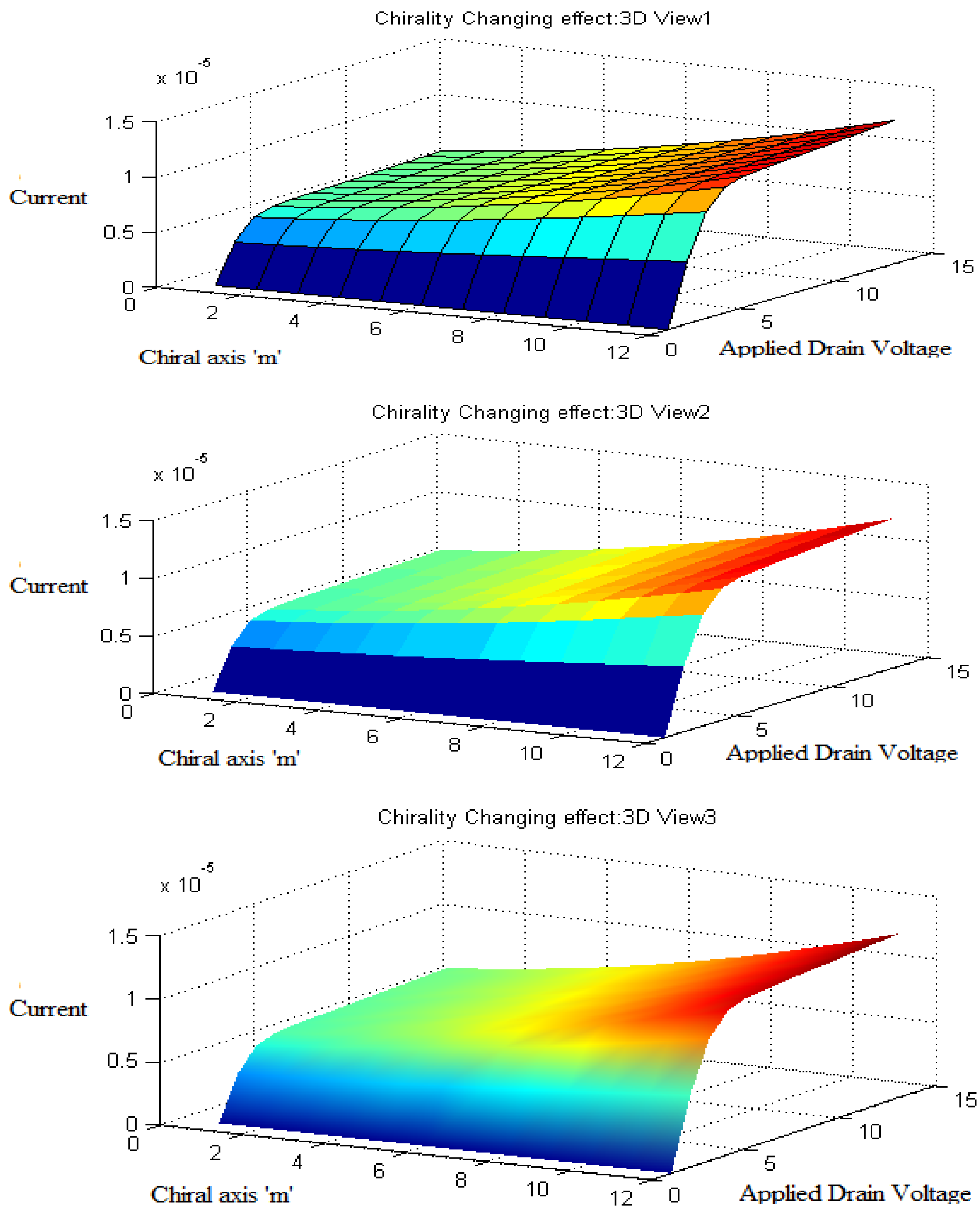

Figure 3.23: Effect of Chiral Axis 'm' variation on I-V characteristics of Carbon Nanotube Field Effect Transistor with Bandgap Strain Factor

3.2.5.3 Tunneling Effect:

The figure 3.24 clearly shows the effect of tunneling on CNTFET. When chiral index n was 11, the smallest amount of current was observed. The value of this current was 7.826×10^{-6} A and for when n was 21 the largest amount of current was found with a value of 1.381×10^{-5} A.

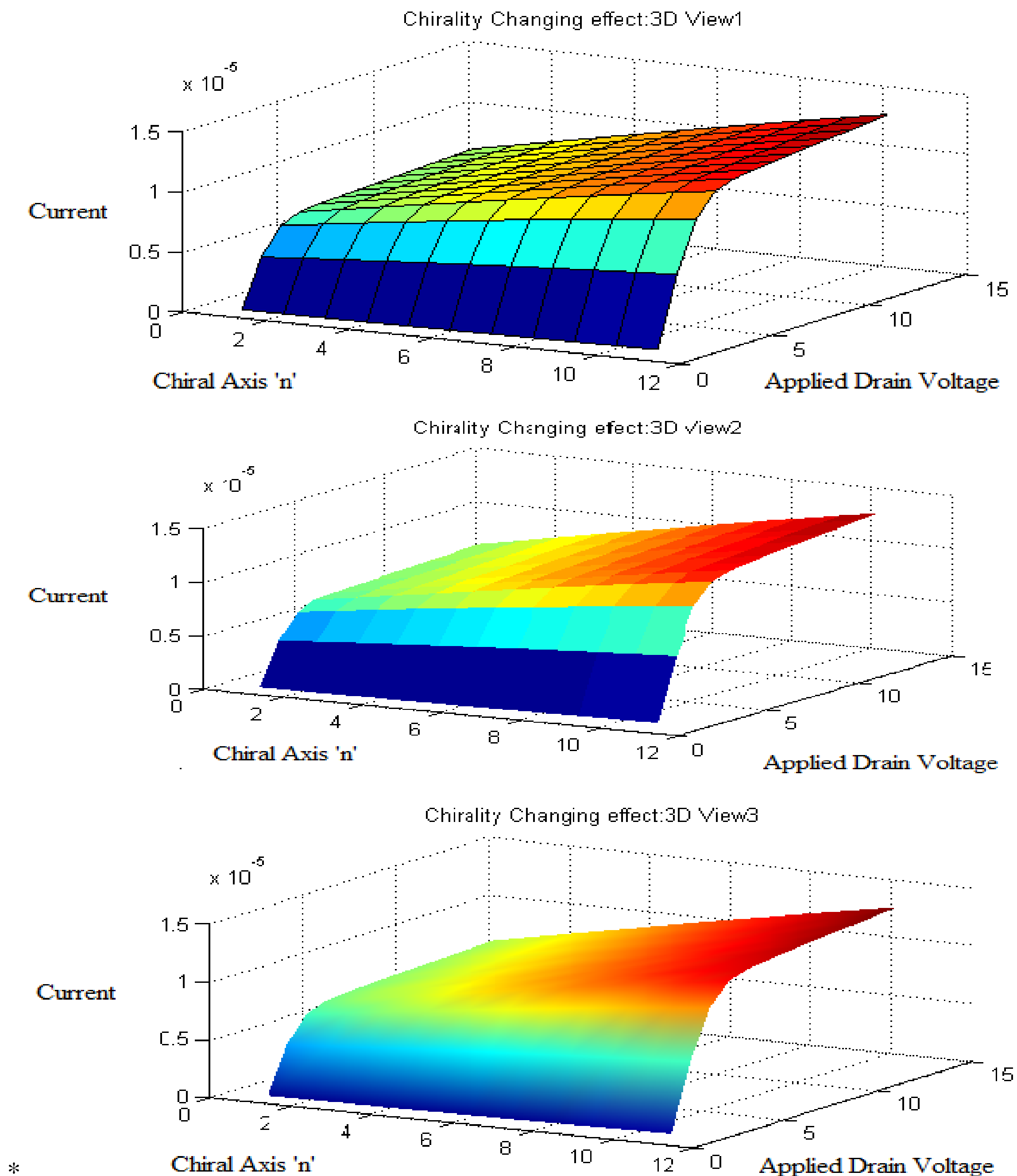

Figure 3.24: Effect of Chiral Axis ‘n’ variation on I-V characteristics of Carbon Nanotube Field Effect Transistor with Tunneling Factor

In figure 3.25, when chiral index m was 1, the smallest amount of current was observed. The value of this current was 8.962×10^{-6} A and for when n was 12 the largest amount of current was found with a value of 2.797×10^{-5} A.

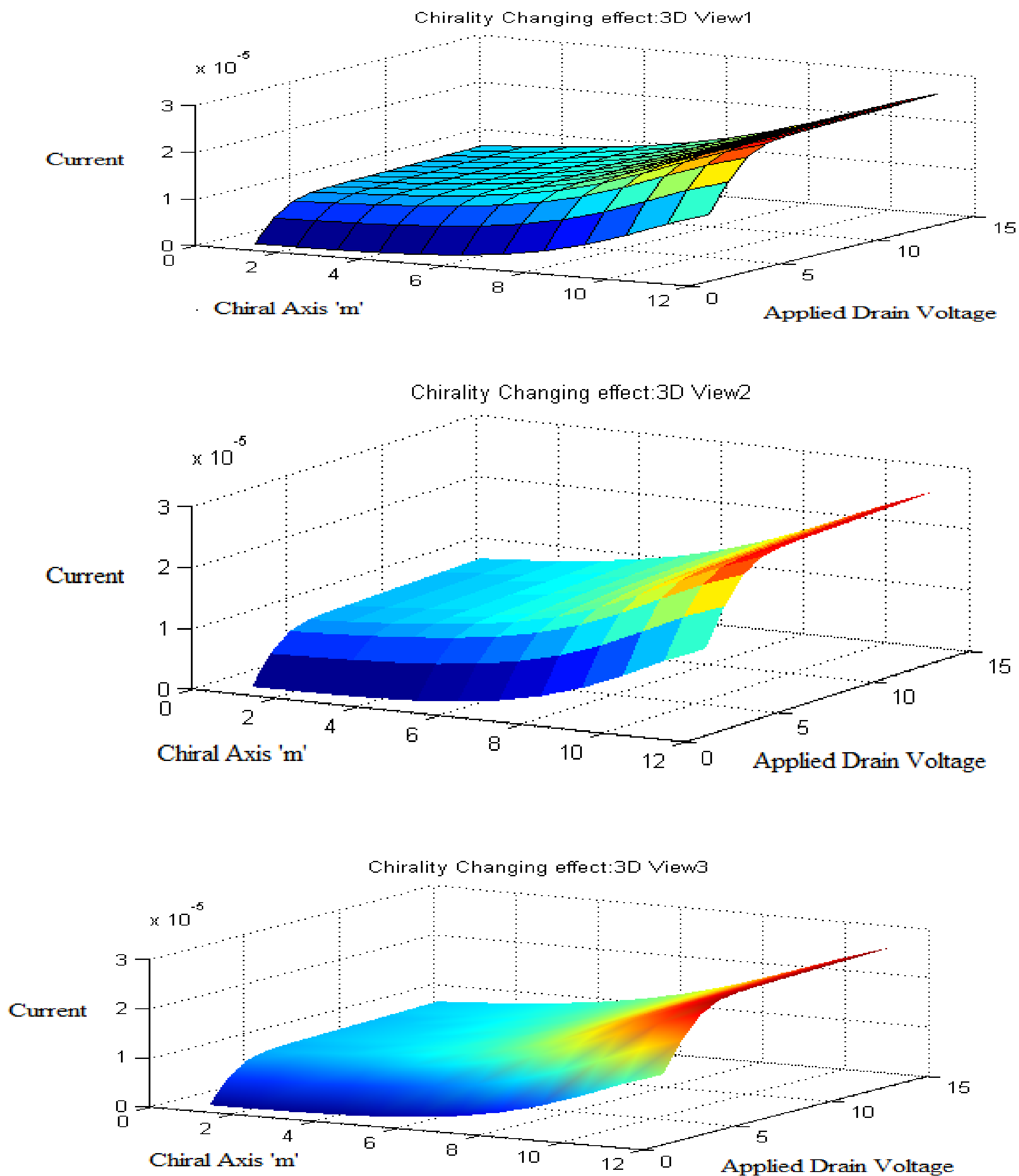

Figure 3.25: Effect of Chiral Axis 'm' variation on I-V characteristics of Carbon Nanotube Field Effect Transistor with Tunneling Factor

3.2.5.4 Combined Non-Ballistic Effect:

From the following figure 3.26, we can clearly observe the combined non-ballistic effect on CNTFET. When n was 11, the lowest amount of current was observed. The value of this current was 5.173×10^{-6} A and when n was 21 the highest amount of current was found with a value of 8.906×10^{-6} A.

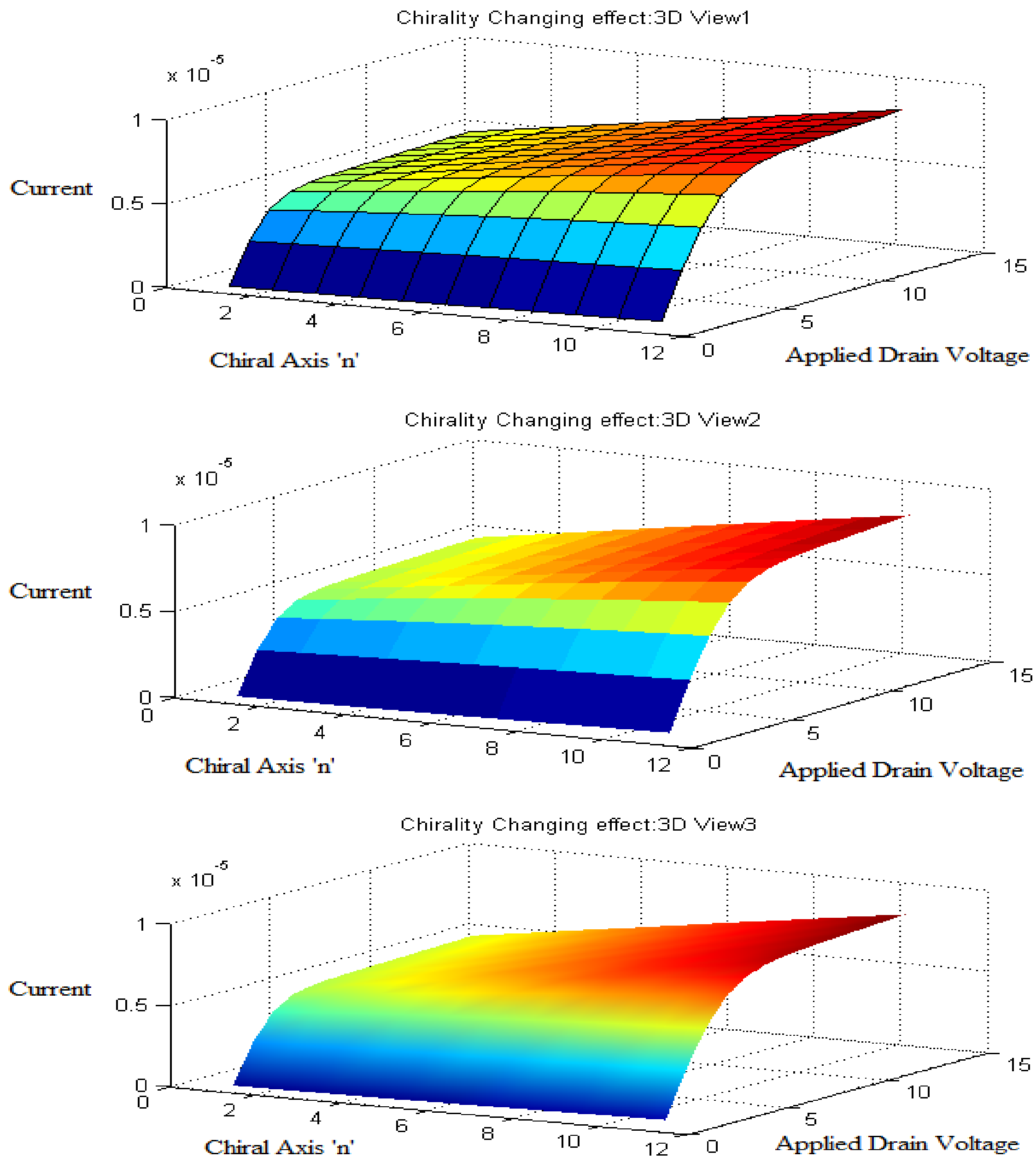

Figure 3.26: Effect of Chiral Axis ‘n’ variation on I-V characteristics of Carbon Nanotube Field Effect Transistor with Combined Non-Ballistic Effect

It can be seen in figure 3.27 that when m was 1, the lowest amount of current was observed. The value of this current was 6.148×10^{-6} A and when m was 12 the highest amount of current was found with a value of 2.679×10^{-5} A.

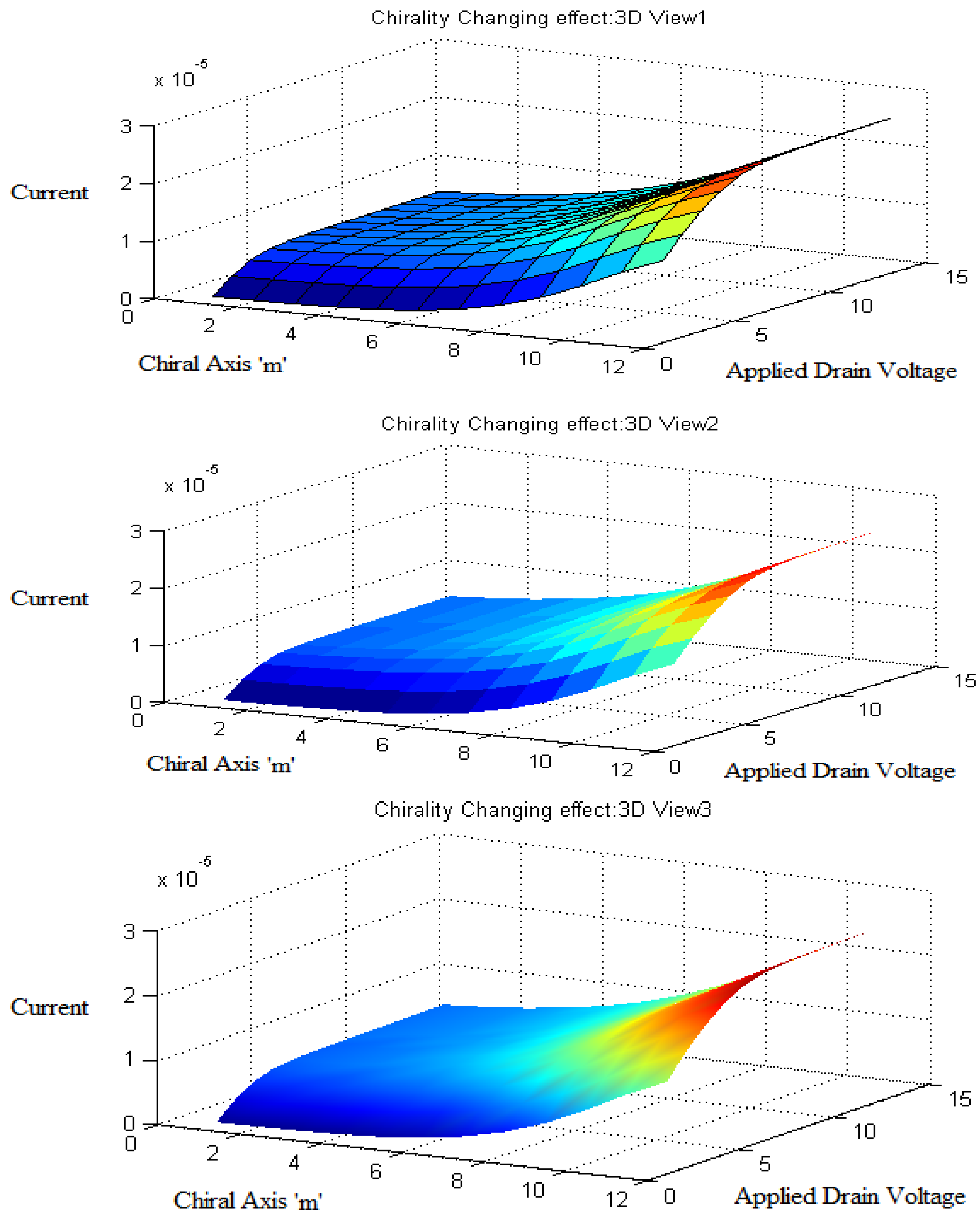

Figure 3.27: Effect of Chiral Axis 'm' variation on I-V characteristics of Carbon Nanotube Field Effect Transistor with Combined Non-Ballistic Effect

From our results, we can deduce that chirality has a very good influence on the performance of carbon nanotube field effect transistor. Drain current increases with the increase of chiral indices n and m.

The deviation from ideal behavior due to non-ballistic effects can be easily observed once the results have been compared with ballistic results found Khan *et al*. [96]. The ballistic simulation was run with the same values of the parameters and it was found that when n was 11, the drain current was 7.231×10^{-6} A and when n was 21, it was 1.312×10^{-5} A. This is clearly superior to the obtained non-ballistic results. The figure 3.28 shows the ballistic characteristics in 3D.

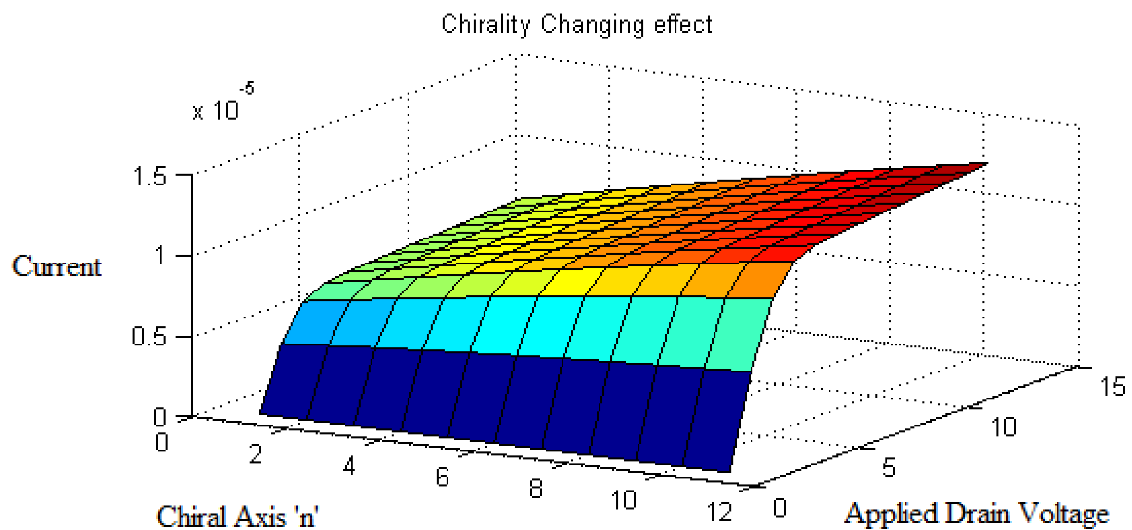

Figure 3.28: Effect of Chiral axis ‘n’ variation on I-V characteristics of Carbon Nanotube Field Effect Transistor with Ballistic Effect [96]

Again, the ballistic simulation [96] was run with the same values of the parameters but this time chiral axis n was kept constant. For this case, it was found that when value of m was 1, the drain current was 8.874×10^{-6} A and when m reached the value of 12, it was 1.346×10^{-5} A. This is clearly superior to the obtained non-ballitic results. The ballistic transport characteristic in 3D is shown in figure 3.29.

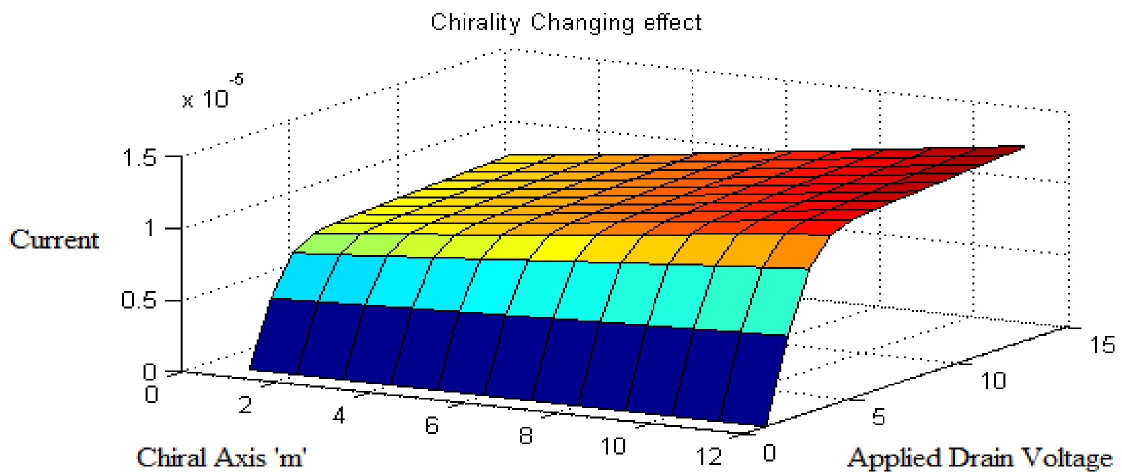

Figure 3.29: Effect of Chiral axis 'm' variation on I-V characteristics of Carbon Nanotube Field Effect Transistor with Ballistic Effect [96]

3.2.6 Variation of I-V characteristics with respect to Gate Voltage V_g:

Change of I-V characteristics by varying gate voltage V_g was also observed. Gate voltage was varied from 0 to 0.6. The other parameters were kept constant. Temperature was taken to be 300 K, gate oxide thickness was 1.5 nm, dielectric constant was 3.9, chiral indices n and m were 13 and 0 respectively. Also, gate control and drain control parameters were fixed at .88 and .035 respectively. Number of bias points taken was 13.

When Elastic scattering was considered, the current when both gate and drain voltage was 0.6 was 8.254×10^{-6} A. The result can be seen in figure 3.30.

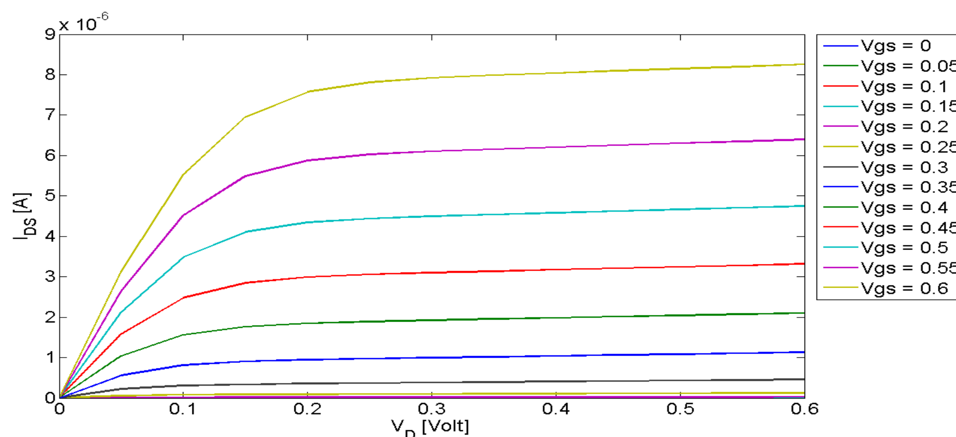

Figure 3.30: Change of I-V characteristics with Gate Voltage when only Elastic Scattering Effect is considered

At the same point, with only bandgap strain, the current was measured at 6.01×10^{-6} A in figure 3.31.

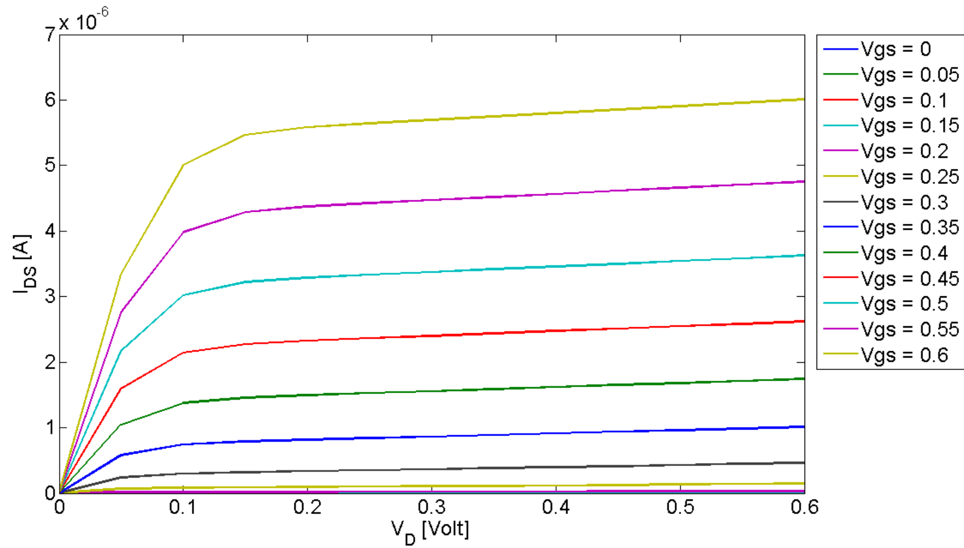

Figure 3.31: Change of I-V characteristics with Gate Voltage when only Bandgap Strain Effect is considered

For the same point, by considering only tunneling effect, 8.684×10^{-6} A current was obtained from figure 3.32.

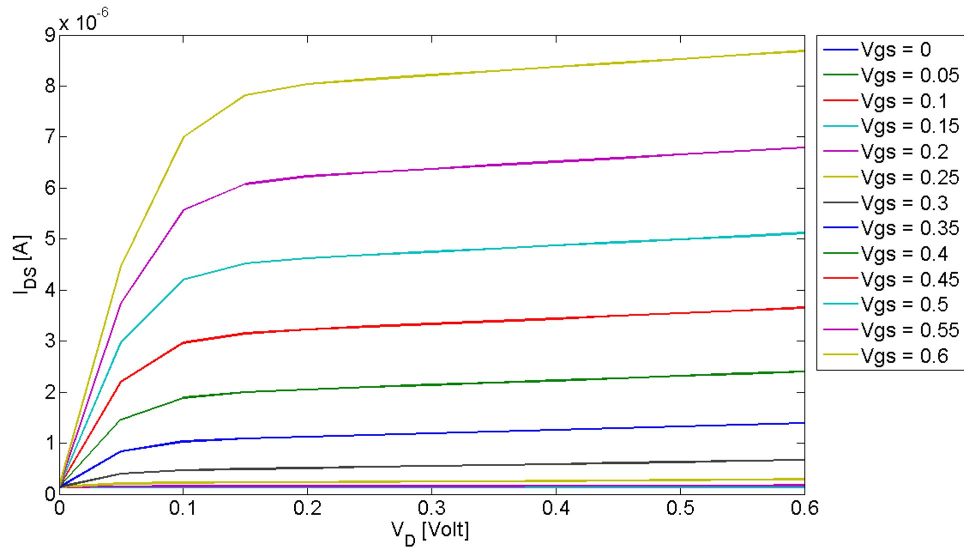

Figure 3.32: Change of I-V characteristics with Gate Voltage when only Tunneling Effect is considered

When all the effects have been considered together, the current at that same point was 5.95×10^{-6} A. This can be observed in figure 3.33.

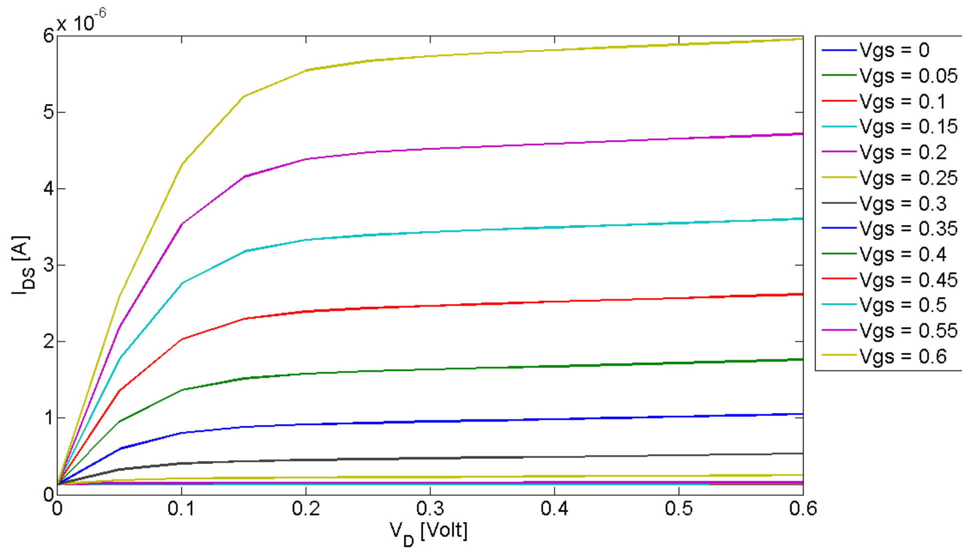

Figure 3.33: Change of I-V characteristics with Gate Voltage when total Non-Ballistic Effect is considered

For ballistic transport, calculated from the model designed by Rahman *et al* [35], the obtained current at the same point was valued at 8.549×10^{-6} A. The result is shown in figure 3.34.

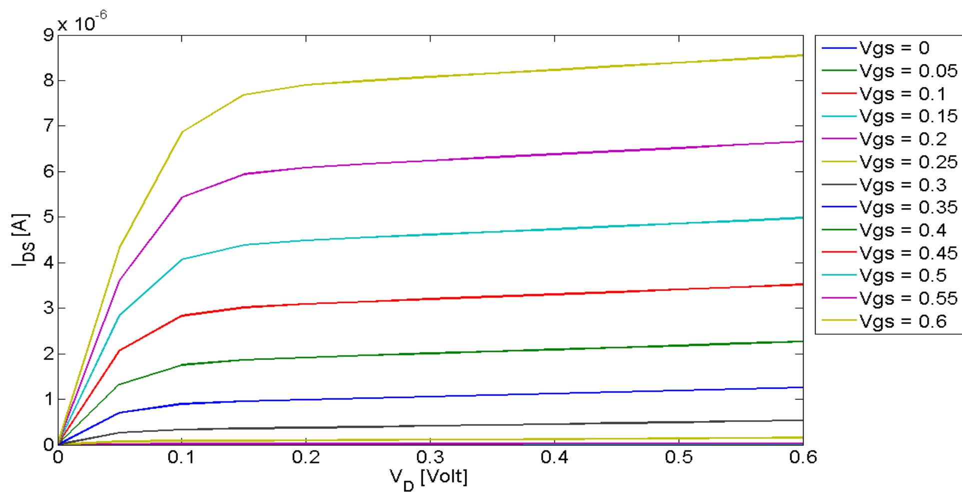

Figure 3.34: Change of I-V characteristics with Gate Voltage when Ballistic Effect is considered [35]

It can be seen when compared to the ballistic results that, bandgap strain affects the performance of the CNTFET the most. Also, another interesting aspect is that tunneling effect yields a higher current than ballistic effect. This is due to the fact that the tunneling current is added to the drain current and increases the total drain current. However, this should be noted that tunneling effect lowers the self-consistent potential and thus worsens the threshold characteristics of the CNTFET [45].

The authenticity of this work can be proved easily by comparing the obtained results with the findings of another research group. The ballistic and non-ballistic effects were compared by Tom J. Kazmierski, Dafeng Zhou, Bashir M. Al-Hashimi and Peter Ashburn in their work "Numerically Efficient Modelling of CNT Transistors With Ballistic and Non-Ballistic Effects For Circuit Simulation" [45]. Their work yields identical results to those of ours. Their results are displayed in the following figure 3.35.

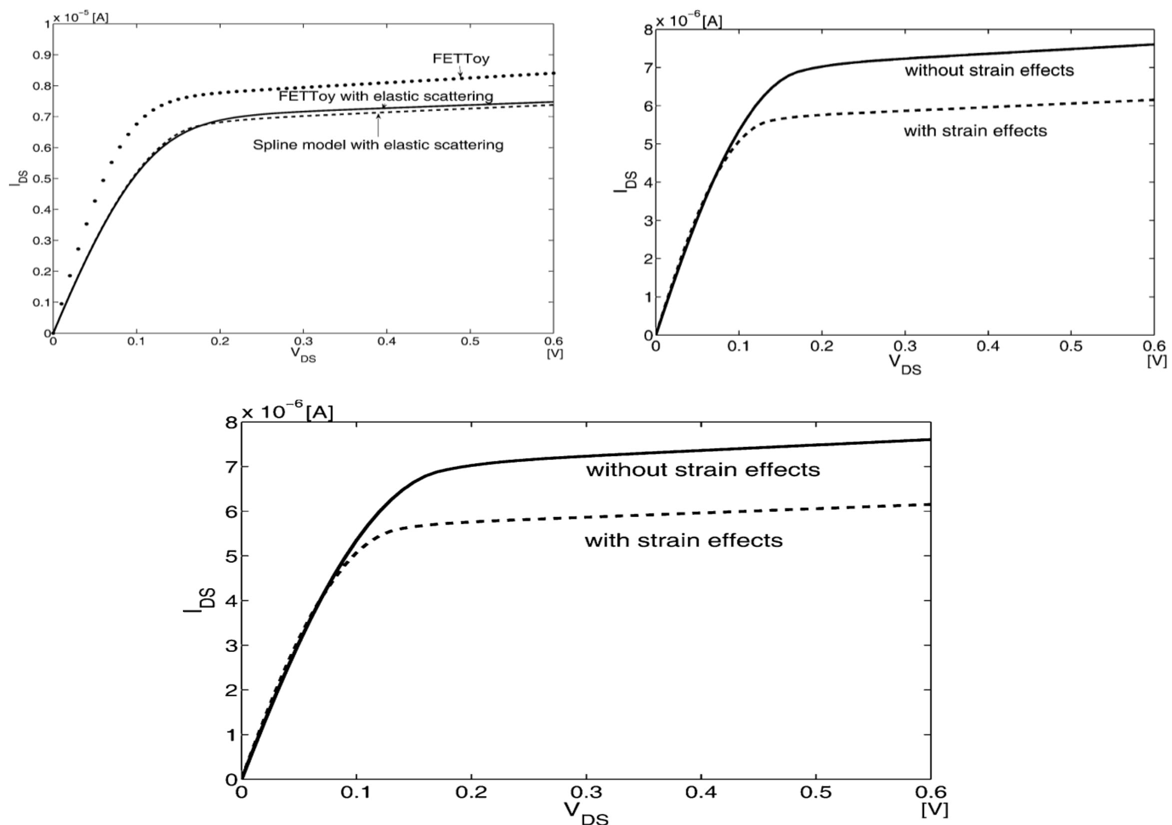

Figure 3.35: Non-Ballistic effects observed by Tom J. Kazmierski, Dafeng Zhou, Bashir M. Al-Hashimi and Peter Ashburn [45]

When compared in the same frame, our work produces extremely similar results and very little deviation from the above mentioned work except for the small deviation in tunneling effect. This was due to making some approximations in the calculations. Moreover, our work produces the combined non-ballistic effect which has not been produced by any other groups so far. Figures 3.36 and 3.37 show the results of the present work.

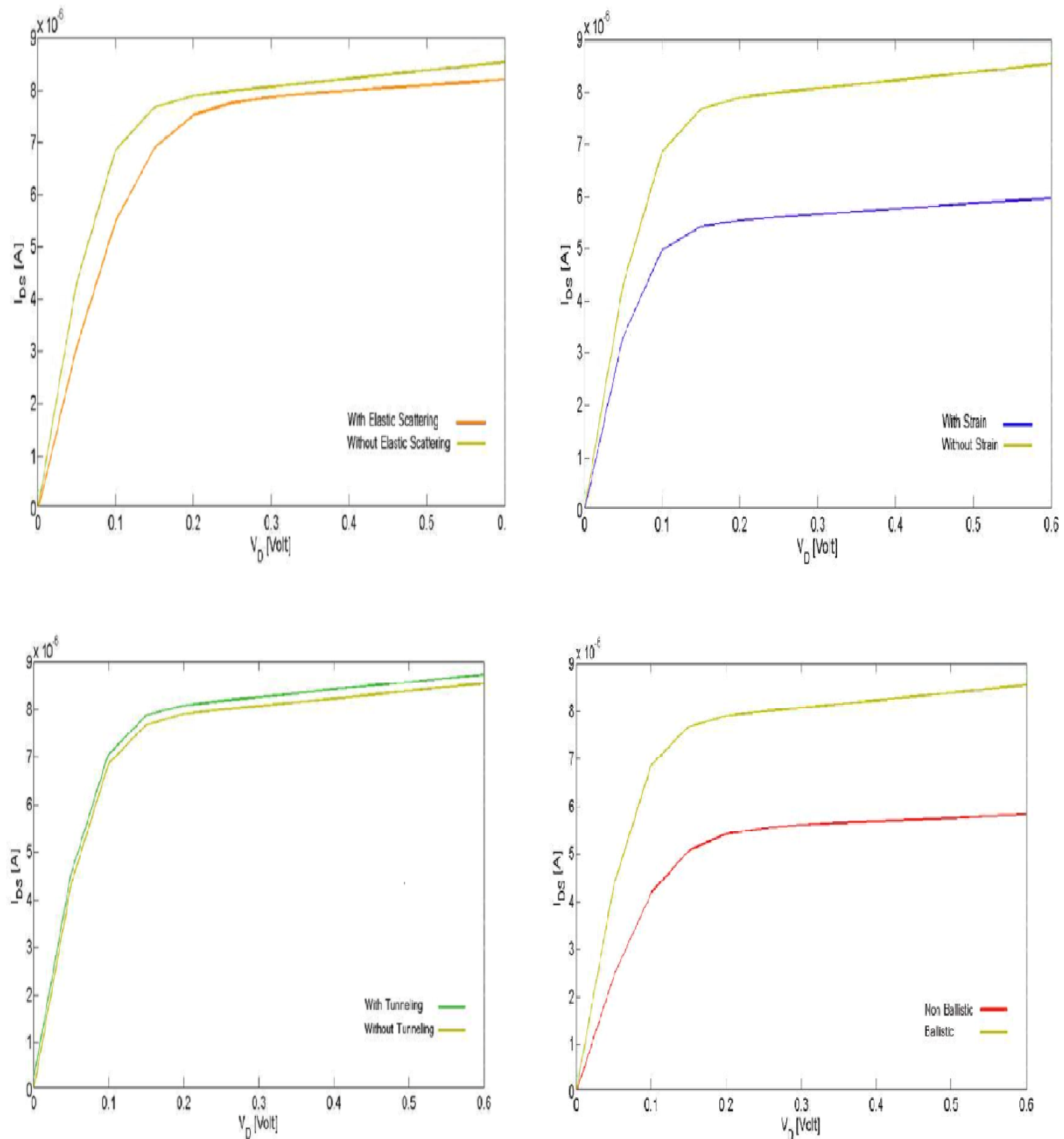

Figure 3.36: Non-Ballistic effects observed and compared with ballistic effects in this work

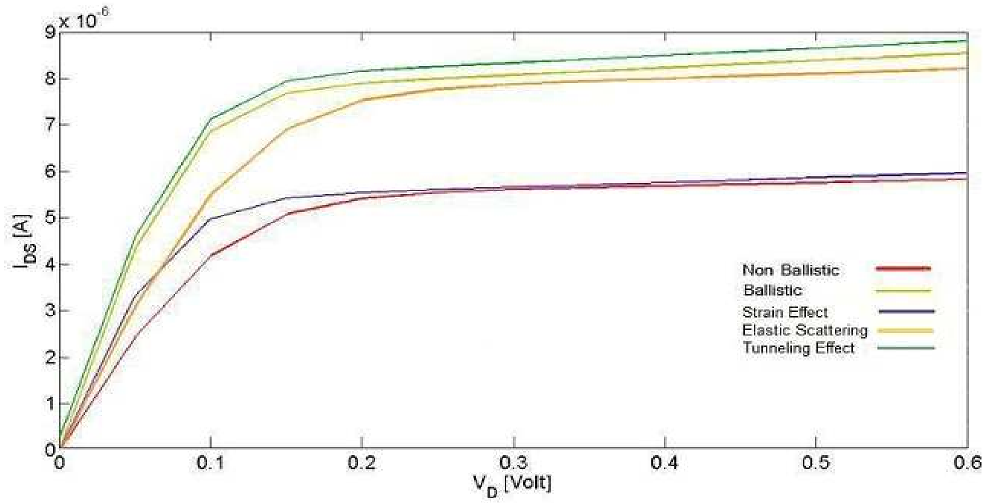

Figure 3.37: Ballistic vs. Non-Ballistic effects as observed in this work

3.2.7 Change in Tunnel Control Parameter with parameters:

Another novel aspect of our work is that here, a tunnel control parameter F was calculated using a different technique and change in F was observed with the change of different parameters, such as, channel length, temperature and chiral indices n and m. Tunnel control parameter is very important in calculating tunneling effect.

$$T_t \approx \frac{\pi^2}{9} e^{-\left(\pi\sqrt{m^* E_g^3}/\sqrt{8q\hbar F}\right)} \quad (51)$$

$$I_t = \frac{4qkT}{h} T_t \sum_{m=1}^{M}\left[\ln\left(1 + e^{(qV_{\text{DSeff}} - E_{geff}/2 - E_F)/K_B T}\right) - \ln\left(1 + e^{qV_{\text{DSeff}} - E_F/K_B T}\right)\right] \quad (52)$$

From the equations (52) and (53) [45], the relation between tunnel control parameter F with the tunneling current can be very easily seen.

3.2.7.1 Change with channel length:

Channel length was varied from 200 nm to 300 nm. Other parameters involved in the calculation were drain voltage V_{DS}, tunneling current I_t, temperature and chiral indices n and m. The other parameters were constant at default values. Drain voltage was fixed at 0.5V, tunneling current was kept at 2.8×10^{-7} A, the temperature was taken to be 300 K and the chiral indices n and m

were taken at 13 and 0 respectively. From figure 3.38, it can be observed that F decreases with the increase of channel length.

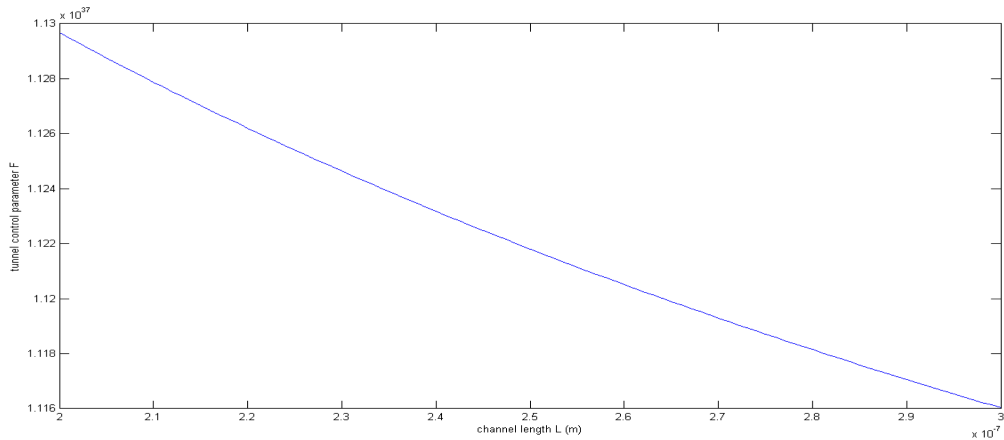

Figure 3.38: Change in tunnel control parameter with Channel Length

3.2.7.2 Change with Temperature:

The temperature was varied from 273 K to 323 K. Other parameters remained constant at their default values. Channel length was chosen to be 300 nm. As shown in the figure 3.39, it was observed that F increases almost linearly with the temperature.

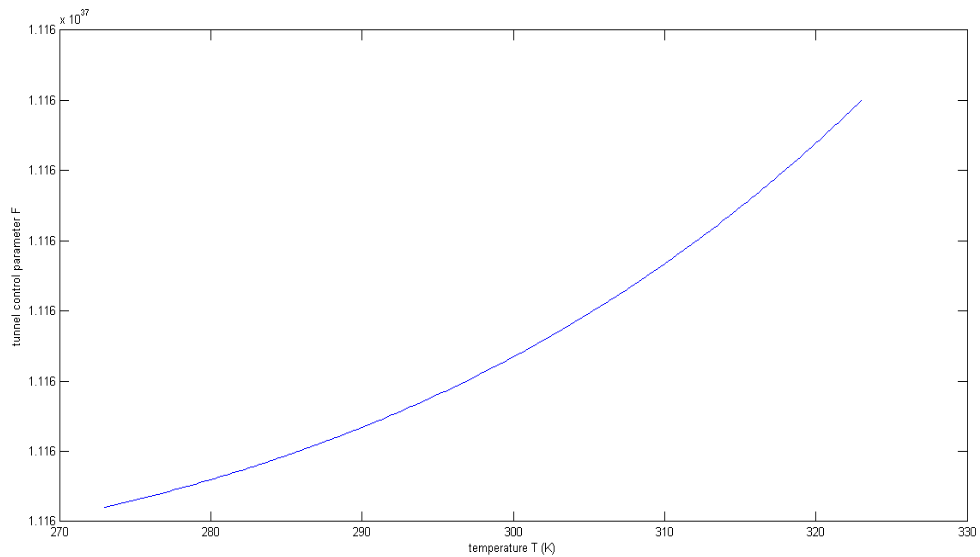

Figure 3.39: Change in tunnel control parameter with Temperature

3.2.7.3 Change with Chiral index n:

Chiral index n was varied from 11 to 23 while the other constants remained fixed at default values. It should be mentioned that the temperature was taken at 300 K. From the obtained result, it was seen that as the value of n increases, the value of F decreases. It can be seen from figure 3.40 that tunnel control parameter is inversely proportional to chiral index n.

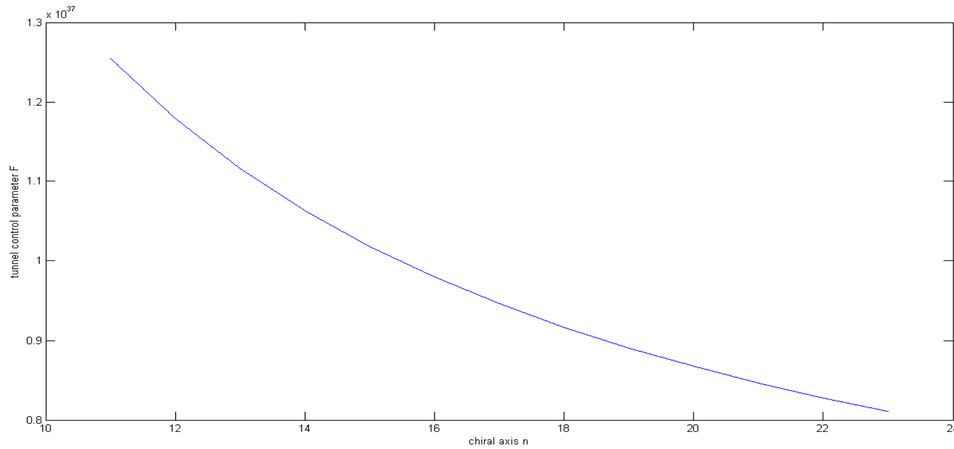

Figure 3.40: Change in tunnel control parameter with Chiral Index n

3.2.7.4 Change with Chiral index m:

Chiral index m was varied from 0 to 12 while n was kept constant at 13. The other parameters involved also maintained their default values. From the output shown in figure 3.41, it was found that tunnel control parameter has an inverse relation with chiral index m.

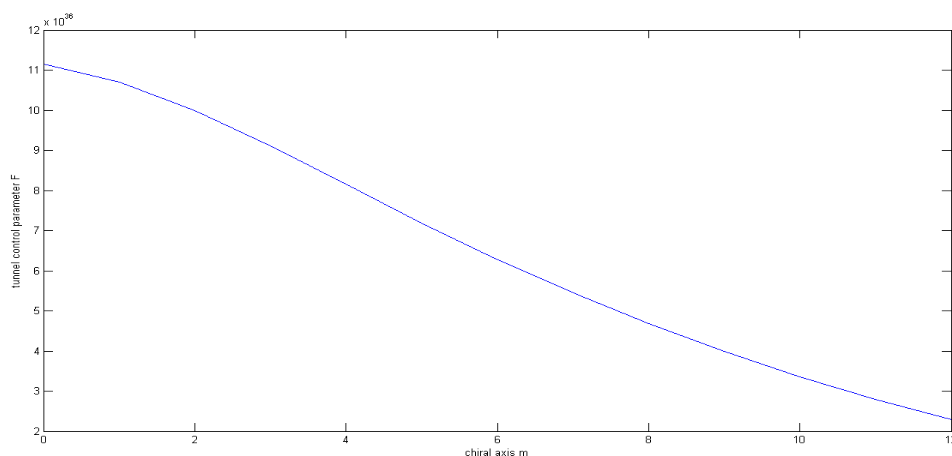

Figure 3.41: Change in tunnel control parameter with Chiral Index m.

3.2.8 Summary

This research investigates the change in non-ballistic characteristics of CNTFET with respect to gate oxide thickness, temperature, dielectric constant and chirality. Also, non-ballistic effects on the performance of CNTFET were studied by comparing the results with previously reported ballistic results. At the same time, the authenticity of the work is proved by comparing the obtained non-ballistic results with already reported non-ballistic outcomes of another group. Very little deviation was observed in the results of the two groups. In the end, change effects of tunnel control parameter with channel length, temperature and chirality were observed. This enabled a new way to study tunneling effect.

So, to summarize the results:

- Electron concentration at the top of the barrier increases with temperature while decreases with chirality.
- Increasing gate oxide thickness reduces drain current.
- Effect of temperature on the performance of CNTFET is very insignificant and can be ignored.
- Drain current increases with the value of dielectric constant.
- Chirality wields a great influence on drain current. Higher the chirality of the nanotube is, the better its performance will be.
- Bandgap strain affects the drain current the most among the non-ballistic effects. Without strain effect, non-ballistic components deviate from the ideal behavior by a very small amount.
- Tunnel control parameter maintains an inverse relation with channel length and chirality while it increases with temperature.

Chapter 4

Conclusions and Future Research

4.1 Conclusion

Carbon nanotube field effect transistor is known as one of the most promising nanotube devices. The research and understanding of CNTFET has been ever progressing rapidly since its evolution about 5-6 years ago and henceforth there exists swift improvements in the performance of this device. Ideal CNT transistor based logic circuits can provide significant energy and performance benefits over the traditional CMOS which created the urge for CNT transistors based devices and its applications in logic circuit design. However nano devices suffer from high defect rates and material variation due to the fundamental limitation of the fabrication process. It is possible to make very small scale transistors due to the nano scale size of CNT and its exceptional property of high current density growth that can bump up the device's performance to a high standard. CNT can have either semiconducting or metallic characteristic, it depends on its chirality. Metallic CNT can be used as wire on circuit boards or electronic interconnections whereas semiconducting CNT can be used as transistor in devices.

Computers models created in MATLAB play a massive role to quantitatively recognize the impact of defects and variation on the electrical characteristics of CNT transistors. The contributions presented in this thesis paper provides fast and accurate simulation models for CNT transistors including ballistic and non-ballistic transport effects based on numerical solution of the theoretical CNT mobile charge density equations. A summary of our results and analysis is given in the next section following our proposed future work.

In our results part, effect of gate oxide thickness was analyzed on the performance of non-ballistic CNTFET. It was seen that gate oxide thickness's influence was quite much on the I-V characteristics of the transistor. It was found that current decreases with gate oxide thickness. So, during the design of CNTFET, gate oxide thickness should be kept low.

The second analysis was done by varying temperature. It was observed that I-V characteristics do not vary that much with the change of temperature. Effect of temperature on the performance of non-ballistic CNTFET can be ignored.

Thirdly, effect of dielectric constant was scrutinized and was found that current increases slowly with increasing dielectric constant. So, by changing the dielectric material in the gate, it is possible to improve the performance of carbon nanotube transistors.

Then, chirality changing effect on the I-V characteristics was studied. It was detected that current increases rapidly with the increasing chirality. Therefore, it was deduced that drain current maintains a positive relationship with chirality.

The main focus of this research was to study the effect of non-ballistic effects on the current-voltage relationship separately and then together. It was observed that bandgap strain affects the current-voltage curve the most and lowers the performance of CNTFET. Tunneling effect and elastic scattering effect have comparatively smaller effect on the performance of the device. Therefore, the combined non-ballistic effect is highly influenced by the bandgap strain.

Another result of this work was the analysis of tunnel control parameter by changing parameters like channel length, temperature and chirality. It was noticed that tunnel control parameter ‘F’ maintains an upward relationship with temperature while it decreases with increasing channel length and chirality.

In the end, by examining the results, it can be safely said that carbon nanotube field effect transistor has huge potential in the electronics industry and this market can be exploited to bring revolutionary changes to the world of electronics.

4.2 Prospected Future Research

Carbon nanotube transistor modeling has a wide number of areas which can be further explored and where there is more scope of development and improvement. Till now our thesis paper has

been focused on the ballistic and non-ballistic effects on the I-V characteristics of CNTFET. The following would be out future prospects:

1) So far we have observed the changes in the I-V curve with parameters such as temperature, gate oxide thickness, chirality and dielectric constant but we would like to further analyze the effects on varying transconductance and conductance as well in ballistic and non-ballistic CNTFET.
2) We have taken the non-ideal effects such as elastic scattering, band gap tuning with strain and tunneling into account. In future we are determined to work with the fourth type of non-ideality called phonon scattering mechanism consisting of acoustic and optical phonon scattering and hence observe the I-V curve we get for this effect by varying the above mentioned parameters accordingly.
3) Then we wish to study and investigate bundled carbon nanotubes and multi walled carbon nanotubes and generate the I-V characteristics curves for the entire criterion mentioned above.
4) In chapter 2 we discussed about the non-ideal effects such as elastic scattering, band gap tuning with strain, tunneling and phonon scattering however, more non-ballistic transport effects of CNT transistors including Schottky contacts and doping effects may significantly affect the performance of CNTFETs. Therefore further analysis of the impacts of such transport effects on the performance of CNTFETs needs to be established along with its numerical expressions representing these effects to be developed.
5) Our thesis work considers on modeling the channel current properties of CNT considering only the inner transistor characteristics. However to develop a model suitable for SPICE simulators more peripheral effects of CNT transistors including parasitics, p-n junctions and substrate leakage need to be implemented. With peripheral effects added, the CNT transistor model may describe both the inner transport characteristics and the interaction between transistors in circuit level simulation.

References

[1] J. Appenzeller, J. Knoch, V. Derycke, R. Martel, S. Wind, and P. Avouris, "Fieldmodulated carrier transport in carbon nanotube transistors," Physical Review Letters, vol. 89, pp. 126801.1-126801.4, 2002.

[2] S. Heinze, J. Tersoff, R. Martel, V. Derycke, J. Appenzeller, and P. Avouris, "Carbon nanotubes as Schottky barrier transistors," Physical Review Letters, vol. 89, pp. 106801.1-106801.4, 2002.

[3] J. Guo, S. Datta, and M. Lundstrom, "A numerical study of scaling issues for Schottky-Barrier carbon nanotube transistors," IEEE Transactions on Electron Devices, vol. 51, pp. 172-177, 2004.

[4] M. Radosavljevic, S. Heinze, J. Tersoff, and P. Avouris, "Drain voltage scaling in carbon nanotube transistors," Applied Physics Letters," Vol. 83, pp. 2435-2437, 2003.

[5] David J. Frank et al, "Device Scaling Limits of Si MOSFETs and Their Application Dependencies," proceedings of the IEEE, vol. 89, no. 3, march 2001.

[6] Chen, Z. et. al. "IDDQ Testing for Deep-Submicron ICs: Challenges and Solutions," IEEE Design and Test of Computers.pp: 24-33, 2002.

[7] Taur, Y., "CMOS design near the limit of scaling," IBM J. Ref. & Dev.,Volume: 46(2): pp: 213-220, 2002.

[8] Compano, R. ed. "Technology Roadmap for Nanoelectronics," Microelectronics Advanced Research Initiative, 2000.

[9] T Surukai, "Perspectives on power aware electronics", Keynote presentation, F, ISSCC Conference, pp.26-29, 2003.

[10] John L. Hennessy and David A. Patterson, "Computer Architecture, A Qualitative Approach", Ed. 3, pp. 14. 55 Carbon Nanotube Field Effect Transistor

[11] Max Schulz, “The end of the road for Silicon?”, Nature, Vol 399, 24 June, 1999.

[12] Jaldappagari Seetharamappa, Shivaraj Yellappa and Francis D’Souza, “Carbon Nanotubes: Next Generation of Electronic Materials,” The Electrochemical Society Interface, Summer 2006.

[13] Paul Holister, Tim Harper and Christina Roman Vas, “Nanotubes White Paper,” CMP Cientifica, January 2003.

[14] Xiaolei Liu,“Synthesis, Devices and Applications of Carbon Nanotubes,” Thesis report, University of Southern California, January 2006.

[15] M. S. Dresselhaus, G. Dresselhaus, Ph. Avouris,“Carbon nanotubes,” Topics in Applied Physics, Springer-Verlag, Berlin, 2001.

[16] T. W. Odom, J. L. Huang et al.,“Atomic structure and electronic properties of single-walled Carbon Nanotubes,” Nature, Volume 391, January, 1998.

[17] P.R. Bandaru., “Electrical Properties and Applications of Carbon Nanotube Structures,” Journal of Nanoscience and Nanotechnology Vol.7, 1–29, 2007.

[18] T.Grace, “An Introduction to Carbon Nanotubes,” Summer, Stanford University, 2003.

[19] Zoheir Kordrostami and Mohammad Hossein Sheikhi (2010). “Fundamental Physical Aspects of Carbon Nanotube Transistors,” Carbon Nanotubes, Jose Mauricio Marulanda (Ed.), ISBN: 978-953-307-054-4, InTech, Available from

[20] Sanjeet Kumar Sinha and Saurabh Chaudhury,“Advantage of Carbon Nannotube Field Effect Transistor (CNTFET) over Double-Gate MOSFET in Nanometre Regime,” National Conference on Computing and Communication Systems (NCCCS), 2012.

[21] P A Alvi et al., “Carbon nanotubes field effect transistors: A review,” Indian Journal of Pure & Applied physics, Vol.43, December, 2005.

[22] Phaedon Avouris et al., “ Carbon Nanotube Electronics” Proceedings of the IEEE, Vol 91, No. 11, November 2003.

[23] Rasmita Sahoo and R. R. Mishra, “Simulations of Carbon Nanotube Field Effect Transistors,” International Journal of Electronic Engineering Research ISSN 0975- 6450 Volume 1 Number 2 (2009) pp. 117–125.

[24] Forro, L. and Schoenberger, C. “Physical Properties of Multi-wall Nanotubes”, Berlin, Germany: Springer-Verlag Berlin Heidelberg, pp: 329-390; 2001.

[25] Avouris et al., "Vertical scaling of carbon nanotube field-effect transistors using top gate electrodes," Applied Physics Letters, 2002.

[26] Dang T., Anghel L., Leveugle R. “CNTFET Basics and Simulation,” International Conference on Design and Test of Integrated Systems in Nanoscale Technology, IEEE Explore 2006.

[27] Guo J., Datta S. and Lundstrom M., “Assessment of Silicon MOS and Carbon Nanotube FET Performance Limits Using a General Theory of Ballistic Transistors,”IEEE.

[28] S. Heinze, J. Tersoff, R. Martel, V. Derycke, J. Appenzeller, and Ph. Avouris, “Carbon Nanotubes as Schottky Barrier Transistors,” Physical Review Letters,Vol.89, 2002.

[29] Jing Guo, Supriyo Datta, and Mark Lundstrom, “A Numerical Study of Scaling Issues for Schottky-Barrier Carbon Nanotube Transistors,” IEEE Transactions on electron devices, Vol.51, No.2, pp. 172-177, 2004.

[30] Mizutani T, Nosho Y, and Ohno Y, “Electrical properties of carbon nanotube FETs,” International Symposium on Advanced Nanodevices and Nanotechnology, Journal of Physics: Conference Series, Vol. 109, pp. 012002, 2008.

[31] P. L. McEuen, M. S. Fuhrer, and H. Park. Single-Walled Carbon Nanotube Electronics. IEEE Trans. on Nanotechnology, 1(1):78–85, Mar. 2002.

[32] Winstead and U. Ravaioli, IEEE Trans. Electron Devices 47, 1241~2000!.

[33] S. Tans et al. Room-temperature Transistor Based on a Single Carbon Nanotube. Nature, 393:49–52, 1998.

[34] S. J. Wind et al. Vertical Scaling of Carbon Nanotube Field-Effect Transistors using Top Gate Electrodes. Applied Physics Letters, 80:3817–3819, May 2002

[35] Anisur Rahman, Jing Guo, Supriyo Datta, and Mark S. Lundstrom.Theory of ballistic nanotransistors. Electron Devices, IEEE, 50(9):1853–1864, September 2003.

[36] Phaedon Avouris, Joerg Appenzeller, Richard Martel, and Shalom J.Wind. Carbon nanotube electronics. Proceedings of the IEEE,91(11):1772–84, November 2003.

[37] Arijit Raychodhury and Kaushik Roy. Carbon nanotube electronics:design of high-performance and low-power digital circuits. IEEE Transactions on Circuits and Systems - I: Fundamental Theory and Applications, 54(11):2391–2401, November 2007.

[38] Jie Deng and H.-S.Philip Wong. A compact spice model for carbonnanotube field-effect transistors including nonidealities and its application - part i: model of the intrinsic channel region. IEEE Transactions on Electron Devices, 54:3186–3194, 2007.

[39] Jie Deng and H.-S.Philip Wong. A compact spice model for carbonnanotube field-effect transistors including non idealities and its application- part ii: full device model and circuit performance benchmarking. IEEE Transactions on Electron Devices, 54:3195–3205, 2007.

[40] Jie Deng and H.-S.Philip Wong. A circuit-compatible SPICE model for enhancement mode carbon nanotube field effect transistors. In 2006 International Conference on Simulation of Semiconductor Processes and Devices, Piscataway, NJ, USA, 6-8 September 2006.

[41] Ming-Hsun Yang, Kenneth B. K. Teo, Laurent Gangloff, William I. Milne, David G. Hasko, Yves Robert, and Pierre Legagneux. Advantages of top-gate, high-k dielectric carbon nanotube field-effect transistors. Applied Physics Letters, 88(11):113507–1–3, March 2006.

[42] Anisur Rahman, Jing Wang, Jing Guo, Sayed Hasan, Yang Liu, Akira Matsudaira, Shaikh S. Ahmed, Supriyo Datta, and Mark Lundstrom. Fettoy 2.0 - on line tool, 14 February 2006. https://www.nanohub.org/resources/220/.

[43] Hamidreza Hashempour and Fabrizio Lombardi. An efficient and symbolic model for charge densities in ballistic carbon nanotube FETs. IEEE-NANO, 1:17–20, 2006

[44] Jie Deng and H.-S.Philip Wong. Modeling and analysis of planar-gate electrostatic capacitance of 1-d fet with multiple cylindrical conducting channels. IEEE Transactions on Electron Devices, 54:2377–2385, 2007.

[45] Tom J. Kazmierski, Dafeng Zhou, Bashir M. Al-Hashimi and Peter Ashburn. A fast, numerical circuit-level model of carbon nanotube transistor. In IEEE Int. Workshop on Design and Test of Defect-Tolerant Nanoscale Architectures (Nanoarch), Santa Clara, CA, 21-22 October 2007

[46] Jean-Christophe Charlier, Xavier Blase, and Stephan Roche. Electronic and transport properties of nanotubes. Reviews of Modern Physics, 79(2):677–732, 2007.

[47] Fei Liu, Kang L. Wang, Chao Li, and Chongwu Zhou. Study of random telegraph signals in single-walled carbon nanotube field effect transistors. IEEE Transactions on Nanotechnology, 5(5):441–445, September 2006.

[48] Akinobu Kanda, Kazuhito Tsukagoshi, Yoshinobu Aoyagi, and Youiti Ootuka. Gate-voltage dependence of zero-bias anomalies in multiwall carbon nanotubes. Phys Rev Lett, 92(3):036801, 2004.

[49] Carter T. White and Tchavdar N. Todorov. Carbon nanotubes as long ballistic conductors. Nature, 393:240–242, 1998.

[50] Jie Jiang, Jinming Dong, H.T Yang, and D.Y Xing. Universal expression for localization length in metallic carbon nanotubes. Physical ReviewB, 64:045409/1–4, 2001

[51] Islamshah Amlani, Jonathan Lewis, King Lee, Ruth Zhang, Jie Deng, and H.-S. Philip Wong. First demonstration of ac gain from a singlewalled carbon nanotube common-source amplifier. In Electron Devices Meeting, 2006. IEDM '06. International, pages 559–562, 11-13 December 2006.

[52] E. D. Minot, Yuval Yaish, Vera Sazonova, Ji-Yong Park, Markus Brink, and Paul L. McEuen. Tuning carbon nanotube band gaps with strain. Physical Review Letters, 90(15):156401/1–4, April 2003.

[53] S. Datta, Electronic Transport inMesoscopic Systems. Cambridge, U.K. Cambridge Univ. Press, 1995, ch. 2.

[54] Jie deng et al., "A Compact SPICE Model for Carbon-Nanotube Field-Effect Transistors Including Nonidealities and Its Application—Part I: Model of the Intrinsic Channel Region," IEEE TRANSACTIONS ON ELECTRON DEVICES, VOL. 54, NO. 12, DECEMBER 2007.

[55] J. Knoch, S. Mantl, and J. Appenzeller, "Comparison of transport properties in carbon nanotube field-effect transistors with Schottky contacts and doped source/drain contacts," Solid State Electron., vol. 49, no. 1, pp. 73–76, Jan. 2005.

[56] J. Chen, C. Klinke, A. Afzali, and P. Avouris, "Self-aligned carbon nanotube transistors with charge transfer doping," Appl. Phys. Lett., vol. 86, no. 12, p. 123 108, Mar. 2005.

[57] Tom J Kazmierski, Dafeng Zhou, Bashir M Al-Hashimi and Peter Ashburn , "Numerically efficient modeling of CNT transistors with ballistic and non-ballistic effects for

circuit simulation," IEEE TRANSACTIONS ON NANOTECHNOLOGY, VOL. 9, NO. 1, JANUARY 2010.

[58] E. O. Kane, "Zener tunneling in semiconductors," J. Phys. Chem. Solids,vol. 12, pp. 181–188, 1959.

[59] E. O. Kane, "Theory of tunneling," J. Appl. Phys., vol. 32, no. 1,pp. 83–91, Jan. 1961.

[60J. Kong, E. Yenilmez, W. Tombler, W. Kim, and H. Dai, "Quantum interference and ballistic transmission in nanotube electron waveguide," Phys. Rev. Lett., vol. 87, no. 10, p. 106 801, Aug. 2001.

[61] S. Frank, P. Poncharal, Z. L.Wang, andW. A. de Heer, "Carbon nanotube quantum resistor," Science, vol. 280, no. 5370, pp. 1744–1746, Jun. 1998

[62] S. O. Koswatta, S. Hasan, and M. S. Lundstrom, "Ballisticity of nanotube field-effect transistors: Role of phonon energy, and gate bias," Appl. Phys. Lett., vol. 89, no. 2, p. 023 125, Jul. 2006

[63] S. O. Koswatta, S. Hasan, M. S. Lundstrom, M. P. Anantram, and D. E. Nikonov, "Non-equilibrium Green's function treatment of phonon scattering in carbon-nanotube transistors," IEEE Trans. Electron Devices, vol. 54, no. 9, pp. 2339–2351, Sep. 2007.

[64] Jing Guo and Mark S. Lundstrom. Role of phonon scattering in carbon nanotube field-effect transistors. Applied Physics Letters, 86:193103–1– 3, 2005.

[65] Asha Balijepalli, Saurabh Sinha, and Yu Cao. Compact modeling of carbon nanotube transistor for early stage process-design exploration. In ISLPED'07: 2007 International Symposium on Low Power Electronics and Design, Portland, OR, United States, 27-29 August 2007.

[66] Yuhua Cheng, Chenming Hu (1999). " MOSFET classification and operation," MOSFET modeling & BSIM3 user's guide. Springer. p. 13. ISBN 0-7923-8575-6.
[67]James D. Plummer, Peter B. Griffin (2001)."Material and Process Limits in Silicon VLSI Technology," PROCEEDINGS OF THE IEEE, VOL. 89, NO. 3, MARCH 2001.
[68] R. Bruce Weisman, Shekhar Subramoney (2006). "Carbon Nanotubes," The Electrochemical Society Interface, Summer 2006.
[69] Rahmat Bin Sanudin, "Characterization of Ballistic Carbon Nanotube Field-Effect Transistor," Thesis report, University Technology Malaysia, November 2005.

[70] Chen, Z. et al,. "IDDQ Testing for Deep-Submicron ICs: Challenges and Solutions," IEEE Design and Test of Computers.pp: 24-33, 2002.

[71] D. Jiménez, X. Cartoixà, E. Miranda, J. Suñé, F. A. Chaves, and S. Roche, "A simple drain current model for Schottky-barrier carbon nanotube field effect transistors," Barcelona,Spain pp: 1-18, 2007.

[72] Choi, W. B. et al., "Aligned carbon nanotubes for nanoelectronics," Institute of Physics Publishing, Volume: 15, pp: 512-516, 2002.

[73] R.F. Peierl, "Quantum Theory of Solids, Clarendon, Oxford," p. 108 (1955).

[74] R. Landauer, IBM J. Res. Dev. 1, 223 (1957); R. Landauer, IBM J. Res. Dev. 32, 306 (1988); D.S. Fisher and P.A. Lee, Phys. Rev. B 23, 6851 (1981); M. Büttiker, Y. Imry, R. Landauer, and S. Pinhas, Phys. Rev. B 31, 6207 (1985); M. Büttiker, Phys. Rev. Lett. 57, 1761 (1986); Y. Imry, Physics of mesoscopic systems, in Directions in Condensed Matter Physics, edited by G. Grinstein and G. Mazenko, World Scientific Press, Singapore (1986); M. Büttiker, IBM J. Res. Dev. 32, 317 (1988); R. Landauer, Physica Scripta T42, 110 (1992).

[75] S. Datta, Electronic Transport in Mesoscopic Systems, Cambridge University

Press, Cambridge, U.K. (1995).

[76] R. Saito, G. Dresselhaus, and M.S. Dresselhaus, Physical Properties of Carbon Nanotubes, Imperial College Press, London (1998).

[77] Z. Yao, C.L. Kane, and C. Dekker, Phys. Rev. Lett. 84, 2941 (2000).

[78] S.J. Tans, M.H. Devoret, H. Dai, A. Thess, R.E. Smalley, L.J. Geerlings, and C. Dekker, Nature 386, 474 (1997).

[79] A. Javey, J. Guo, Q. Wang, M. Lundstrom, and H. Dai, Nature 424, 654 (2003).

[80] D. Mann, A. Javey, J. Kong, et al., Nano Lett. 3, 1541 (2003).

[81] J.Y. Park, S. Rosenblatt, Y. Yaish, et al., Nano Lett. 4, 517 (2004).

[82] M. Freitag, Local Electronic Functionality in Carbon Nanotube Devices, thesis, University of Pennsylvania, Philadelphia (2002).

[83] C.L. Kane, E.J. Mele, R.S. Lee, et al., Europhys. Lett. 41, 683 (1998).

[84] L.M. Woods and G.D. Mahan, Phys. Rev. B 61, 10651 (2000).

[85] M. Bockrath, W. Liang, D. Bozovic, et al., Science 291, 283 (2001).

[86] V.H. Crespi, M.L. Cohen, and A. Rubio, Phys. Rev. Lett. 79, 2093 (1997).

[87] A. Javey, J. Guo, M. Paulsson, et al., Phys. Rev. Lett. 92, 106804 (2004).

[88]W. Shockley and G.L. Pearson, *Phys. Rev.* 74, 232 (1948).

[89]D. Kahng and M.M. Atalla, Silicon-Silicon Dioxide Field Induced Surface Devices, IRE Solid-State Device Research Conference, Carnegie Institute of Technology, Pittsburgh, PA (1960).

[90] S.J. Tans, A.R.M. Verschueren, and C. Dekker, *Nature* 393, 49 (1998).

[91] R. Martel, T. Schmidt, H.R. Shea, et al., *Appl. Phys. Lett.* 73, 2447 (1998).

[92] J. Tersoff, M. Freitag, J.C. Tsang, and Ph. Avouris, cond-mat/0411537 (2004).

[93] M.S. Fuhrer, B.M. Kim, T. Dürkop, and T. Brintlinger, *NanoLett.* 2, 755 (2002).

[94] T. Dürkop, S.A. Getty, E. Cobas, and M.S. Fuhrer, *NanoLett.* 4, 35 (2004).

[95] A. Javey, J. Guo, Q. Wang, M. Lundstrom, and H. Dai, *Nature* 424, 654 (2003).

[96] Sabbir Ahmed Khan, Mahmudul Hasan, Zahangir Alom, Sourav Mahmood and Prof. Sharif Mohammad Mominuzzaman, A Novel Approach Towards Multiple Parameters Modelling of Mosfet-like Carbon Nanotube Field Effect Transistor, Carbon, Brazil, 2013.

Appendix A

1) MATLAB Operational Code:

```
disp('Choice 1 for non-ballistic variation:');
disp('Choice 2 for F variation:');
choice=input('Select=');

switch choice
    case 1

disp('Choice 1 for assigning the values of thickness(t):');
disp('Choice 2 for assigning the values of temparature(T):');
disp('Choice 3: for assigning the values of dielectric
constant(epsr):');
disp('Choice 4: for assigning the values of chiral axis(n):');
disp('Choice 5: for assigning the values of chiral axis(m):');
choice=input('Enter the value=');

% modified by Sabbir 31/08/2012
% last modified by Nirjhor Tahmidur Rouf 30/08/2013

switch choice
   case 1
      %insert minimum and maximum value.
       tmin=input('Insert minimum Gate insulator thickness
value=');
       tmax=input('Insert maximum Gate insulator thickness
value=');

      % Gate Insulator Dielectric Constant, epsr
        epsr = [];
        while isempty(epsr)
            fprintf('   Gate Insulator Dielectric Const.:   ');
            epsr = input('epsr = ');
            if isempty(epsr)
                epsr = 3.9; % Default value
                fprintf('\b\b 3.9 (Using Default ...)\n');
            end
        end

        % NT Diameter, d (m)
%         d = [];
```

```
%           while isempty(d)
%               fprintf('   NanoTube Diameter (m):
');
%               d = input('d = ');
%               if isempty(d)
%                   d = 1.0e-9; % Default value
%                   fprintf('\b\b 1.0e-9 (Using Default ...)\n');
%               end
%           end

        %Calculation for Chairality(n,m).
        m = [];
        while isempty(m)
            fprintf('  Chiral axis m:                 ');
            m = input('m = ');
            if isempty(m)
                m = 0; % Default value
                fprintf('\b\b 0 (Using Default ...)\n');
            end
        end

        n =[];
        while isempty(n)
            fprintf(' Chiral axis  n:                 ');
            n = input('n = ');
            if isempty(n)
                n = 13; % Default value
                fprintf('\b\b 13 (Using Default ...n>m
always)\n');
            end
        end
        % Calculation of Diameter from Chiral axis(n,m)
%           a = []; % graphene basis vector
%           a = 2.461e-10;
%           d=(a*(m^2+m*n+n^2)^0.5)/3.1416
%
%           fp = fopen('our_results.txt','a');
%
%           fprintf(fp,'\nfor n = %d, m = %d, value of d = %e',
n,m,d);
%
%           fclose(fp);
%
        % Temperature, T (K)
        T = [];
        while isempty(T)
            fprintf('   Temperature (K):                    ');
```

```
            T = input('T = ');
            if isempty(T)
                T = 300; % Default value
                fprintf('\b\b 300 (Using Default ...)\n');
            end
            fprintf('\n');
        end

% Terminal Voltage:
%===========================================
        fprintf('Terminal Voltage:\n');
        fprintf('=================\n');
        % Number of Bias Points, NV
        NV = [];
        while isempty(NV)
            fprintf('   Number of Bias Points:  ');
            NV = input('NV = ');
            if isempty(NV)
                NV = 13; % Default value
                fprintf('\b\b 13 (Using Default ...)\n');
            end
        end

        % Voltage Range, VI,VF (V)
        VI = [];
        VF = [];
        while isempty(VI) | isempty(VF)
            fprintf('   Voltage Range (V):\n');
            fprintf('\t\t\t');
            VI = input('(Initial)  VI = ');
            if isempty(VI)
                VI = 0; % Default value
                fprintf('\b\b 0 (Using Default ...)\n');
            end
            fprintf('\t\t\t');
            VF = input('(Final)  VF = ');
            if isempty(VF)
                VF = 0.6; % Default value
                fprintf('\b\b 0.6 (Using Default ...)\n');
            end
            fprintf('\n');
        end

% Analytical Model:
%===========================================
        fprintf('Analytical Model:\n');
        fprintf('=================\n');
```

```
        % Source Fermi Level, Ef (eV)
        Ef = [];
        while isempty(Ef)
            fprintf('    Source Fermi Level (eV):     ');
            Ef = input('Ef = ');
            if isempty(Ef)
                Ef = -0.32; % Default value
                fprintf('\b\b -0.32 (Using Default ...)\n');
            end
        end

        % Get Control Parameter, alphag
        alphag = [];
        while isempty(alphag)
            fprintf('    Gate Control Parameter:      ');
            alphag = input('alphag = ');
            if isempty(alphag)
                alphag = 0.88; % Default value
                fprintf('\b\b 0.88 (Using Default ...)\n');
            end
        end

        % Drain Control Parameter, alphad
        alphad = [];
        while isempty(alphad)
            fprintf('    Drain Control Parameter:     ');
            alphad = input('alphad = ');
            if isempty(alphad)
                alphad = 0.035; % Default value
                fprintf('\b\b 0.035 (Using Default ...)\n');
            end
            fprintf('\n');
        end
        % Call Main Program
        % ================================
%         file=1;
%         for t=tmin:0.5:tmax
%              results = CNTFETToy( t,d,epsr,T, VI,VF,NV,
Ef,alphag,alphad );
%
%              xlswrite('result.xlsx',results,file);
%
%              file=file+1;
%         end
       % MOdified code without excel
file????????????????????????????///
        file=1;
```

```
        for t=tmin:0.25e-9:tmax
             results = CNTFETToy( t,n,m,epsr,T, VI,VF,NV,
Ef,alphag,alphad );

             AVg(:,file)=results(:,1);
             AVd(:,file)=results(:,2);
             AI(:,file)=results(:,3);
             AD(:,file)=results(:,4);

            % xlswrite('result.xlsx',results,file);

             file=file+1;
        end

        for i=1:size(AI,2)
            xtest=AI(:,i);
            mat=vec2mat(xtest,13);
            pv(:,i)=max(mat,[],2);
            %AIavg(i)=mean(pv);
        end

% Creating modified figure by Sabbir Ahmed Khan 31/08/12
points = linspace(-2, 0, 20);
[X, Y] = meshgrid(points, -points);
% Faceted Shading
subplot(2, 2, 1);
surf(pv,'DisplayName','pv','YDataSource','pv'); view(30, 30);
shading faceted;
title('Effect of Gate Oxide Thickness: View1');

% Flat Shading
subplot(2, 2, 2);
surf(pv,'DisplayName','pv','YDataSource','pv'); view(30, 30);
shading flat;
title('Effect of Gate Oxide Thickness:View2');

% Interpolated Shading
subplot(2, 2, 3);
surf(pv,'DisplayName','pv','YDataSource','pv'); view(30, 30);
shading interp;
title('Effect of Gate Oxide Thickness:View3');

% Shading Commands
subplot(2, 2, 4, 'Visible', 'off');
text(0, .5, sprintf('%s\n%s\n%s\n%s', ...
```

```
    '3D View1(shading faceted)', '3D View2(shading flat)', '3D
View3(shading interp)','"Current is inversely proportional to
Gate Oxide Thickness"'), ...
    'VerticalAlignment', 'middle', ...
    'FontName', 'Bell MT', ...
    'FontWeight', 'bold', ...
    'FontSize', 13);


     %% Final touch by Sabbir Ahmed Khan 02/09/2012......

   case 2
      % Inserting minimum and amximum temperature value
       Tmin=input('Insert minimum temperature value=');
       Tmax=input('Insert maximum temparature value=');

       % Gate Insulator Thickness, t (m)
        t = [];
        while isempty(t)
            fprintf('   Gate Insulator Thickness (m):       ');
            t = input('t = ');
            if isempty(t)
                t = 1.5e-9; % Default value
                fprintf('\b\b 1.5e-9 (Using Default ...)\n');
            end
        end

         % Gate Insulator Dielectric Constant, epsr
        epsr = [];
        while isempty(epsr)
            fprintf('   Gate Insulator Dielectric Const.:   ');
            epsr = input('epsr = ');
            if isempty(epsr)
                epsr = 3.9; % Default value
                fprintf('\b\b 3.9 (Using Default ...)\n');
            end
        end

        % Calculating Chairality(n,m)
        m = [];
        while isempty(m)
            fprintf('   m:              ');
            m = input('Chiral axis m = ');
            if isempty(m)
                m =0; % Default value
                fprintf('\b\b 0 (Using Default ...)\n');
            end
```

```
        end

        n =[];
        while isempty(n)
            fprintf('    n:                  ');
            n = input('Chiral axis n = ');
            if isempty(n)
                n = 13; % Default value
                fprintf('\b\b 13 (Using Default ...n>m
always)\n');
            end
        end

        % Terminal Voltage:
%===========================================
        fprintf('Terminal Voltage:\n');
        fprintf('=================\n');
        % Number of Bias Points, NV
        NV = [];
        while isempty(NV)
            fprintf('    Number of Bias Points:   ');
            NV = input('NV = ');
            if isempty(NV)
                NV = 13; % Default value
                fprintf('\b\b 13 (Using Default ...)\n');
            end
        end

        % Voltage Range, VI,VF (V)
        VI = [];
        VF = [];
        while isempty(VI) | isempty(VF)
            fprintf('    Voltage Range (V):\n');
            fprintf('\t\t\t');
            VI = input('(Initial)  VI = ');
            if isempty(VI)
                VI = 0; % Default value
                fprintf('\b\b 0 (Using Default ...)\n');
            end
            fprintf('\t\t\t');
            VF = input('(Final)  VF = ');
            if isempty(VF)
                VF = 0.6; % Default value
                fprintf('\b\b 0.6 (Using Default ...)\n');
            end
            fprintf('\n');
        end
```

```
% Analytical Model:
%============================================
        fprintf('Analytical Model:\n');
        fprintf('=================\n');
        % Source Fermi Level, Ef (eV)
        Ef = [];
        while isempty(Ef)
            fprintf('    Source Fermi Level (eV):     ');
            Ef = input('Ef = ');
            if isempty(Ef)
                Ef = -0.32; % Default value
                fprintf('\b\b -0.32 (Using Default ...)\n');
            end
        end

        % Get Control Parameter, alphag
        alphag = [];
        while isempty(alphag)
            fprintf('    Gate Control Parameter:      ');
            alphag = input('alphag = ');
            if isempty(alphag)
                alphag = 0.88; % Default value
                fprintf('\b\b 0.88 (Using Default ...)\n');
            end
        end

        % Drain Control Parameter, alphad
        alphad = [];
        while isempty(alphad)
            fprintf('    Drain Control Parameter:     ');
            alphad = input('alphad = ');
            if isempty(alphad)
                alphad = 0.035; % Default value
                fprintf('\b\b 0.035 (Using Default ...)\n');
            end
            fprintf('\n');
        end


        % Call Main Program
        % ================================

        % MOdified code without excel file by sabbir and
Zahangir????????????????????????????///
        file=1;
        for T=Tmin:1:Tmax
```

```
            results = CNTFETToy( t,n,m,epsr,T, VI,VF,NV,
Ef,alphag,alphad );

            AVg(:,file)=results(:,1);
            AVd(:,file)=results(:,2);
            AI(:,file)=results(:,3);
            AD(:,file)=results(:,4);

           % xlswrite('result.xlsx',results,file);

            file=file+1;
        end

        for i=1:size(AI,2)
            xtest=AI(:,i);
            mat=vec2mat(xtest,13);
            pv(:,i)=max(mat,[],2);
            %AIavg(i)=mean(pv);
        end
        % Create a grid of x and y points
% Creating modified figure by Sabbir Ahmed Khan 31/08/12
points = linspace(-2, 0, 20);
[X, Y] = meshgrid(points, -points);
% Faceted Shading
subplot(2, 2, 1);
surf(pv,'DisplayName','pv','YDataSource','pv'); view(30, 30);
shading faceted;
title('Effect of Temperature: View1');

% Flat Shading
subplot(2, 2, 2);
surf(pv,'DisplayName','pv','YDataSource','pv'); view(30, 30);
shading flat;
title('Effect of Temperature: View2');

% Interpolated Shading
subplot(2, 2, 3);
surf(pv,'DisplayName','pv','YDataSource','pv'); view(30, 30);
shading interp;
title('Effect of Temperature: View3');

% Shading Commands
subplot(2, 2, 4, 'Visible', 'off');
text(0, .5, sprintf('%s\n%s\n%s\n%s', ...
    '3D View1(shading faceted)', '3D View2(shading flat)', '3d
View3(shading interp)','"Ballistic consideration reduce
Temperature changing effect"'), ...
```

```
    'VerticalAlignment', 'middle', ...
    'FontName', 'Bell MT', ...
    'FontWeight', 'bold', ...
    'FontSize', 13);

       %%Final touch by Sabbir Ahmed Khan 02/09/2012...
    case 3
        %%%% Inserting minimum and maximum value%%%%%%%%
       epsrmin=input('Insert minimum dielectric constant=');
       epsrmax=input('Insert maximum dielectric constant=');
       t = [];
        while isempty(t)
            fprintf('   Gate Insulator Thickness (m):       ');
            t = input('t = ');
            if isempty(t)
                t = 1.5e-9; % Default value
                fprintf('\b\b 1.5e-9 (Using Default ...)\n');
            end
        end


        % NT Diameter, d (m)
%         d = [];
%         while isempty(d)
%             fprintf('   NanoTube Diameter (m):
');
%             d = input('d = ');
%             if isempty(d)
%                 d = 1.0e-9; % Default value
%                 fprintf('\b\b 1.0e-9 (Using Default ...)\n');
%             end
%         end

        %Calculation for Chairality(n,m).
        m = [];
        while isempty(m)
            fprintf('  Chiral axis m:                 ');
            m = input('m = ');
            if isempty(m)
                m = 0; % Default value
                fprintf('\b\b 0 (Using Default ...)\n');
            end
        end

        n =[];
        while isempty(n)
            fprintf(' Chiral axis  n:                 ');
```

```
            n = input('n = ');
            if isempty(n)
                n = 13; % Default value
                fprintf('\b\b 13 (Using Default ...n>m
always)\n');
            end
        end
        % Calculation of Diameter from Chiral axis(n,m)
%         a = []; % graphene basis vector
%         a = 2.461e-10;
%         d=(a*(m^2+m*n+n^2)^0.5)/3.1416
%
%         fp = fopen('our_results.txt','a');
%
%         fprintf(fp,'\nfor n = %d, m = %d, value of d = %e',
n,m,d);
%
%         fclose(fp);
%
        % Temperature, T (K)
        T = [];
        while isempty(T)
            fprintf('   Temperature (K):                    ');
            T = input('T = ');
            if isempty(T)
                T = 300; % Default value
                fprintf('\b\b 300 (Using Default ...)\n');
            end
            fprintf('\n');
        end

% Terminal Voltage:
%===========================================
        fprintf('Terminal Voltage:\n');
        fprintf('=================\n');
        % Number of Bias Points, NV
        NV = [];
        while isempty(NV)
            fprintf('   Number of Bias Points:  ');
            NV = input('NV = ');
            if isempty(NV)
                NV = 13; % Default value
                fprintf('\b\b 13 (Using Default ...)\n');
            end
        end

        % Voltage Range, VI,VF (V)
```

```
        VI = [];
        VF = [];
        while isempty(VI) | isempty(VF)
            fprintf('   Voltage Range (V):\n');
            fprintf('\t\t\t');
            VI = input('(Initial)  VI = ');
            if isempty(VI)
                VI = 0; % Default value
                fprintf('\b\b 0 (Using Default ...)\n');
            end
            fprintf('\t\t\t');
            VF = input('(Final)  VF = ');
            if isempty(VF)
                VF = 0.6; % Default value
                fprintf('\b\b 0.6 (Using Default ...)\n');
            end
            fprintf('\n');
        end

% Analytical Model:
%===========================================
        fprintf('Analytical Model:\n');
        fprintf('=================\n');
        % Source Fermi Level, Ef (eV)
        Ef = [];
        while isempty(Ef)
            fprintf('   Source Fermi Level (eV):     ');
            Ef = input('Ef = ');
            if isempty(Ef)
                Ef = -0.32; % Default value
                fprintf('\b\b -0.32 (Using Default ...)\n');
            end
        end

        % Get Control Parameter, alphag
        alphag = [];
        while isempty(alphag)
            fprintf('   Gate Control Parameter:     ');
            alphag = input('alphag = ');
            if isempty(alphag)
                alphag = 0.88; % Default value
                fprintf('\b\b 0.88 (Using Default ...)\n');
            end
        end

        % Drain Control Parameter, alphad
        alphad = [];
```

```
        while isempty(alphad)
            fprintf('   Drain Control Parameter:     ');
            alphad = input('alphad = ');
            if isempty(alphad)
                alphad = 0.035; % Default value
                fprintf('\b\b 0.035 (Using Default ...)\n');
            end
            fprintf('\n');
        end
        % Call Main Program
        % ================================
%         file=1;
%         for t=tmin:0.5:tmax
%              results = CNTFETToy( t,d,epsr,T, VI,VF,NV,
Ef,alphag,alphad );
%
%              xlswrite('result.xlsx',results,file);
%
%              file=file+1;
%         end
%%%%%%%%%%%%%%%%%%%%%%%%%%%%%% MOdified code without excel
file????????????????????????????///
        file=1;
        for epsr=epsrmin:.5:epsrmax
             results = CNTFETToy( t,m,n,epsr,T, VI,VF,NV,
Ef,alphag,alphad );

             AVg(:,file)=results(:,1);
             AVd(:,file)=results(:,2);
             AI(:,file)=results(:,3);
             AD(:,file)=results(:,4);

            % xlswrite('result.xlsx',results,file);

             file=file+1;
        end

        for i=1:size(AI,2)
            xtest=AI(:,i);
            mat=vec2mat(xtest,13);
            pv(:,i)=max(mat,[],2);
            %AIavg(i)=mean(pv);
        end

% Creating modified figure by Sabbir Ahmed Khan 31/08/12
points = linspace(-2, 0, 20);
[X, Y] = meshgrid(points, -points);
```

```
% Faceted Shading
subplot(2, 2, 1);
surf(pv,'DisplayName','pv','YDataSource','pv'); view(30, 30);
shading faceted;
title('Dielectric constant changing effect: 3D View1');

% Flat Shading
subplot(2, 2, 2);
surf(pv,'DisplayName','pv','YDataSource','pv'); view(30, 30);
shading flat;
title('Dielectric constant changing effect: 3D View2');

% Interpolated Shading
subplot(2, 2, 3);
surf(pv,'DisplayName','pv','YDataSource','pv'); view(30, 30);
shading interp;
title('Dielectric constant changing effect: 3D View3');

% Shading Commands
subplot(2, 2, 4, 'Visible', 'off');
text(0, .5, sprintf('%s\n%s\n%s\n%s', ...
    'View1(shading faceted)', 'View2(shading flat)',
'View3(shading interp)','"Current increasing with increasing
Dielectric Constant"'), ...
    'VerticalAlignment', 'middle', ...
    'FontName', 'Bell MT', ...
    'FontWeight', 'bold', ...
    'FontSize', 13);


     %% Last touch by Sabbir Ahmed Khan 02/09/12

%%%%%%%%%%%%%%%%%%%%%%%%%%%%%%%%%%%%%%END%%%%%%%%%%%%%%%%%%%%
%%%%%%%%%%%%%%%%%%%%%%%%%%%%%%%



       case 4
      %insert minimum and maximum value.
       nmin=input('Insert minimum Chiral axis value=');
       nmax=input('Insert maximum Chieal axis value=');
        % Gate Insulator Thickness, t (m)
        t = [];
        while isempty(t)
            fprintf('   Gate Insulator Thickness (m):        ');
            t = input('t = ');
            if isempty(t)
```

```
                t = 1.5e-9; % Default value
                fprintf('\b\b 1.5e-9 (Using Default ...)\n');
            end
        end
      % Gate Insulator Dielectric Constant, epsr
        epsr = [];
        while isempty(epsr)
            fprintf('   Gate Insulator Dielectric Const.:    ');
            epsr = input('epsr = ');
            if isempty(epsr)
                epsr = 3.9; % Default value
                fprintf('\b\b 3.9 (Using Default ...)\n');
            end
        end

        % NT Diameter, d (m)
%         d = [];
%         while isempty(d)
%             fprintf('   NanoTube Diameter (m):
');
%             d = input('d = ');
%             if isempty(d)
%                 d = 1.0e-9; % Default value
%                 fprintf('\b\b 1.0e-9 (Using Default ...)\n');
%             end
%         end

        %Calculation for Chairality(n,m).
        m = [];
        while isempty(m)
            fprintf('  Chiral axis m:                   ');
            m = input('m = ');
            if isempty(m)
                m = 0; % Default value
                fprintf('\b\b 0 (Using Default ...n>m
always)\n');
            end
        end


        % Calculation of Diameter from Chiral axis(n,m)
%         a = []; % graphene basis vector
%         a = 2.461e-10;
%         d=(a*(m^2+m*n+n^2)^0.5)/3.1416
%
%         fp = fopen('our_results.txt','a');
%
```

```
%         fprintf(fp,'\nfor n = %d, m = %d, value of d = %e',
n,m,d);
%
%         fclose(fp);

        % Temperature, T (K)
        T = [];
        while isempty(T)
            fprintf('   Temperature (K):                    ');
            T = input('T = ');
            if isempty(T)
                T = 300; % Default value
                fprintf('\b\b 300 (Using Default ...)\n');
            end
            fprintf('\n');
        end

% Terminal Voltage:
%==========================================
        fprintf('Terminal Voltage:\n');
        fprintf('=================\n');
        % Number of Bias Points, NV
        NV = [];
        while isempty(NV)
            fprintf('   Number of Bias Points:  ');
            NV = input('NV = ');
            if isempty(NV)
                NV = 13; % Default value
                fprintf('\b\b 13 (Using Default ...)\n');
            end
        end

        % Voltage Range, VI,VF (V)
        VI = [];
        VF = [];
        while isempty(VI) | isempty(VF)
            fprintf('   Voltage Range (V):\n');
            fprintf('\t\t\t');
            VI = input('(Initial)  VI = ');
            if isempty(VI)
                VI = 0; % Default value
                fprintf('\b\b 0 (Using Default ...)\n');
            end
            fprintf('\t\t\t');
            VF = input('(Final)  VF = ');
            if isempty(VF)
                VF = 0.6; % Default value
```

```
                fprintf('\b\b 0.6 (Using Default ...)\n');
            end
            fprintf('\n');
        end

% Analytical Model:
%===========================================
        fprintf('Analytical Model:\n');
        fprintf('=================\n');
        % Source Fermi Level, Ef (eV)
        Ef = [];
        while isempty(Ef)
            fprintf('    Source Fermi Level (eV):     ');
            Ef = input('Ef = ');
            if isempty(Ef)
                Ef = -0.32; % Default value
                fprintf('\b\b -0.32 (Using Default ...)\n');
            end
        end

        % Get Control Parameter, alphag
        alphag = [];
        while isempty(alphag)
            fprintf('    Gate Control Parameter:      ');
            alphag = input('alphag = ');
            if isempty(alphag)
                alphag = 0.88; % Default value
                fprintf('\b\b 0.88 (Using Default ...)\n');
            end
        end

        % Drain Control Parameter, alphad
        alphad = [];
        while isempty(alphad)
            fprintf('    Drain Control Parameter:     ');
            alphad = input('alphad = ');
            if isempty(alphad)
                alphad = 0.035; % Default value
                fprintf('\b\b 0.035 (Using Default ...)\n');
            end
            fprintf('\n');
        end
        % Call Main Program
        % ================================
%          file=1;
%          for t=tmin:0.5:tmax
```

```
%               results = CNTFETToy( t,d,epsr,T, VI,VF,NV,
Ef,alphag,alphad );
%
%               xlswrite('result.xlsx',results,file);
%
%               file=file+1;
%          end
       % MOdified code without excel
file????????????????????????????///
        file=1;
        for n=nmin:1:nmax
             results = CNTFETToy( t,n,m,epsr,T, VI,VF,NV,
Ef,alphag,alphad );

             AVg(:,file)=results(:,1);
             AVd(:,file)=results(:,2);
             AI(:,file)=results(:,3);
             AD(:,file)=results(:,4);

            % xlswrite('result.xlsx',results,file);

             file=file+1;
        end

        for i=1:size(AI,2)
            xtest=AI(:,i);
            mat=vec2mat(xtest,13);
            pv(:,i)=max(mat,[],2);
            %AIavg(i)=mean(pv);
        end



% Creating modified figure by Sabbir Ahmed Khan 31/08/12
points = linspace(-2, 0, 20);
[X, Y] = meshgrid(points, -points);
% Faceted Shading
subplot(2, 2, 1);
surf(pv,'DisplayName','pv','YDataSource','pv'); view(30, 30);
shading faceted;
title('Chirality Changing effect:3D View1');

% Flat Shading
subplot(2, 2, 2);
surf(pv,'DisplayName','pv','YDataSource','pv'); view(30, 30);
shading flat;
title('Chirality Changing effect:3D View2');
```

```
% Interpolated Shading
subplot(2, 2, 3);
surf(pv,'DisplayName','pv','YDataSource','pv'); view(30, 30);
shading interp;
title('Chirality Changing effect:3D View3');

% Shading Commands
subplot(2, 2, 4, 'Visible', 'off');
text(0, .5, sprintf('%s\n%s\n%s\n%s', ...
    '3D View1(shading faceted)', '3D View2(shading flat)', '3D
View3(shading interp)','"Increasing Chiral axis increase the
diameter resulting increase Current"'), ...
    'VerticalAlignment', 'middle', ...
    'FontName', 'Bell MT', ...
    'FontWeight', 'bold', ...
    'FontSize', 13);

%%Final touc by Sabbir ahmed Khan 02/09/12

%surf(pv,'DisplayName','pv','YDataSource','pv');figure(gcf)
       %grid on
       %legend('300K','350K','400K','450K','500K','550K')

%?????????????????????????????????????????????????????????????
        case 5
      %insert minimum and maximum value.
       mmin=input('Insert minimum Chiral axis value=');
       mmax=input('Insert maximum Chiral axis value=');
      % Gate Insulator Thickness, t (m)
        t = [];
        while isempty(t)
            fprintf('   Gate Insulator Thickness (m):       ');
            t = input('t = ');
            if isempty(t)
                t = 1.5e-9; % Default value
                fprintf('\b\b 1.5e-9 (Using Default ...)\n');
            end
        end
      % Gate Insulator Dielectric Constant, epsr
        epsr = [];
        while isempty(epsr)
            fprintf('   Gate Insulator Dielectric Const.:   ');
            epsr = input('epsr = ');
            if isempty(epsr)
                epsr = 3.9; % Default value
                fprintf('\b\b 3.9 (Using Default ...)\n');
```

```
            end
        end

        % NT Diameter, d (m)
%          d = [];
%          while isempty(d)
%              fprintf('   NanoTube Diameter (m):
');
%              d = input('d = ');
%              if isempty(d)
%                  d = 1.0e-9; % Default value
%                  fprintf('\b\b 1.0e-9 (Using Default ...)\n');
%              end
%          end

        %Calculation for Chairality(n,m).

        n =[];
        while isempty(n)
            fprintf(' Chiral axis  n:              ');
            n = input('n = ');
            if isempty(n)
                n = 13; % Default value
                fprintf('\b\b 13 (Using Default ...n>m
always)\n');
            end
        end
        % Calculation of Diameter from Chiral axis(n,m)
%          a = []; % graphene basis vector
%          a = 2.461e-10;
%          d=(a*(m^2+m*n+n^2)^0.5)/3.1416
%
%          fp = fopen('our_results.txt','a');
%
%          fprintf(fp,'\nfor n = %d, m = %d, value of d = %e',
n,m,d);
%
%          fclose(fp);

        % Temperature, T (K)
        T = [];
        while isempty(T)
            fprintf('   Temperature (K):                    ');
            T = input('T = ');
            if isempty(T)
                T = 300; % Default value
                fprintf('\b\b 300 (Using Default ...)\n');
```

```
            end
            fprintf('\n');
        end

% Terminal Voltage:
%===========================================
        fprintf('Terminal Voltage:\n');
        fprintf('=================\n');
        % Number of Bias Points, NV
        NV = [];
        while isempty(NV)
            fprintf('   Number of Bias Points:  ');
            NV = input('NV = ');
            if isempty(NV)
                NV = 13; % Default value
                fprintf('\b\b 13 (Using Default ...)\n');
            end
        end

        % Voltage Range, VI,VF (V)
        VI = [];
        VF = [];
        while isempty(VI)  isempty(VF)
            fprintf('   Voltage Range (V):\n');
            fprintf('\t\t\t');
            VI = input('(Initial)  VI = ');
            if isempty(VI)
                VI = 0; % Default value
                fprintf('\b\b 0 (Using Default ...)\n');
            end
            fprintf('\t\t\t');
            VF = input('(Final)  VF = ');
            if isempty(VF)
                VF = 0.6; % Default value
                fprintf('\b\b 0.6 (Using Default ...)\n');
            end
            fprintf('\n');
        end

% Analytical Model:
%===========================================
        fprintf('Analytical Model:\n');
        fprintf('=================\n');
        % Source Fermi Level, Ef (eV)
        Ef = [];
        while isempty(Ef)
            fprintf('   Source Fermi Level (eV):    ');
```

```
            Ef = input('Ef = ');
            if isempty(Ef)
                Ef = -0.32; % Default value
                fprintf('\b\b -0.32 (Using Default ...)\n');
            end
        end

        % Get Control Parameter, alphag
        alphag = [];
        while isempty(alphag)
            fprintf('   Gate Control Parameter:     ');
            alphag = input('alphag = ');
            if isempty(alphag)
                alphag = 0.88; % Default value
                fprintf('\b\b 0.88 (Using Default ...)\n');
            end
        end

        % Drain Control Parameter, alphad
        alphad = [];
        while isempty(alphad)
            fprintf('   Drain Control Parameter:    ');
            alphad = input('alphad = ');
            if isempty(alphad)
                alphad = 0.035; % Default value
                fprintf('\b\b 0.035 (Using Default ...)\n');
            end
            fprintf('\n');
        end
        % Call Main Program
        % ================================
%          file=1;
%          for t=tmin:0.5:tmax
%               results = CNTFETToy( t,d,epsr,T, VI,VF,NV,
Ef,alphag,alphad );
%
%               xlswrite('result.xlsx',results,file);
%
%               file=file+1;
%          end
       % MOdified code without excel
file???????????????????????????///
        file=1;
        for m=mmin:1:mmax
             results = CNTFETToy( t,n,m,epsr,T, VI,VF,NV,
Ef,alphag,alphad );
```

```
            AVg(:,file)=results(:,1);
            AVd(:,file)=results(:,2);
            AI(:,file)=results(:,3);
            AD(:,file)=results(:,4);

           % xlswrite('result.xlsx',results,file);

            file=file+1;
        end

        for i=1:size(AI,2)
            xtest=AI(:,i);
            mat=vec2mat(xtest,13);
            pv(:,i)=max(mat,[],2);
            %AIavg(i)=mean(pv);
        end




% Creating modified figure by Sabbir Ahmed Khan 31/08/12
points = linspace(-2, 0, 20);
[X, Y] = meshgrid(points, -points);
% Faceted Shading
subplot(2, 2, 1);
surf(pv,'DisplayName','pv','YDataSource','pv'); view(30, 30);
shading faceted;
title('Chirality Changing effect:3D View1');

% Flat Shading
subplot(2, 2, 2);
surf(pv,'DisplayName','pv','YDataSource','pv'); view(30, 30);
shading flat;
title('Chirality Changing effect:3D View2');

% Interpolated Shading
subplot(2, 2, 3);
surf(pv,'DisplayName','pv','YDataSource','pv'); view(30, 30);
shading interp;
title('Chirality Changing effect:3D View3');

% Shading Commands
subplot(2, 2, 4, 'Visible', 'off');
text(0, .5, sprintf('%s\n%s\n%s\n%s', ...
```

```
    '3D View1(shading faceted)', '3D View2(shading flat)', '3D
View3(shading interp)','"Increasing Chiral axis increase the
diameter resulting increase Current"'), ...
    'VerticalAlignment', 'middle', ...
    'FontName', 'Bell MT', ...
    'FontWeight', 'bold', ...
    'FontSize', 13);
%%final touch by Sabbir Ahmed Khan 02/09/12


%surf(pv,'DisplayName','pv','YDataSource','pv');figure(gcf)
       %grid on
       %legend('300K','350K','400K','450K','500K','550K')

%??????????????????????????????????????????????????????????????
    otherwise
        disp('You can change the inside value interms of running
the code')
end


case 2

    %% modified by Nirjhor Tahmidur Rouf 13/07/2013

disp('Choice 1: for assigning the values of channel
length(L):');
disp('Choice 2: for assigning the values of temperature(T):');
disp('Choice 3: for assigning the values of chiral axis(n):');
disp('Choice 4: for assigning the values of chiral axis(m):');
choice=input('Enter the value=');



switch choice
   case 1
      %insert minimum and maximum value.
       L_min=input('Insert minimum channel length value=');
       L_max=input('Insert maximum channel length value=');

      % drain-source voltage, VDS
        VDS = [];
        while isempty(VDS)
            fprintf('   drain-source voltage:   ');
            VDS = input('VDS = ');
            if isempty(VDS)
                VDS = .5; % Default value
```

```
            fprintf('\b\b .5 (Using Default ...)\n');
        end
    end


    % tunneling current, It
    It = [];
    while isempty(It)
        fprintf('    tunneling current:    ');
        It = input('It = ');
        if isempty(It)
            It = 2.8000e-007; % Default value
            fprintf('\b\b 2.8000e-007 (Using Default
...)\n');
        end
    end


    % Temperature, T
    T = [];
    while isempty(T)
        fprintf('    temperature:    ');
        T = input('T = ');
        if isempty(T)
            T = 300; % Default value
            fprintf('\b\b 300 (Using Default ...)\n');
        end
    end


    % chirality
    n = [];
    while isempty(n)
        fprintf('    chiral axis n:    ');
        n = input('n = ');
        if isempty(n)
            n = 13; % Default value
            fprintf('\b\b 13 (Using Default ...)\n');
        end
    end

    m = [];
    while isempty(m)
        fprintf('    chiral axis m:    ');
        m = input('m = ');
        if isempty(m)
            m = 0; % Default value
```

```
            fprintf('\b\b 0 (Using Default ...)\n');
        end
    end

    i=1;
    for L=L_min:1e-9:L_max
        F(1,i)=tunnel_control_parameter(It,VDS,L,T,n,m);
        i=i+1;
    end

    L=L_min:1e-9:L_max;

    figure(1)
    plot(L,F, '-*')
    xlabel('channel length L (m)')
    ylabel('tunnel control parameter F')




case 2
   %insert minimum and maximum value.
    T_min=input('Insert minimum temperature value=');
    T_max=input('Insert maximum temperature value=');

   % drain-source voltage, VDS
     VDS = [];
     while isempty(VDS)
         fprintf('   drain-source voltage:    ');
         VDS = input('VDS = ');
         if isempty(VDS)
             VDS = .5; % Default value
             fprintf('\b\b .5 (Using Default ...)\n');
         end
     end


   % tunneling current, It
     It = [];
     while isempty(It)
         fprintf('   tunneling current:    ');
         It = input('It = ');
         if isempty(It)
             It = 2.8000e-007; % Default value
             fprintf('\b\b 2.8000e-007 (Using Default
...)\n');
         end
```

```
  end


% channel length, L
  L = [];
  while isempty(L)
      fprintf('    channel length:    ');
      L = input('L = ');
      if isempty(L)
          L = 300e-9; % Default value
          fprintf('\b\b 300e-9 (Using Default ...)\n');
      end
  end


% chirality
  n = [];
  while isempty(n)
      fprintf('    chiral axis n:    ');
      n = input('n = ');
      if isempty(n)
          n = 13; % Default value
          fprintf('\b\b 13 (Using Default ...)\n');
      end
  end

  m = [];
  while isempty(m)
      fprintf('    chiral axis m:    ');
      m = input('m = ');
      if isempty(m)
          m = 0; % Default value
          fprintf('\b\b 0 (Using Default ...)\n');
      end
  end

  i=1;
  for T=T_min:.25:T_max
      F(1,i)=tunnel_control_parameter(It,VDS,L,T,n,m);
      i=i+1;
  end

  T=T_min:.25:T_max;

  figure(1)
  plot(T,F, '-*')
  xlabel('temperature T (K)')
```

```
        ylabel('tunnel control parameter F')


    case 3
       %insert minimum and maximum value.
        n_min=input('Insert minimum chiral axis n value=');
        n_max=input('Insert maximum chiral axis n value=');

       % drain-source voltage, VDS
         VDS = [];
         while isempty(VDS)
             fprintf('    drain-source voltage:    ');
             VDS = input('VDS = ');
             if isempty(VDS)
                 VDS = .5; % Default value
                 fprintf('\b\b .5 (Using Default ...)\n');
             end
         end


       % tunneling current, It
         It = [];
         while isempty(It)
             fprintf('    tunneling current:    ');
             It = input('It = ');
             if isempty(It)
                 It = 2.8000e-007; % Default value
                 fprintf('\b\b 2.8000e-007 (Using Default
...)\n');
             end
         end


       % channel length, L
         L = [];
         while isempty(L)
             fprintf('    channel length:    ');
             L = input('L = ');
             if isempty(L)
                 L = 300e-9; % Default value
                 fprintf('\b\b 300e-9 (Using Default ...)\n');
             end
         end



       % temperature
```

```
    T = [];
    while isempty(T)
        fprintf('   temperature:   ');
        T = input('T = ');
        if isempty(T)
            T = 300; % Default value
            fprintf('\b\b 300 (Using Default ...)\n');
        end
    end

  % chirality
    m = [];
    while isempty(m)
        fprintf('   chiral axis m:   ');
        m = input('m = ');
        if isempty(m)
            m = 0; % Default value
            fprintf('\b\b 0 (Using Default ...)\n');
        end
    end

    i=1;
    for n=n_min:1:n_max
        F(1,i)=tunnel_control_parameter(It,VDS,L,T,n,m);
        i=i+1;
    end

    n=n_min:1:n_max;

    figure(1)
    plot(n,F, '-*')
    xlabel('chiral axis n')
    ylabel('tunnel control parameter F')



case 4
  %insert minimum and maximum value.
   m_min=input('Insert minimum chiral axis m value=');
   m_max=input('Insert maximum chiral axis m value=');

  % drain-source voltage, VDS
    VDS = [];
    while isempty(VDS)
        fprintf('   drain-source voltage:   ');
        VDS = input('VDS = ');
        if isempty(VDS)
```

```
            VDS = .5; % Default value
            fprintf('\b\b .5 (Using Default ...)\n');
        end
    end


  % tunneling current, It
    It = [];
    while isempty(It)
        fprintf('   tunneling current:   ');
        It = input('It = ');
        if isempty(It)
            It = 2.8000e-007; % Default value
            fprintf('\b\b 2.8000e-007 (Using Default
...)\n');
        end
    end


  % channel length, L
    L = [];
    while isempty(L)
        fprintf('   channel length:   ');
        L = input('L = ');
        if isempty(L)
            L = 300e-9; % Default value
            fprintf('\b\b 300e-9 (Using Default ...)\n');
        end
    end


    T = [];
    while isempty(T)
        fprintf('   temperature:   ');
        T = input('T = ');
        if isempty(T)
            T = 300; % Default value
            fprintf('\b\b 300 (Using Default ...)\n');
        end
    end


  % chirality
    n = [];
    while isempty(n)
        fprintf('   chiral axis n:   ');
        n = input('n = ');
```

```
            if isempty(n)
                n = 13; % Default value
                fprintf('\b\b 13 (Using Default ...)\n');
            end
        end


        i=1;
        for m=m_min:1:m_max
            F(1,i)=tunnel_control_parameter(It,VDS,L,T,n,m);
            i=i+1;
        end

        m=m_min:1:m_max;

        figure(1)
        plot(m,F, '-*')
        xlabel('chiral axis m')
        ylabel('tunnel control parameter F')


end

end
```

2) MATLAB Physics Code:

```
function [results_our] = CNTFETToy( t,n,m,epsr,T,
VI,VF,NV,Ef,alphag,alphad )

% function [I,V,Uscf,N] = CNTFETToy( t,d,epsr,T, VI,VF,NV,
Ef,alphag,alphad )
%     Inputs:
%    ----------------
%        t - insulator thickness (m)
%        d - NT diameter (m)
%        epsr - insulator dielectric constant
%        T - Temp (K)
%
%        VI - Initial Voltage
%        VF - Final Voltage
%        NV - # of bias points
%
%        Ef - Fermi Level
%        alphag - gate control parameter
```

```
%       alphad - drain control parameter
%
%   Outputs:
%   ------------------
%       I = Current
%       V = Voltage
%       Uscf = Self Consistent Potential
%       N = Free charge
%
% Based on FETToy Originally developed by : Anisur Rahman
%   Reference:
%   [1] A. Rahman, J. Guo, S. Datta, and M. Lundstrom,
%   "Theory of Ballistic Nanotransistors", to appear in IEEE
TED, 2003.
%
% Adapted for CNTFETToy by : Jing Wang
% Latest Version Updated by : Sayed Hasan (05/24/2004)
%----------------------------------------------------------------
-----------

%%%%%%%%%%%%%%%%%%%%%%%%%%%%%%%%%%%%%%%%%%%%%%%%%%%%%%%%%%%%%%%%
%%%%%%%%%%%%%%%%%%%%%
%% Original Note by Anisur Rahman
%%
%%--------------------------------------------------------------
--------------------%%
%% Name: FETToy
%%
%% Written by Anisur Rahman, Purdue University, Dec 24, 2002
%%
%% email: rahmana@purdue.edu
%%
%% Routines used: input.m, plot_output.m, fermi.m, Uscf_zero.m,
write_results.m    %%
%%
%%
%% Reference:
%%
%% [1] A. Rahman, J. Guo, S. Datta, and M. Lundstrom,
%%
%% "Theory of Ballistic Nanotransistors", to appear in IEEE TED,
2003.             %%
%%
%%
%% Analytically calculates the ballistic I-V of a Double Gate
ultra thin body      %%
```

```
%% MOSFET assuming that only the lowest unprimed subband is
occupied (All          %%
%% constants are in MKS unit except energy, which is in eV)
%%
%%%%%%%%%%%%%%%%%%%%%%%%%%%%%%%%%%%%%%%%%%%%%%%%%%%%%%%%%%%%%%%%
%%%%%%%%%%%%%%%%%%%%%

% FETToy for CNTFETs ...

% Physical constants(modified by Sabbir)
% Last modified by Nirjhor Tahmidur Rouf 20/8/2013

m0=0.91e-30;    hbar=1.05e-34;      q=1.6e-19;    eps0=8.85e-12;
kB=1.38e-23;  a = 2.461e-10;
f=9.798e36;
hbar=1.05e-34;          %reduced Planck's constant (m^2-kg-/s)

%non-ballistic effect parameters
L=300e-9;               %channel length
lambda_eff=200e-9;      %elastic scatterin MFP (m)
d0=1.5e-9;              %reference diameter (m)
sigma=2.7;              %overlap integral of tight bonding c-c
model (eV)
r0=.2;                  %poisson's ratio
chi=.1;                 %distortion factor under strain
h=6.626e-34;            %Planck's constant (m^2-kg-/s)
EF=-.32;                %fermi energy (eV)



d=(a*(m^2+m*n+n^2)^0.5)/3.1416;
kT=kB*T/q;                           % Thermal voltage.
V=linspace(VI,VF,NV);                % Voltage (gate or drain)
steps.

Cins=2*pi*epsr*eps0/log((t+d/2)/(d/2));
CG=Cins;
C_SIG=CG/alphag;                     % C_SIG=sum of capacitors
(see eq. (7b) in [1]).
U0=q/C_SIG;                          % Charging energy (eq. (8b)
in [1]).

% for CNTFETs (calculate D0 and EG)
dd=d;                    % tube diameter
a_cc=1.42e-10;           % C-C bond length
t0=3.0;                  % Overlap Integral TB parameter
D0=8/(3*pi*a_cc*t0);     % DOS [1/(m*eV)]
```

```
EG=2*a_cc*t0/dd;         % Band Gap [eV]
N0=N_CNT(D0,EG,kT,Ef);  % Electron concentration at the top of
the barrier in neutral device.
I0=(2*q*kB*T/pi/hbar);  % Valley degeneracy is 2

p=mod(n-m,3);
phi=atan((sqrt(3)*m)/(m+(2*n)));        %chiral angle
m_eff=.19*m0;                           %effective mass of
electron


% Start Usual calculation
N=zeros(NV,NV);          % Mobile charge density.
I=zeros(NV,NV);          % Current.
Ef_mat=zeros(NV,NV);     % Source Fermi level.
Esub_max=zeros(NV,NV);  % Energy at the top of the barrier.

%calculate EG_eff

diff_EG_strain=3*sigma*(1+r0)*sign(2*p+1)*cos(3*phi);
%rate of change of EG with distortion factor

EG_eff=EG+(diff_EG_strain*chi);
%effective bandgap due to strain

% CQ=zeros(NV,1);          % Qauntum Capacitance
% v_ave=zeros(NV,1);       % average velocity

fp = fopen('our_results_iv.txt','w');
fprintf(fp, '%s', 'New Run\n');
count_print = [];
count_print = 0; %for printing purpose
results_our = zeros(NV*NV, 4);
results_our(1,4) = d;
for kVg=1:NV             % Bias loop begins.
    Vg=V(kVg);
    for kV=1:NV
        Vd=V(kV);
        VDS_eff=(L/(L+((d/d0)*lambda_eff)))*Vd;    % calculating
VDS_eff(non-ballistic effect)
        mu1=Ef;   mu2=mu1-VDS_eff;
% Source and drain fermi levels.
        UL=-(alphag*Vg)-(alphad*VDS_eff);
% Laplace potential.
        Uscf=fzero(@Uscf_zero,0,optimset('tolx',1e-
12),D0,EG_eff,mu1,mu2,kT,UL,U0,N0);
```

```
        fermi_flag=1; if (mu1-Uscf)/kT<-20, fermi_flag=0; end
        dN=N_CNT(D0/2,EG_eff,kT,mu1-
Uscf)+N_CNT(D0/2,EG_eff,kT,mu2-Uscf)-N0;    % Mobile charge
induced by gate and drain

        N(kV,kVg)=dN;
        eta1=(mu1-Uscf)/kT; eta2=(mu2-Uscf)/kT;

        Tt=(pi^2/9)*exp(-
(pi*sqrt(m_eff*(EG_eff^3))/(sqrt(8)*q*hbar*f)));
        Itemp=I0*Tt*((log(1+exp((VDS_eff-(EG_eff/2)-EF)/kT)))-
(log(1+exp((VDS_eff-EF)/kT))));
        It=abs(Itemp);

        % Vd changes along fixed column and Vg changes along
fixed row.
        IDS(kV,kVg)=I0*(fermi(eta1,fermi_flag,0)-
fermi(eta2,fermi_flag,0));
        I=IDS+It;

        fprintf(fp, 'Vg = %f, VDS_eff = %f, I= %e\t', Vg,
VDS_eff, I(kV, kVg));

        results_our(kVg*kV,1) = Vg;
        results_our(kVg*kV,2) = VDS_eff;
        results_our(kVg*kV,3) = I(kV, kVg);
        count_print = count_print + 1;
        if(mod(count_print, 3) == 0)
            fprintf(fp, '\n');
        end
        Esub_max(kV,kVg)=Uscf;
        Ef_mat(kV,kVg)=mu1;

        % Added by Sayed Hasan 5/26/2004
        Us(kV,kVg) = Uscf;

        % Quantum Capacitance and velocity calculation added by
Sayed Hasan 05/28/2004
        if ((kV==2)|(kV==NV)),
            deltaU = 0.002*kT;
            if (kV==2),
                N_U2 =  N_CNT(D0/2,EG_eff,kT,mu1-
Uscf+deltaU/2)+N_CNT(D0/2,EG_eff,kT,mu2-Uscf+deltaU/2)-N0;
                N_U1 =  N_CNT(D0/2,EG_eff,kT,mu1-Uscf-
deltaU/2)+N_CNT(D0/2,EG_eff,kT,mu2-Uscf-deltaU/2)-N0;
                CQ(1, kVg) = q*(N_U2-N_U1)/deltaU;
```

```
                %q*(N_CNT(D0/2,EG,kT,mu1-Uscf+0.001*kT)-
N_CNT(D0/2,EG,kT,mu1-Uscf-0.001*kT))/(0.002*kT);
            elseif (kV==NV),
                N_U2 =  N_CNT(D0/2,EG_eff,kT,mu1-
Uscf+deltaU/2)+N_CNT(D0/2,EG_eff,kT,mu2-Uscf+deltaU/2)-N0;
                N_U1 =  N_CNT(D0/2,EG_eff,kT,mu1-Uscf-
deltaU/2)+N_CNT(D0/2,EG_eff,kT,mu2-Uscf-deltaU/2)-N0;
                CQ(2, kVg) = q*(N_U2-N_U1)/deltaU;
                %CQ(2, kVg)=q*(N_CNT(D0/2,EG,kT,mu1-
Uscf+0.001*kT)-N_CNT(D0/2,EG,kT,mu1-Uscf-0.001*kT))/(0.002*kT);
                v_ave(kVg)=I(kV,kVg)/q/(dN+N0);
            end

        end
    end
end                      % Bias loop ends.
fclose(fp);
% Transconductance, gm and output conductance, gd and vinjare
calculated at highest gate and drain biases
gm=(I(NV,NV)-I(NV,NV-1))/(V(NV)-V(NV-1));
gd=(I(NV,NV)-I(NV-1,NV))/(V(NV)-V(NV-1));
Av=gm/gd;
vinj=I(NV,NV)/(q*N(NV,NV));



% Calculate S and DIBL  %%%%%%%%%%%%%%%%%% added by Jing Wang
09/09/2003
Ie1=log10(I(NV,:));
Ie2=log10(I(2,:));
vv1=interp1(Ie1,V,log10(I(NV,1)),'spline');
vv2=interp1(Ie1,V,log10(2*I(NV,1)),'spline');
vv3=interp1(Ie2,V,log10(I(NV,1)),'spline');
S=(vv2-vv1)/log10(2)*1000;
DIBL=(vv3-vv1)/(V(NV)-V(2))*1000;

% Calculate channel conductance (cc) and transconductance (tc)
as a function of Vgs %%%%%%%%%%%%%%%%%% added by Jing Wang
11/05/2003
cc=I(2,:)'./(V(2)-V(1));
tc=zeros(NV,1);
for i=2:NV
    tc(i)=(interp1(V,I(NV,:),V(i)+0.0005,'spline')-
interp1(V,I(NV,:),V(i)-0.0005,'spline'))/0.001;
    %tc(i)=(exp(interp1(V,log(I(NV,:)),V(i)+0.0005))-
exp(interp1(V,log(I(NV,:)),V(i)-0.0005)))/0.001;
end
```

```
tc(1)=(exp(interp1(V,log(I(NV,:)),V(1)+0.0005,'spline'))-
exp(interp1(V,log(I(NV,:)),V(1)-0.0005,'spline')))/0.001;


%%%%%%%%%%%%%%%  OUTPUT (Sayed Hasan: 5/25/2004)
%%%%%%%%%%%%%%%%%%%%%%%%%%%%%%%%%%%%
plot_output1;                % Plot results
save_charge;                % Save q*N
save_current;               % Save I
save_uscf;                  % Save Us
write_results;              % Write results in results.m file
save rawdata;               % save matlab variables
```

3) Tunnel Control Parameter:

```
function [F]=tunnel_control_parameter(It,VDS,L,T,n,m)


%   Inputs
%---------------
%   L-channel length (m)
%   It-tunneling current (A)
%   VDS-drain-source voltage (V)
%   T- temperature (K)
%   n-chiral axis n
%   m-chiral axis m


%% Name: Tunnel Control Parameter Calculator
%% modified by Nirjhor Tahmidur Rouf 20/06/2013


lambda_eff=200e-9;      %elastic scatterin MFP (m)
d0=1.5e-9;              %reference diameter (m)
a_cc=1.42e-10;          %c-c bond legth (m)
t0=3;                   %bonding energy c-c (eV)
sigma=2.7;              %overlap integral of tight bonding c-c
model (eV)
r0=.2;                  %poisson's ratio
chi=.1;                 %distortion factor under strain
q=1.6e-19;              %charge of electron (C)
h=6.626e-34;            %Planck's constant (m^2-kg-/s)
KB=1.38e-23;            %Boltzmann constant (m^2-kg/S^2/K)
m0=9.11e-31;            %electron mass (kg)
hbar=1.05e-34;          %reduced Planck's constant (m^2-kg-/s)
```

```
a=.246e-9;                %needed to calculate diameter
EF=-.32;                  %fermi energy (eV)

%usual calculation

d=(a/pi)*sqrt(n^2+(n*m)+m^2);           %cnt diameter
EG=(2*a_cc*t0)/d;                       %bandgap
p=mod(n-m,3);
phi=atan((sqrt(3)*m)/(m+(2*n)));        %chiral angle
m_eff=.19*m0;                           %effective mass of
electron

%calculate VDS_eff

VDS_eff=(L/(L+((d/d0)*lambda_eff)))*VDS;

%calculate EG_eff

diff_EG_strain=3*sigma*(1+r0)*sign(2*p+1)*cos(3*phi);
%rate of change of EG with distortion factor

EG_eff=EG+(diff_EG_strain*chi);

%calculate Tt (tunneling effect)

I0=(4*q*KB*T/h);
I1=log(1+(exp((((VDS_eff)-(EG_eff/2)-EF)*q)/(KB*T))));
I2=log(1+(exp((((VDS_eff)-EF))/(KB*T)*q)));

temp_1=I0*(I1-I2);
Tt=It/temp_1;

%calculate F

if Tt>0
    numerator=pi*sqrt(m_eff*(EG_eff^3));
    Tt1=log(Tt*9/(pi^2));
    denumerator=sqrt(8)*q*hbar*Tt1;
    F=-(numerator/denumerator);
else
    numerator=2*pi*sqrt(m_eff*((EG_eff)^3));
    Tt1=log(Tt^2*81/(pi^4));
    denumerator=sqrt(8)*q*hbar*Tt1;
    F=-(numerator/denumerator);
end

end
```

4) Tunneling Reproducing Code:

```
close all;
clear all;
clc

x=[0 .07698 .136 .1368 .561 .5 .6 .371 .451 .4914 .5014 .5991
.1361 .2009 .1361 .2009 .15 .16052 .1671 .17237 .17895 .18552
.189473];
%VDS data from graph
y=[0 .443 .638 .6384 .8 .755 .833 .7316 .7449 .7511 .7562 .8318
.6381 .7002 .6381 .7002 .6666 .6777 .6861 .6866 .6944 .6972 .7];
%current with tunneling effect data from graph
x_b=[0 .07286 .1376 .1572 .1779 .2619 .5965 .6];    %VDS data for
ballistic from graph
y_1=[0 .4101 .6252 .6611 .674 .6935 .7376 .738];    %current
without tunneling effect data
y_b=1e-5.*y_1;                                      %multiplying
with 1e-5 to get proper order of IDS
VDS=0:.0000001:.6;
x1=unique(x);
y1=unique(y);
y2=1e-5*y1;                                         %multiplying
with 1e-5 to get proper order of IDS

IDS=interp1(x_b,y_b,VDS);
%interpolating to get more data points for ballistic current
IDS_t=interp1(x1,y2,VDS);
%interpolating to get more data points for current with
tunneling effect
It=IDS_t-IDS;                                       %tunneling
current

%plot IDS_t vs VDS, IDS vs VDS, It vs VDS
figure(1)
plot(VDS,IDS_t);

xlabel('VDS [V]');
ylabel('IDS [A]');
hold all;
plot(VDS,IDS)
plot(VDS,It)
legend('IDS with tunneling effect','IDS without tunneling
effect','tunneling current')
```

APPENDIX B

MATHEMATICAL DERIVATION FOR BALLISTIC CNTFET SIMULATION

This section presents the mathematical derivation of current-voltage (I-V) characteristic for ballistic CNTFET. FigureB-1 illustrates how the states at the top of the barrier are filled using E-k relationship. The energy reference is the top of barrier at zero terminal voltage. The source Fermi level, E_{f1}, drain Fermi level, E_{f2}, and potential at top of barrier are expressed with respect to the energy reference.

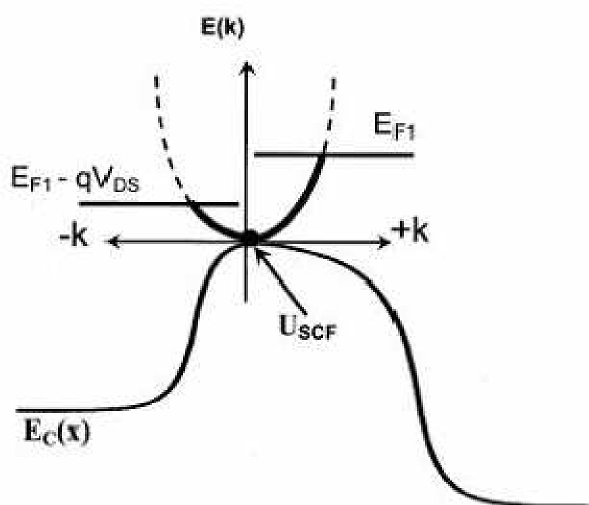

Figure 1: Illustration of how k-states at top of the barrier are filled by the two fermi levels.

The positive k-states are occupied according to source Fermi level as

$$N_1 = 1/A \sum_{k2>0,kz} f(E-E_{fl}) = \iint_{k2>0,kz} 2d^2 \times k/(2\pi)^2 \times f(E-E_{fl})$$

$$= \int_{-\infty}^{\infty} f(E-E_{fl})\, dE \times ½ \int_{S(E)} \frac{1}{2\pi^2 |\nabla E(k)|} dS \qquad (1)$$

Where S(E) is a constant energy in k-space, dS is an element area on this surface and $\frac{dE}{|\nabla E(k)|}$ is the distance between the surfaces S(E+dE) and S(E). Defining the density-of-states (DOS) as

$$D\,(E-U_{scf}) = \int_{S(E-Uscf)} \frac{dS}{2\pi\hat{}2\,|\nabla E(k)|} \qquad (2)$$

We finally have, $N_1 = {}^1/_2 \int_{-\infty}^{\infty} D(E-U_{scf})\, f(E-E_{fl})\, dE$ (3)

The integral for N_1 can be analytically defined as

$$N_1 = k_B\, T\, 2m^* /(2\pi(h/2\pi)^2) * \log\,(1+ e^{(E_{f1} - U_{scf}/k_B T)}) \qquad (4)$$

A similar expression for N_2, states occupied according to drain Fermi level

$$N_2 = k_B\, T\, 2m^* /(2\pi(h/2\pi)^2) * \log\,(1+ e^{(E_{f2} - U_{scf}/k_B T)}) \qquad (5)$$

Current for positive k-states is evaluated as

$$I_1 = q/A \sum_{k2>0,kz} V_x\, f\,(E-E_{fl})$$

$$= \iint_{k2>0,kz} d^2*k/(2\pi)^2 * f\,(E-E_{fl})$$

$$= \int_{-\infty}^{\infty} f\,(E-E_{fl})\, dE * q/2 * ½ \int_{B(E)} \frac{dS}{2\pi^2|} |V_x\, |1/\nabla E(k)|$$

$$= \int_{-\infty}^{\infty} f\,(E-E_{fl}) * q/2 * v'_x\,(E-U_{scf}) * D\,(E-U_{scf}) dE \qquad (6)$$

Where v'_x (E) is the average value of v'_x over the constant energy surface, S(E), expressed as

$$v'_x\,(E-U_{scf}) = \int_{S(E-Uscf)} \frac{dS}{2\pi^2|} |V_x\, |1/\nabla E(k)| \,/\, \int_{S(E-Uscf)} \frac{dS}{2\pi^2} 1/|\nabla E(k)| \qquad (7)$$

Defining the current density-of-states as

$$J\,(E-U_{scf}) = q/2\, V_x\,(E-U_{scf}) * D\,(E-U_{scf}) \qquad (8)$$

Thus we have,

$$I_1 = \int_{-\infty}^{\infty} J\,(E-U_{scf})\, f\,(E-E_{fl})\, dE \qquad (9)$$

In general, for the 2D electron density, the v'_x (E) can be analytically evaluated to obtain

$$J\,(E-U_{scf}) = {}^1/_2\, q\,(2/\pi \sqrt{2(E-Uscf)/m*})^2 /D \qquad (10)$$

Where, the factor $2/\pi$ appears because of averaging v'_x over all possible k values at energy E-$U_{scf.}$ I_1 can be analytically integrated to obtain

$$I_1=1/2\ q\ k_b\ T\ 2m^* / (\pi(h^2))/ \sqrt{2KT/\pi m*}\ \log(1 + e^{Ef1-Uscf/kBT}) \qquad (11)$$

Similar expression exists for current at negative k-states

$$I_2=1/2\ q\ k_b\ T\ 2m^* / (\pi(h^2))/ \sqrt{2KT/\pi m*}\ \log(1 + e^{Ef2-Uscf/kBT}) \qquad (12)$$